UiT
THE ARCTIC UNIVERSITY OF NORWAY

Faculty of Science and Technology
Department of Physics and Technology

Case Study of a Large-Scale Solar and Wind Power Hybrid System at Fakken Wind Farm, Troms

Charlotte Tiller

EOM- 3901 Master thesis in Energy, Climate and Environment- June 2017

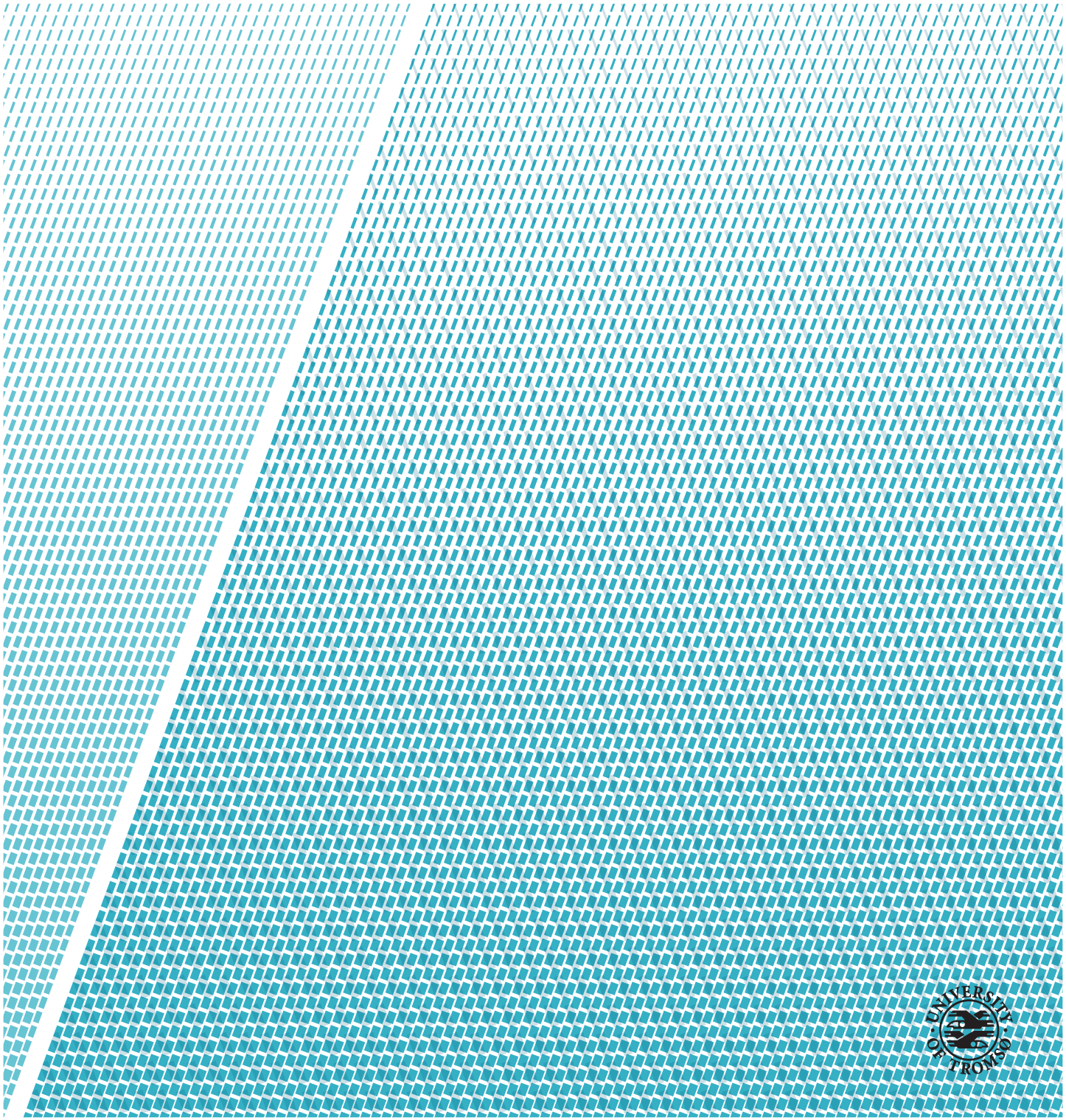

Abstract

The objective of this thesis is to investigate the feasibility of a large scale hybrid system at Fakken, Troms. There is already an existing 54 MW wind farm at site. The wind farm has considerably higher power production during winter compared to summer, and the electricity grid is therefore not fully exploited during summer. Adding a solar panel utility to the site could be a solution to this issue. This thesis is centralized around simulating the hybrid system using *HOMER Pro*. This tool requires a whole year of data to perform a simulation. Since only three months of observed radiation are available, will *WRF* simulated solar radiation data be used in the *HOMER* simulations. To evaluate the feasibility of such a system is an anti correlation analysis between the solar and wind resources at site conducted. A negative correlation would be optimal. The anti correlation analysis is performed on observed wind and solar radiation for February, March and April 2017. A similar analysis is conduced on simulated solar radiation data and measured wind data for a whole year as well. The analysis do not show any anti correlation on small to middle time scales. Only on a very large time scale is the anti correlation significantly high.

The *WRF model* fails in producing a reliable solar radiation source partly because it overestimates the radiation levels and also because it has an offset in the daily profile of the radiation. Measures are taken for scaling the radiation to obtain more reliable results, but the offset is not corrected for.

A 20 MW solar power system is simulated together with the pre-existing wind far, with a grid constraint of 54 MW. Sensitivity analysis are performed on several physical, technical and economic parameters that might affect the feasibility of the system. Under the most realistic conditions simulated, did the system not qualify as an economic feasible system. There is possible to extract large amounts of power from the system if the right measures are taken, but it was not enough for the system to become profitable.

Acknowledgements

Jeg vil gjerne takke alle som har bidratt til å gjøre denne oppgaven mulig for meg å skrive. Det har vært et spennende prosjekt å avslutte studiet med.

Tusen takk til prof. Tobias Boström som tok seg tid til å være min veileder selv om han er opptatt med foreldrepermisjon. Også takk til veileder Svein Erik Thyrhaug som har bidratt med viktig veiledning og datakilder.

Tusen takk til Ynge Birkelund, som simulerte soldata som vi ikke kunne klart oss uten.

Takk til alle på kontoret som har bidratt til god stemning gjennom hele semesteret.

Spesielt takk til my "My partner in crime", Karoline Ingebrigtsen for 5 år med fantastisk studiesamarbeid!

Contents

List of Figures

List of Tables

Nomenclature

δ	Declination angle
HRA	Hour angle
LSTM	Local standard time meridian
ϕ	Latitude
K	Kelvin
AM	air mass
α	Azimuth angle
ϵ	Elevation angle
d	Day number in a year
h	Hour
S_{tiltet}	Irradiation incident on a tilted surface
$S_{\text{horizontal}}$	Irradiation incident on a horizontal surface
I_{sc}	Short circuit current
V_{oc}	Open circuit voltage
ρ	Air density
A	area (covered by a wind turbines wingspan)
V	Wind speed
P	Power
P_w	Power per unit area in the wind
I_L	Light generated current
I_0	Dark saturation current
V	Voltage
T	Absolute temperature in Kelvin
q	Electron charge
G_{sc}	Solar constant ($1.367 kW/m^2$) η

Abbreviations

AC	Alternating Current
DC	Direct Current
CF	Capacity Factor
BJT	Bipolar Junction Transistor
PV	Photo voltaic
HRES	Hybrid Renewable Energy System
BoS	Balance of System
MPPT	Maximum Power Point Tracking
EoT	Equation of Time
LT	Local Time
TC	Time Correction Factor
FF	Fill Factor
ARC	Anti Reflective Coating
BoS	Balance of System for Solar installations
WRF	Weather Forecasting and Research Program
WPS	WRF Prepocessing System
ARW	Advanced Research WRF
PWM	Pulse Width Modulation
NPV	Net Present Value
LCOE	Levelized Cost Of Energy

1 Introduction

1.1 Objective

This thesis is written in collaboration with Troms Kraft, who is interested in expanding Fakken wind farm by transforming it into a hybrid renewable energy system by adding photovoltaic panels to the plant. The main motivation behind this is to improve the utilization of the electricity grid that is not fully exploited during large parts of the year due to the varying wind resources at site. The power production peaks during winter and gradually decline when summer approaches. It is reasonable to believe that solar energy could even this difference out, in the same time as it enables Troms Kraft to elevate its power production without grid expansion requirements. Troms Kraft's power supply is currently vulnerable to rain water accumulation in the reservoirs. The energy security could in theory be improved by harvesting power from a bigger selection of sources.

Although solar power is an emerging technology globally, has its capabilities at high latitudes not been thoroughly investigated yet. It is mainly viewed as an infeasible technology choice for North of Norway due to moderate solar radiation, high installation costs and low electricity prices. The yearly electricity demand profile is also opposite of the solar energy production profile. This issue is irrelevant for the case study at Fakken since the motive is to increase production during summer. Photovoltaic systems costs has also dropped rapidly over the recent years, while the efficiency has improved. Fakken has the advantage of cold temperatures which has a major positive impact on the efficiency

Figure 1.1: Map of Fakken modifiend from Norgeskart[**?**]. The pyranometer location and transformer station is marked in yellow

of PV modules.

This thesis is a feasibility analysis of the addition of solar energy to the pre existing wind farm. The analysis will focus on the viability of the technical solutions available both when it comes to energy harvesting and cost efficiency. The analysis will evolve around the following:

- A correlation analysis of the solar and wind resources at site.
- Simulations in the computer tool *Homer* for several technological solutions.
- Economical analysis of the solutions.

The aim behind the correlation analysis is to investigate how the time varies on a wide spectrum of time scales. Since the objective is to improve the grid capacity utilization will a negative correlation be optimal. A negative correlation between the solar and wind resources creates the opportunity of uniting two intermittent and unstable energy sources to join forces and cooperate in generating a smooth power flow.

Since solar panels are not yet common to install at high latitudes, and because Troms Kraft has limited experience with solar power in general, will a rather comprehensive theory chapter create the necessary foundation for the further work in in this thesis. The theory chapter will explain the main features of solar energy generation, and focuses on how the site specific conditions might

affect the power output of the hybrid system.

In the third chapter will the data sources, programming tools and the methodology be explained. A pyranometer was installed at Fakken in January 2017 to measure the global solar radiation at site. However, since *Homer* needs a whole year of solar resources in order to conduct a simulation. To overcome this obstacle was an alternative approach required. The solution was to use the *WRF* model to simulate the global solar radiation at Fakken during 2016. The *WRF* simulations were also conducted at Holt in Tromsø to construct a basis for evaluating the success of the *WRF* model in simulating the radiation. When the data sources and program tools have been sufficiently described will the chapter proceed in explaining the simulation strategy and describe how the feasibility of the system will be evaluated. At last will also the inputs to the different technological case scenarios be viewed. The results and the discussion are assigned to chapter 4. First will the results from the *WRF* simulation be presented and compared to observed radiation at Holt following with the correlation analysis between wind and solar resources at Fakken. The next part concerns the simulation analysis of the hybrid system. The first part of this section will be a technical evaluation on how different PV installations respond to physical parameters like ground reflectance, radiation and efficiencies. Based on the findings from this section will some scenarios appear more relevant for further investigation. Some scenarios will be relevant because they respond well to the actual or presumed physical conditions and for being technically realistic approaches. Other will be investigated further because they might seem relevant for future scenarios when it is assumed that the technologies have reached further maturity. Some satellite images presenting Fakken's exposure to sunshine for parts of the year will in the end be displayed. Based on the findings in the result and discussion chapter, will a conclusion be made on if it is feasible to install a large scale PV utility to the existing wind farm at Fakken.

1.2 Fakken Wind Farm

Fakken Wind farm is located at Vannøya in Troms. The power plant was finalized 2. June 2012 and has a lifetime of 25 years [1]. It consists of 18 V90-3.0MW wind turbines from Vestas, each with a power rating of 3 MW, giving a total capacity of 54 MW [1]. Approximately 139 GWh is produced annually [1]. If all the turbines operated at their rated power all the time would the total of 18 turbines have an annual production of

$$3MW \cdot 18 \cdot 365 \cdot 24h = 473GWh$$

Hence can the capacity factor at Fakken be calculated:

$$CF = \frac{139GWh}{473GhWh} \cdot 100\% \approx 29.4\%$$

Each turbine is connected to a transformer that elevates the voltage from 1 kV to 22 kV. Another transformer collects the 22 kV power from all the turbines and steps it up further to 66 kV and connects it to the grid. Most of the energy produced at Fakken is consumed in Tromsø by feeding power to the 66 kV grid from Vannøya to a coupling station at Kvaløya. Any excess power is transformed further up to 132 kV and transported south towards Balsfjorden or north towards Ullsfjorden. Approximately 4 MW is consumed locally at Vannøya, and there is a 50 MVA limit on the 66 kV line from Fakken to Kvaløya, which gives power production restrictions at site. The capacity of the electricity grid is to a varying degree covered by wind power production during the winter season. The hourly production for January 2013 is displayed in figure 1.6 to demonstrate the intermittent nature of wind power production.

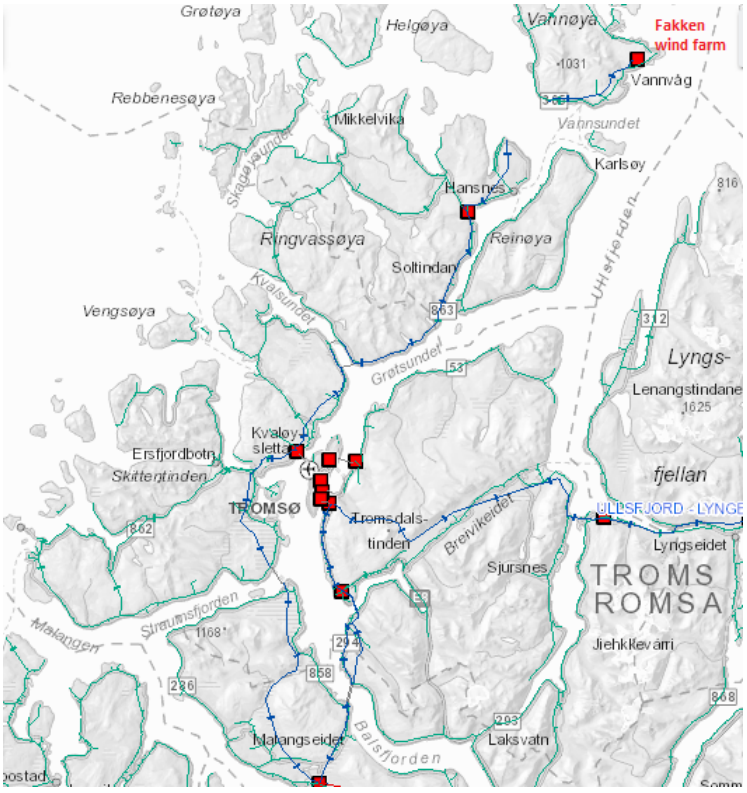

Figure 1.2: Local electricity grid slightly modified from [37]

Figure 1.3 shows the average hourly power production during each week

at Fakken over three years (2013-2015). The figure is plotted using matlab and is based on production data in MWh received from Troms Kraft. The corresponding hourly average consumption data during each week for Troms Kraft concession area is also plotted for year 2013-2015 in figure 1.4.

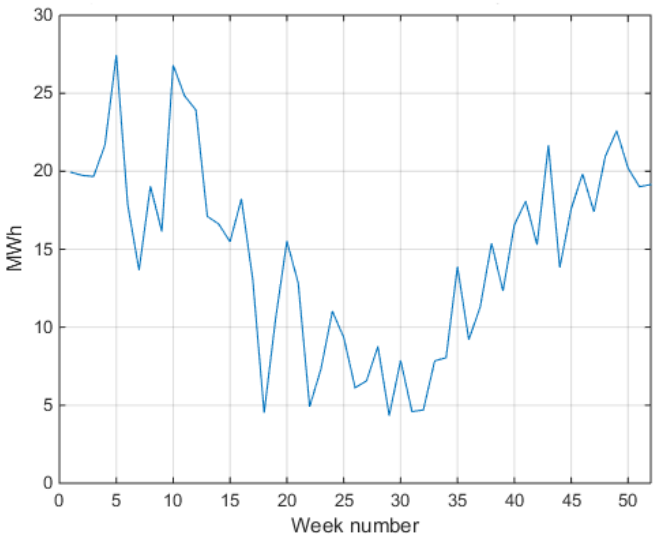

Figure 1.3: Average hourly power production for each week at Fakken wind farm from 2013-2015

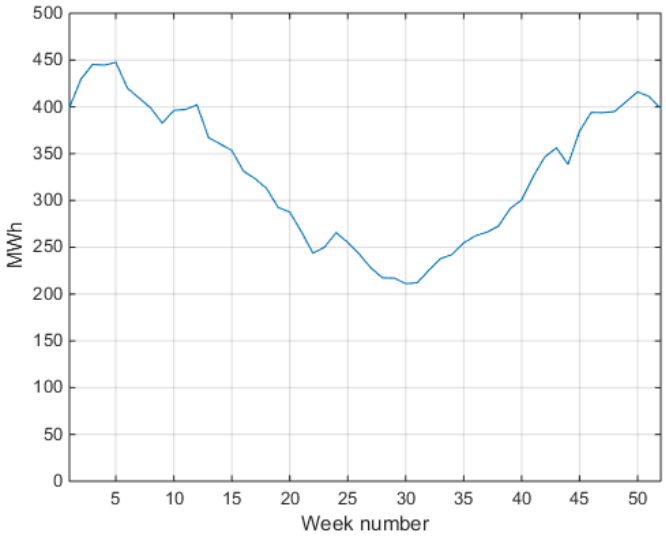

Figure 1.4: Average weekly consumption from 2013-2015 for the entire concession area of Troms Kraft

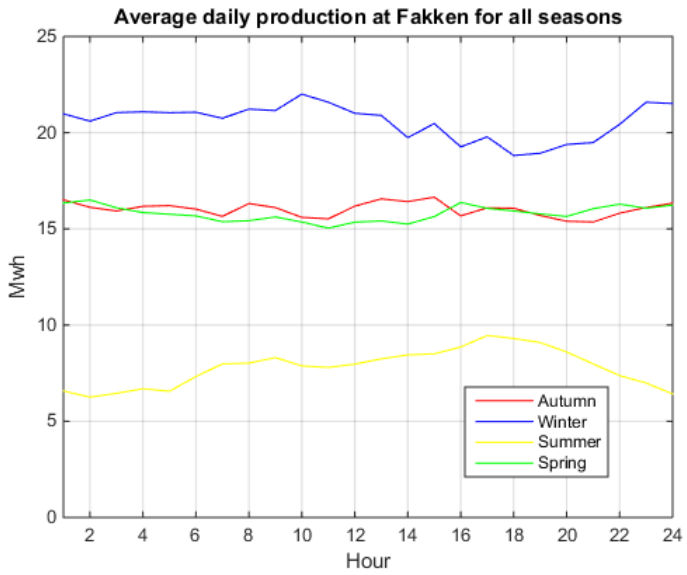

Figure 1.5: Average daily production profile distinguished between the four seasons with hourly values

The figures 1.4 and 1.3 shows that there is strong seasonal variations in both the consumption and the production. The figures also show that the consumption always exceeds the production and the power restriction on the electricity grid of 50 MW. Figure 1.5 exposes how the average daily production varies seasonally. The seasons are for this plot defined as:

- Spring: March, April and May
- Summer: June, July and August
- Autumn: September, October and November
- Winter: December, January and February

Production is highest at winter time producing roughly 20 MW on average. During spring and autumn, the production is approximately 16-17 MW. The average production is significantly lower during summer, with roughly 6-8 MW. By using an average curve are the fluctuating effects of the wind evened out. The production for January 2013 is shown in figure 1.6 which clearly shows how much the production varies in time.

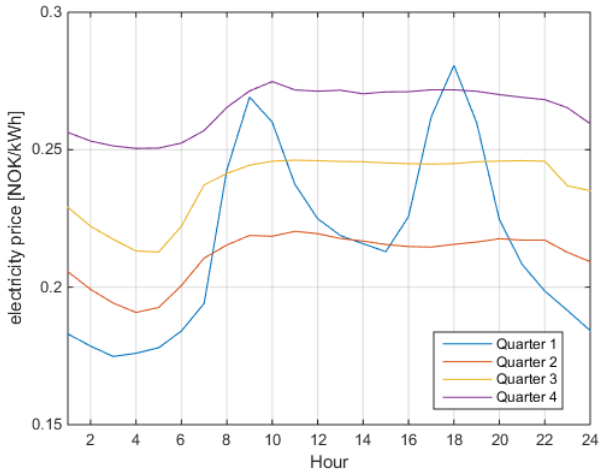

Figure 1.7: Daily profile of electricity prices for each quarter of the year

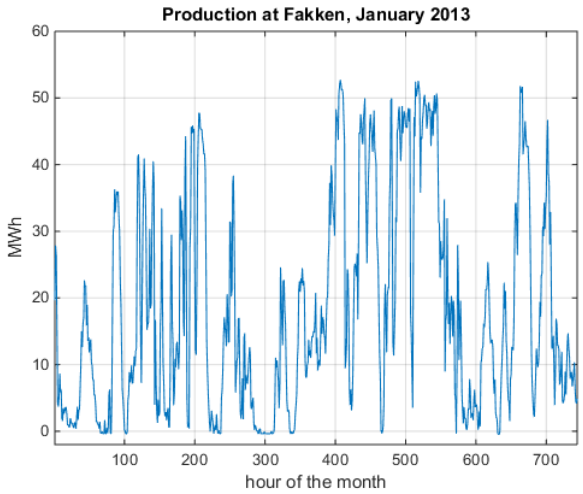

Figure 1.6: Plot of the hourly production at Fakken during january 2013

Figure 1.6 proves that the production cover the grid restrain from time to time, but the overall production is less than optimal. January is also one of the most productive months.

Fakken is the only wind farm owned by Troms kraft, and the rest of the power production is based on hydro power [1]. A PV plant in North of Norway will clearly produce most power during summer. Figure 1.7 displays the daily profile of the electricity prices for each quarter of the year. The prices are highest during daytime for all quarters which is an advantage for solar power

production. The average prices for each quarter are; first quarter(Jan, Feb, Mar): 0.2161 NOK/kWh, second quarter (Apr, May, Jun): 0.2113 NOK/kWh , third quarter (Jul, Aug, Sep): 0.2377 NOK/kWh and the last quarter (Oct, Nov, Dec): 0.2649 NOK/kWh. The second quarter has the lowest electricity prices and this is the same quarter period it is assumed that solar power production will peak. However, in combination with hydro power, which is easily stored, capturing solar energy during summer allows more water to be stored for times when energy consumption is higher and water accumulation into the dams are lower. The excess electricity can be fed to the grid when energy prices are more favourable. As a bonus might the energy security be improved since a PV plant can reduce the electricity production's dependence of rain water.

Wind power generators

The wind turbines are connected to induction generators. The stator is directly connected to the three phase grid, and its power flow must therefore be kept at constant voltage amplitude and frequency by keeping the rotation of the magnetic field fixed at 1500 rpm. To allow for power transfer both from and towards the rotor, does the power converters apply pulse width modulations (PWM). The PWM also enable reactive power control of the generator [3]. This power transfer is what enable the stator to feed the grid with constant power while the turbine is enabled to rotate at varying speed [4]. The average total turbine power consumption between 2013-2015 was 48.47 kW/h, but the consumption is highly variable as figure 1.8 shows.

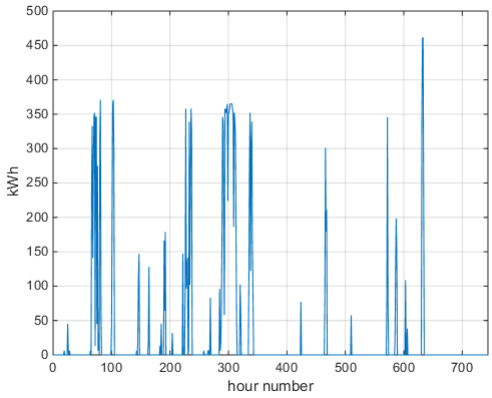

Figure 1.8: Consumption from all the 18 turbines for each hour during January 2013 [1]

2

Solar Power Theory

Solar energy is by far the most abundant source of energy available on earth [16]. Every single hour, the earth's surface receives more energy than the entire global population needs annually [7]. However, only a fraction of this is practical to extract [7]. Without the indefatigable irradiation from the sun, we could not burn fossil fuels or biomass and we would not have wind, wave, hydro or solar energy at all, because they are all directly or indirectly solar powered. Only photovoltaic panels converts the energy from the sun straight in to electricity. Compared to other energy sources are PV-panels gentle to the environment both locally and globally. Solar panes emits no green house gases during operation, and they have no fast moving parts which makes them harmless to wildlife.

2.1 Irradiation, Air Mass and Scattering

The irradiation at the top of the atmosphere is on average higher than at the surface of earth. This is due to scattering of the radiation as it moves through the atmosphere.

The proportion of energy that is lost due to scattering depends on the path length that the light has to travel through the atmosphere until it reaches the surface of earth. This quantity is measured as *air mass* and is given by equation

2.1

$$AM = \frac{\text{Optical path length to sun}}{\text{Optical path length if sun is directly overhead}} = \frac{1}{sin(\alpha)} \tag{2.1}$$

α is the angle between the surface of the earth and the suns position (elevation angle). This equation neglects the earth's and the atmosphere's curvature [15].

The path length will vary depending on the latitude of the location, the season and the time of the day. But air mass is not the only factor affecting the irradiation. Differences in local weather conditions, pollution and water vapour in the atmosphere can also influence the amount of energy available in the sunshin [7]. As a consequence of scattering is the sunlight divided into two parts, namely direct and diffuse radiation. As opposed to direct sunlight, diffuse radiation travels from all directions in the atmosphere [7]. On average does the diffuse light count for 15% of the total radiation, but this number increases with latitude as the air mass expands [15].

The surface of the earth also reflect some portion of the radiation received from the sun. This fraction is called albedo, and this radiation can also be exploited in photovoltaic applications, particularly with bifacial panels, which will be further discussed in section 2.8.3 [8].

2.2 Sun's Movement and Optimum Angle of Attack

To achieve the highest flux of radiation on a solar cell, it is most efficient to place the solar panel such that the direct sunlight hits the surface at a 90° angle. If the sky is seen as a two dimensional dome, only two coordinates are needed to describe the position of the sun on the sky, namely the azimuth, and the elevation/altitude angle (see figure 2.1). These angles are not fundamental, but are determined by the fundamental quantities *hour angle*, *declination angle* and the *latitude* [16].

Considering earth's rotation, tilt and orbit will the solar panels require the installation of sophisticated tracking systems in order to have optimal incident angle at all times. Tracking systems increases the cost of the system quite substantially compared to stationary panels, which is by far the most common configuration. Different tracking topologies will be discussed in section 2.8.2.

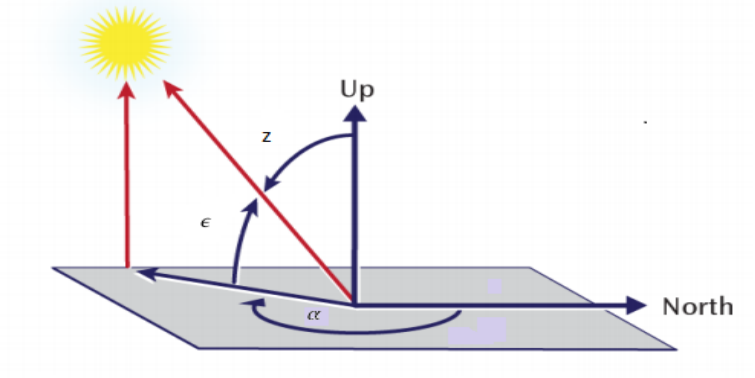

Figure 2.1: Azimuth and elevation angle [24]

2.2.1 Declination Angle

The declination angle, δ, is the angle between the equator and an imaginary line from the center of the earth to the center of the sun [7]. The declination angle varies throughout the year due to the tilt of the earth and its rotation around the sun, and can be calculated by equation 2.2.

$$\delta = sin^{-1}\left(sin(23,45^\circ)sin\left(\frac{360}{365}(d-81)\right)\right) \tag{2.2}$$

where d is the day number of the year.

2.2.2 Hour Angle

In order to achieve the *Hour Angle*, HRA, some other variables needs to be discussed. Earth rotates 360° every day, and with 24 time zones, this gives a rotation of 15° each hour. Every time zone has its own 'Local Standard Time Meridian', LSTM, that is calculated by equation 2.3, and is given in hours.

$$LSTM = 15^\circ \cdot \Delta T_{GMT} \tag{2.3}$$

where ΔT_{GMT} is the time difference between the local time and the Greenwich mean time.
The Equation of Time, EoT, takes into account that earth's orbit around the sun is an ellipse and that the earth is tilted. It is an empirical equation given

by 2.4, and the unit is in minutes.

$$EoT = 9,87sin(2B) - 7,53cos(B) - 1,5sin(B) \tag{2.4}$$

in which

$$B = \frac{360}{365}(d - 81)$$

Time zones are human inventions and the real solar time for one particular locations will differ from the solar time at an other location inside the same time zone. This can be corrected for by using the Time Correction factor, TC, given by 2.5 with unit of minutes.

$$TC = 4 \cdot (\lambda - LSTM) + EoT \tag{2.5}$$

Now the Local Solar Time, LST, is represented by 2.6. Local time, LT, can differ from LST because of the eccentricity and human adjustments.

$$LST = LT + \frac{TC}{60} \tag{2.6}$$

Now finally, the Hour Angle, HRA can be presented as 2.7

$$HRA = 15^{\circ}(LST - 12) \tag{2.7}$$

2.2.3 Elevation Angle

The altitude/elevation angle is described as the angle measured from the horizontal line to the position of the sun at the sky. This angle will be zero at sunrise and sunset, and at the equator it can reach 90°at noon at the solar equinoxes. The elevation angle ϵ can be calculated by equation 2.8

$$\epsilon = sin^{-1}[sin(\delta)sin(\phi) + cos(\delta)cos(\phi)cos(HRA)] \tag{2.8}$$

where ϕ is the latitude and HRA is the hour angle [7].

2.2.4 Azimuth Angle

Now, we only need to find an expression for the azimuth angle, α, which is described as the compass direction the incident sunlight comes from. It can be

calculated by equation 2.9:

$$\alpha = cos^{-1}\left(\frac{sin(\delta)cos(\phi) - cos(\delta)sin(\phi)cos(HRA)}{cos(\epsilon)}\right) \tag{2.9}$$

[7]

2.2.5 Radiation Incident on a Tilted Surface

The tilt angle, β, is the angle defined as the angle stretching from the horizontal plane to the PV panel [7]. The relationship between the radiation at a horizontal surface and a tilted surface is

$$G_{\text{tilted}} = \frac{G_{\text{horizontal}} \cdot sin(\epsilon + \beta)}{sin(\epsilon)} \tag{2.10}$$

[7].

2.3 Structure of Solar Cells

In PV cells, we exploit the photovoltaic effect by letting photons from the sun be absorbed by a semiconductor to separate electrons from the atom and making conduction possible. Figure 2.2 shows the cross section of a single cell. If the material absorbs photons with energy higher than the band gap, electrons will detatch from the crystal, and, provided that the electron do not recombine with a hole in the crystal first, be collected at the contacts and provide power to the external load [7]. Hou et. al [10] reports typical PV efficiencies from 2013 presented in table 2.1

Table 2.1: Typical efficiency values for silicon solar cells (2013) [10]

mono-crystalline Si cell efficiency Si	17 – 19.5%
mono-crystalline Si module efficiency	16 – 18%
multi-crystalline Si cell efficiency	16 – 18.5%
multi-crystalline Si module efficiency	15 – 16%

These values are only 4 years old, but might still be outdated. The best performing cell efficiencies recorded are reported by NREL (National renewable energy laboratory) [95] to be around 22-25 % for crystalline silicon solar cells in2017. The module efficiency will be somewhat lower.

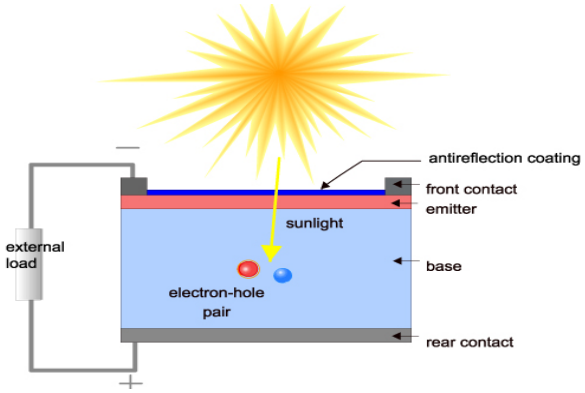

Figure 2.2: Structure of solar cell [7]

2.4 IV Curve

The current produced by a solar cell is expressed by equation 2.11. The IV-curve is displayed in figure 2.3

$$I = I_L - I_0 \left[exp\left(\frac{qV}{nkT}\right)\right] \tag{2.11}$$

where
I_0 is the dark saturation current, also called the leakage current, driving recombination. This is dependant on the temperature, material quality and the doping level [7].
I_L is the light generated current.
q is the electron charge
T is the absolute temperature
V is the voltage over the solar cell
n is the ideality factor (usually a value between 1 and 2)
k is the Boltzmann factor

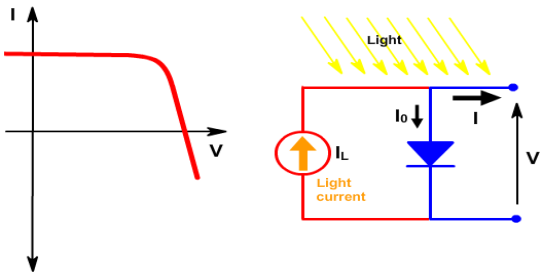

Figure 2.3: IV Curve of solar cell under illumination [7]

The maximum power point on the IV-curve has a voltage V_m and a current I_m so the fill factor is given by equation 2.12 [14]

$$FF = \frac{I_m V_m}{I_{sc} V_{oc}} \tag{2.12}$$

The efficiency of a solar cell is the fraction of the power output to the input power from the sun (equation 2.13) [14]

$$\eta = \frac{I_{mp} V_{mp}}{P_{in}} \tag{2.13}$$

To achieve the maximum power extraction we need a load resistance of $R_{ch} = V_{mp}/I_{mp}$, which is called the characteristic resistance. Then we will achieve the maximum power density as displayed in figure 2.4 [7].

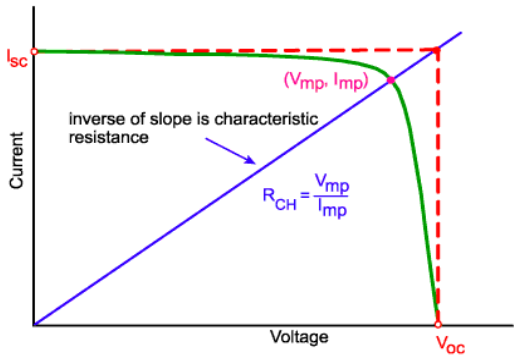

Figure 2.4: Maximum Power Point achieved by Characteristic resistance [7]

2.5 Module Design

For power production, solar cells are interconnected in parallel and/or series to form PV modules. The modules are capable of producing higher power output than the cells would on their own [14]. By connecting the cells in series, the output voltage increases, and by parallel connecting them, the output current rises[14]. The modules can be interconnected to form PV-arrays [14].

The PV- modules are series connected into strings. Furthermore, the strings are connected in parallels to form PV-arrays. A commonly applied configuration PV-arrays is shown in figure 2.5. The number of modules in one string will determine the voltage level of the array while the number of strings determines the power level. Each string needs a blocking diode in order to avoid current flow between the strings [11].

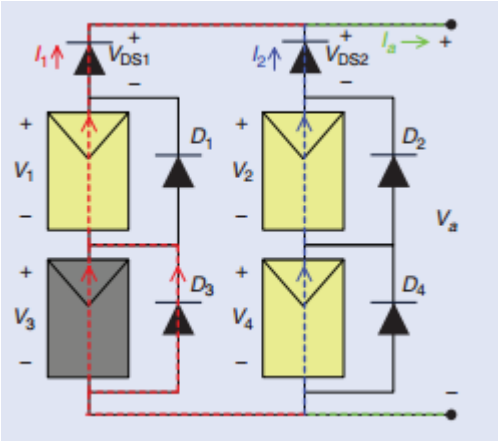

Figure 2.5: Series- parallel connected modules forms a PV-array. This configuration has two modules in series in each string and two strings in parallel [11]

2.6 Mismatch in modules

Mismatches in modules/cells are sources of power loss, but can also give rise to serious damages to the module [14]. Mismatches can occur from many reasons. Some of the most common sources are:

- Cells in module do not have identical electrical properties. It is particularly common that cells possess differences in V_{oc} or I_{sc} under otherwise equal conditions.

- Different shading of the cells in the module, or other external circum-

stances. Partial shading of the module cause mismatch in I_{sc}.

- Breaking of the protective glass.

[14]

Mismatch due to difference in I_{sc} or V_{oc}: If there is mismatch in V_{oc} a series connection, it will only affect the cell with the mismatch. For instance, if one of 60 cells gets lower V_{oc} than the rest, its power output will drop, but the production from the other cells will remain, resulting in an modest power drop for the module. If there is a mismatch in the I_{sc}, all the cells in the series connection will be bound to produce the same current as the one with the lowest production, and the power loss will be more severe, and could additionally give rise to serious damage on the module. The cell with the lowest production will start operating in reverse bias, and swithch from producing power to consuming power. The power produced by all the other cells will dissipate in the bad cell, giving elevated temperatures (hot spot), and could lead to permanent damage on the cell, either because of the high temperature, or breakdown[14]. A high voltage production is usually wanted, but because of mismatching in series connections, some safety measures must be taken.

To avoid destruction of the cells/modules, bypass diodes can be connected in parallel with the cells, with opposite polarity. If a cell is reverse biased, the diode will become forward biased and start conducting such that damage is avoided [14]. However, having a bypass diode for each cell is not cost efficient, and the conventional strategy is to connect one bypass diode to each module [7]. If one module is shaded or for some other reason is underpreforming will the current in the string will be elevated compared to the current in the shaded module, and the bypass diode becomes activated [11]. The bypass diodes are also displayed in figure 2.5. Mismatching between the modules makes the appearance of the string having multiple maximum power points [11].

For a parallel connection, a mismatch in I_{sc} will only give lower power output for that particular cell, and only slightly lower output for the module. A mismatch in V_{oc}, will give å more severe power loss, but will normally not lead to damages to the cells [14].

The structure of the modules and arrays in connection with power converters will be considered further in section 2.4; Solar Power Integration to Grid.

2.7 Standard Testing Conditions and Environment at Fakken

2.7.1 STC and NOCT

To enable the comparison of different solar cells they are all tested under the same conditions, called standard testing conditions (STC). The power output that solar cells has under these conditions are noted as W_p, and corresponds to the rated power of the cells [14]. The standard testing conditions have the following characteristics:

- Spectrum corresponding to AM of 1.5.
- irradiance of $1000 W/m^2$ on the cell surface.
- cell temperature of $25°C$

Since these conditions are unrealistic for the environments that most solar cells operates, the nominal operating temperature conditions (NOCT) can also be used for testing the efficiency. NOCT holds the following characteristics:

- irradiance of $800 W/m^2$ on the cell surface.
- Air temperature of $25°C$
- wind velocity of 1 m/s.
- Back side of the panels are open and surrounding air can cool them.
- efficiency of zero [54]

2.7.2 Temperature

The efficiency of the solar module is highly dependent on the cell temperature [7]. It is most convenient to express the temperature dependent efficiency in terms of the ambient temperature and the irradiation. An expression satisfying this requirement is equation 2.14

$$\eta_c = \eta_{STC}\left[1 - \mu\left(T_a - T_{c,STC} + G_T\frac{T_{C,NOCT} - T_{a,NOCT}}{G_{NOCT}}(1 - \eta_{STC})\right)\right] \tag{2.14}$$

η_c is the cell efficiency
η_{STC} represents the cell efficiency under STC, which is taken to be 20% in the simulation below.
μ is the temperature coefficient, taken to be $0.0047/C°$.
T_a is the ambient temperature
$T_{c,STC}$ is the cell temperature under STC conditions ($25°C$)
G_T is the solar irradiance at the location and is taken to be constant at 700 kW and independent of the ambient temperature
$T_{C,NOCT}$ is the cell temperature at NOCT conditions. This value is depending on the module design and the materials used [7]. In the simulation below, this value is set to $48°C$, which is a typical value[7]
$T_{a,NOCT}$ represents the ambient temperature under NOCT, which is $20°C$
G_{NOCT} is the irradiation at NOCT, namely $800kW/m^2$ [29].

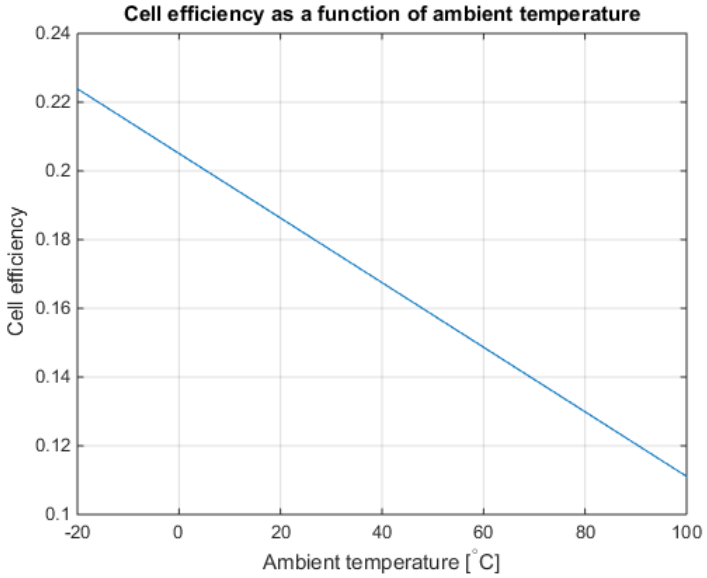

Figure 2.6: Effect of ambient temperature on cell efficiency

Figure 2.14 shows that an increase in temperature give lower efficiency. This is a major advantage for solar cell application in high latitudes such as Vannøya. The equation also predicts an efficiency higher than 20% when temperatures are below $0°C$. Equation 2.14 does not take wind speed into account, so the climatic cooling effects can be assumed to be even higher than figure 2.6 suggests for a given ambient temperature.

Gokmen et al. [35] proved in 2016 that wind can significantly help reduce the cell temperature by several degrees Celsius. The quantitative cooling effect of wind on PV panels has not yet been comprehensively investigated by

researchers compared to other factors that affects cell efficiency. However, by not considering the effects of wind in energy calculations, the power output can be underestimated by several percent's, especially during hot summer days [35].

2.7.3 Derating Factor

The derating factor is a power reduction factor that is not dependent on temperature, but accounts for the following parameters:

- DC losses such as MPPT efficiency, mismatch effects and DC wiring.
- AC losses such as transformer and AC wiring losses.
- Other losses. This can be due to shading, dust, inverter efficiencies, degradation and sun tracking efficiency.

Great uncertainty lies in calculating this factor as it depend on a high number of variables in addition of being highly site specific. It is therefore impossible to predict a certain derating factor for a PV plant on Fakken to this date, but some qualified guesses can be made. Roberts et al. reports that expected values of the derating factor lies between 0.62 and 0.92, and a typical value is 0.8 [52]. Because of high wind speed and probably low dust accumulation, will the derating factor be assumed to be high at Fakken.

The real PV power output can expressed in terms of the solar cell efficiency under STC as:

$$P_{PV} = P_{PV,STC} \cdot f_{PV} \cdot \mu \cdot \left(\frac{G_T}{G_{T,STC}} \right) \tag{2.15}$$

$P_{PV,STC}$ is the power capacity under standard test conditions
f_{PV} is the derating factor
μ is the derating factor caused by difference in temperature
G_T is the global radiation on the panel
$G_{T,STC}$ is the global radiation under standard test conditions [53].

The solar panels will also experience degradation over the years, meaning that the efficiency will gradually decrease. Jordan and Kurtz [72] tested numerous panels and systems and found a median degradation value of $0.5\%/year$ during this test.

2.8 Installation topologies for high absorption

The most important installation factors affecting the performance of a PV module are:

- Optimal angle of attack for highest possible photon absorption.
- Ensuring the lowest possible cell temperature.
- Strive to eliminate shading.

2.8.1 Stationary Monofacial Panels

The rule of thumb when installing PV panels is to make them face south with a tilted angle similar to the latitude of the specific location [35]. This setup maximizes the amount of solar energy available for the panels througout the year [7]. The panels needs a steeper angle to optimize production during winter, while lower tilt angles will maximise production at summer [7]. The motive at Fakken is to increase the production during summer. However, high wind speeds will probably make the panels more efficient with high tilt angle [35], while low tilt angles are better at absorbing diffuse radiation during overcast weather conditions [50]. High tilt angles better exploit the surrounding albedo and is therefore beneficial during periods of snow cover on the ground while simultaneously reduce snow accumulation on the panels. Homer does not take into account the effect of wind when calculating power output. On the other hand, is the aim of this study to increase production during summer, and favours lower slopes.

2.8.2 Tracking

The energy output from PV-panels can be increased by $10 - 100\%$ by using a tracking system compared to stationary panels. How much the power production will increase depends on the time period in question and the climatic and geographical conditions at site [8]. Tracking can be executed in one or two axis, and an overview of differet tracking topologies are shown in figure 2.7. In the dual-axis topology the panel can move both according to the azimuth and elevation angle of the sun. Tracking systems are also distinguished by how they track the suns orientation. Passive systems moves according to the precalculated astronomical position of the sun, while active tracking strategies have optical sensors installed, which determines how the sun orientates at the sky [50]. Off the additional energy produced by a tracking PV system compared to a system consisting of stationary panels, will $2 - 3\%$ be consumed

by enabeling the tracking [8]. The advantages of using tracking panels might be lost during cloudy weather since over 90% of the solar radiation might become diffuse, and tracking the sun might even give lower output than just having the panels oriented horizontally [50]. The problem with this position is that snow will easily accumulates on the panels. Also, if there is snow cover on the ground, the albedo effect of this might defeat the diffuse light in the sky, so that the energy yield will be better of facing the sun. Quesada et al. [50] have done a comprehensive study aiming to find the most appropriate tracking algorithm for PV panels at high latitudes with special focus on cloudy conditions. A theoretical method on isotropic sky conditions was used and the model was implemented on an experimental study on a grid connected photovoltaic system in Montreal in Canada, an area where cloudy weather often is accompanied by snowfall.

The critical hourly solar radiation , I_c is defined as the irradiation in which a horizontally oriented solar panel receives more radiation than a panel following the sun. I_c is calculated according to equation 2.16

$$I_c = K_{t_c} \cdot I_{H,0} \tag{2.16}$$

were K_{t_c} is the hourly clearness index and $I_{H,0}$ is the extraterrestrial solar radiation on a horizontal surface.

The results from the study shows that the presence of high a albedo (as in snow), the critical hourly solar radiation is significantly decreased. During cloudy summer days, and winter days with low albedo the panels are better off being oriented horizontally. If the ground serves a high albedo, the net effect of using tracking is only slightly positive $(1,5\%)$, and the losses caused by the motoric movement of the panels are not even counted for. An experiment compared the tracking strategy to a fixed south-facing 60°-tilted position and showed that the stationary panel performed 0.9% better than the panel following the sun. The effect is assumed to be even higher when snow cover is present. The study concludes with that tracking is disadvantageous on cloudy summer days, and slightly advantageous on cloudy winter days. Under clear sky conditions the tracking is advantageous. The results might be different with active trackers that detects the lightest spot independent of the solar position.

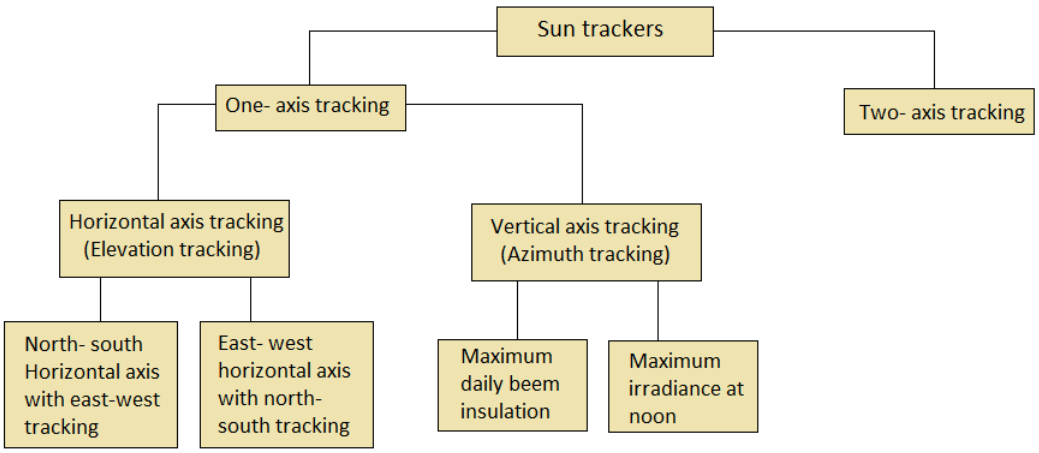

Figure 2.7: Overview if different tracking strategies simplified from [8]

2.8.3 Bifacial Panels

Some of the solar radiation that hits the earth will be reflected back to the atmosphere, and this fraction is called albedo [8]. Bifacial solar panels differs from standard solar cells by containing photovoltaic material on both panel sides, enabling bifacial photon absorption [46]. The cells will exploit the surrounding albedo radiation and other reflections and direct radiation hitting the rear side of the cell to produce more electric power [47]. The energy output can be expected to be $10 - 20\%$ higher with bifacial cells relative to standard monofacial cells [47]. The albedo in the surroundings will be essential for the effect of using bifacial panels over monofacial. By replacing the covering metal rear plate with semiconductor material, the cell becomes transparent to infra red radiation, and the cell temperature will therefore be lower than in the case of monofacial operation [46]. As explored in section 2.7.2, will this result in higher cell efficiency. Bifacial cells are expected to become more commonly applied in the future and will be an important factor for decreasing the cost of PV- technology [46] [47]. Fertig et al. recommends the use of bifacial solar cells in order to reduce the levelized cost of electricity [47].

To find the optimal angle for bifacial panels are a complicated affair [49], and will strongly depend on the surrounding topology. The high albedo effect of surfaces covered by snow is shown in figure 2.8. The high albedo for snow for short wavelengths correspond very nicely to the wavelengths absorbed by silicon solar cells (highest for short wavelengths and and dropping around 1100 nm) [7]. The use of bifacial cells can therefore be beneficial at areas covered in snow parts of the year. The albedo factor for other surfaces such as grass and sandstone are also displayed in figure 2.8. Bifacial panels can not be simulated in Homer Energy, so other methods needs to be used to get a hold of the effect.

Figure 2.8: Albedo of different materials [48]

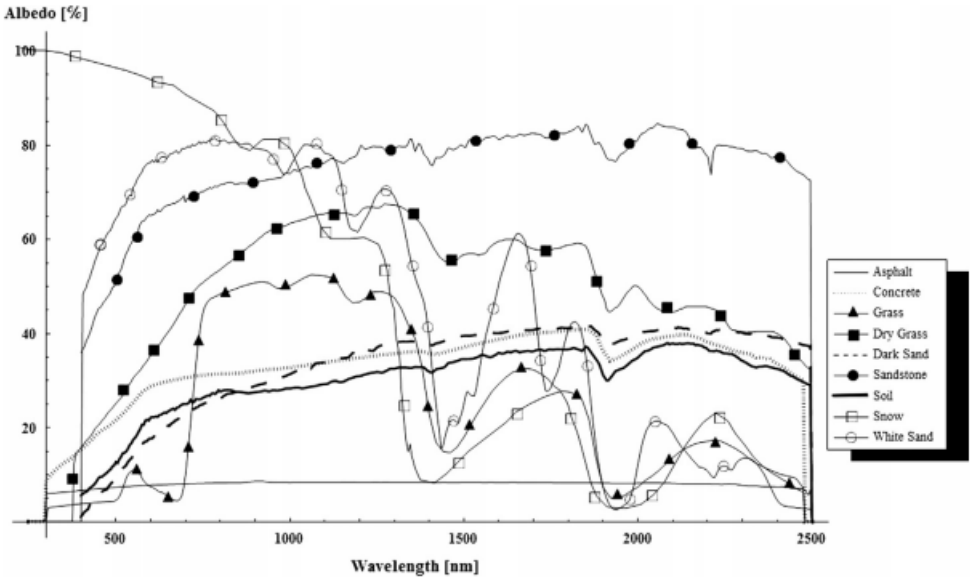

Fig. 2. The albedo spectrum for the selected materials for industrial (solar farm) PV applications.

Surface Cover	Albedo
Grass (summer)	0.25
Dry grass	0.28-0.32
Soil	0.17
Fresh snow cover	0.80-0.90
Old snow cover	0.45-0.70
Water surface ($\epsilon > 45°$)	0.05
Water surface ($45° > \epsilon > 30°$)	0.08
Water surface ($30° > \epsilon > 20°$)	0.12
Water surface ($20° > \epsilon > 10°$)	0.22
Bare rocks	0.05-0.15

Table 2.2: Albedo effect from different surface covers [70], [74]. ϵ represents the elevation angle

2.9 Solar Power Integration to Grid

The Solar power plant is supposed to collaborate with the existing wind farm in feeding the grid at Vannøya with power. The solar power fed to the grid will need to possess certain characteristics when it comes to frequency, voltage level and power quality. The process of converting the raw power produced by the PV- array into electricity for the grid takes measures in maximizing the amount of power extracted at all levels of irradiation, while using strategies for mitigating problems arising by differential shading of the modules [11].

For a traditional grid connected PV system, the conversion from raw DC-power to the refined AC power, is carried out in two main steps. The first step usually involves boosting the DC power from the PV array by using a DC-DC converter in addition to applying maximum power point tracking (MPPT) techniques to trace the most optimal operating point on the IV-curve. The next step is to transfer this power into AC power, with the right requirements for the grid, using DC-AC inverters [14]. For hybrid applications will the power fed to the grid from wind and PV be controlled by a regulator. This will be briefly discussed in section 2.10.

It is important to keep in mind that the power conversion systems will introduce conduction, swithcing and harmonic losses to the system, and so the overall efficiency for the power plant will be lower than the efficiency of the solar cells alone [5].

This thesis conciders 6 configurations used for grid connecting the PV array. [11] [60]. These are:

- **Centralized configuration:** The dominant configuration for utility scale PV systems [59]. The array consists of a parallel connected strings that are all connected to the same inverter that converts the DC power from the array into a AC power to be fed directly into the grid. Notice that the DC-DC stage is omitted which means that the module configuration itself needs to provide high enough voltage for grid integration without being boosted. Since the system do not include a DC-DC converter, the MPPT must be carried out by the DC-AC inverter. This is usually a configuration used for high power PV arrays. If the voltage is not sufficiently high, the configuration must be modified to include a DC-DC converter at the DC side of the inverter, or using a transformer on the AC side to increase the voltage [11]. A figure of this configuration is shown in figure 2.9.

- **String configuration:** Instead of having all of the power created by the array going through the same inverter, all the strings are connected to their own DC-AC inverter. The MPPT system is carried out individually for each string, which could reduce mismatch losses. The AC power from each string is collected and fed to the grid. This is in effect the same configuration as the centralized configuration, except that more converters are needed. Just like for the centralized configuration, if the voltage is too low, a DC-DC converter can be introduced on the DC-side, or a transformer can be added on the AC-side. A model of this configuration is shown in figure 2.9.

- **Multistring configuration:** Each string is connected to its own DC-DC boost converter. The MPPT is implemented in the DC-DC converters, and the tracking is therefore conducted for each string. The DC boosted power produced by each string is then collected into one single DC-AC inverter that is connected to the three-phased grid. This is a configuration of high efficiency. A figure of this configuration is shown in figure 2.9

- **AC module configuration:** Each module is being MPPT controlled by inserting DC-AC converters on each of them. By having each module indiviually MPPT-tracked, mismatch losses are reduced. This configuration is more expensive than the others, but can be the right choice if the array is exposed to partial shading [11], [56]. A model of the configuration can be seen in figure 2.9.

- **Modular Configuration** Each string has its own DC-DC converter that also conducts MPPT. The boosted DC power from all the converters are collected on a DC bus. From the DC bus, many DC-AC inverters are connected which produce the necessary power for grid connection. The configuration can be seen in figure 2.9

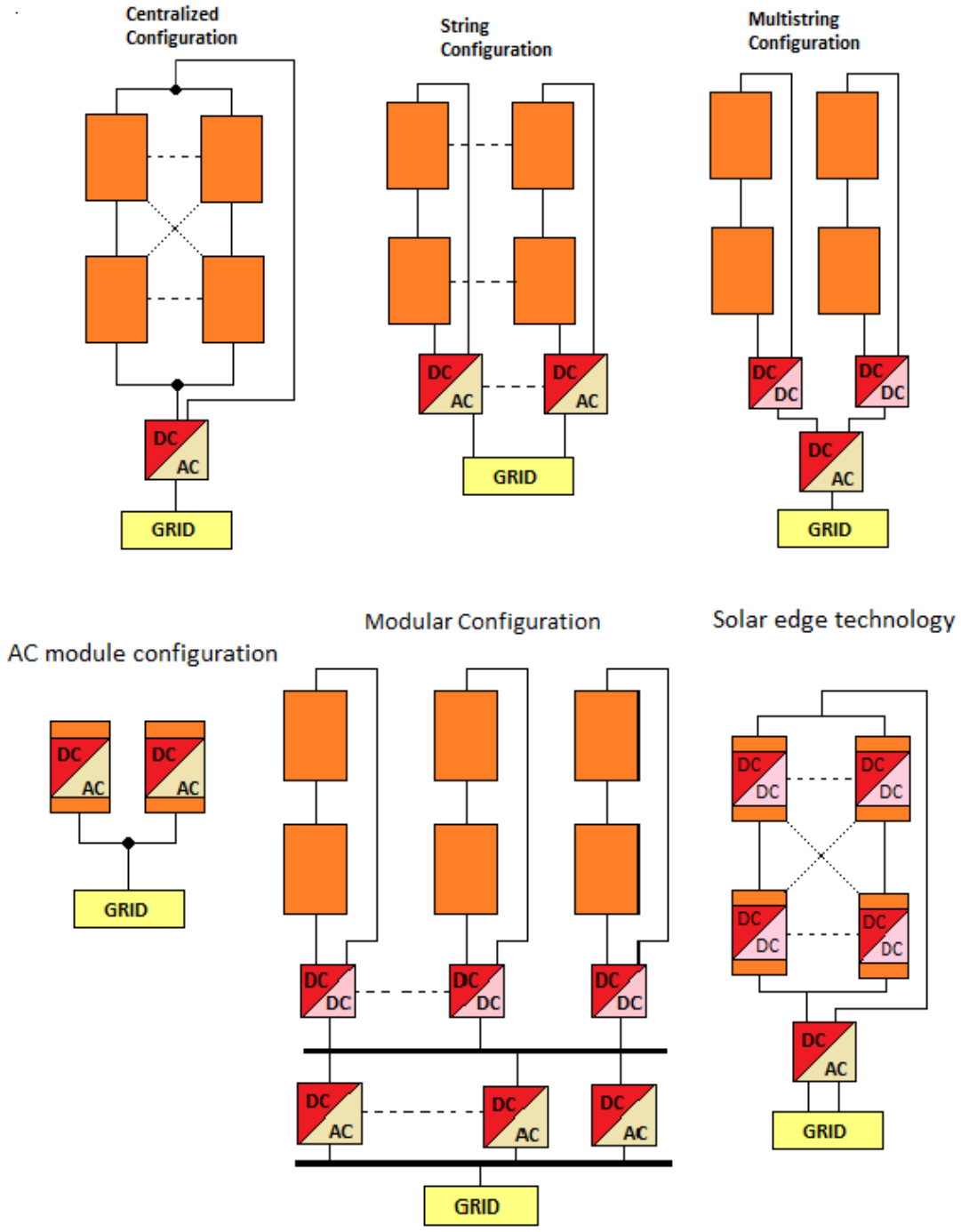

Figure 2.9: Model of centralized, string, multistring AC module, modular and solar edge configurations inspired by [11] and [60]

- **Solar edge solution** MPPT is carried out for each module individually by DC-DC converters. The DC power from the whole system is collected and inverted to AC power by an inverter. This solution yields 2% – 25% higher power output compared to traditional solutions with one inverter per string [60]. The topology is shown in figure 2.9.

The efficiency of the inverting process is determined by the configurations described above, but also on the efficiency of the actual inverters. The inverter technology is under continuously improvement. Fedkin and Dutton [79] reports a normal efficiency of 90-95 % of standard inverters, but higher efficiencies have also been demonstrated [80] and commercialized [77]. SMA have already 98 % efficient inverters available. It is also assumed that the efficiency can exceed 99 % in the future [78].

2.10 Hybrid system

As we have seen are the nature of renewable energy sources such as solar and wind intermittent. Studies show that by integrating two ore more renewable energy sources into a hybrid renewable energy system (HRES) can, to some extent overcome this issue [42], making the system more reliable [41]. A HRES can obtain higher efficiency than each of the renewable energy components could achieve alone [42]. In times when wind production is absent, the solar cells might still operate and feed the grid. It is common to add a storage unit as a part of the hybrid system in order to increase the reliability of the system. Care must be taken in finding the optimal sizes of the system components so that it strikes the balance between being cost effective and a reliable energy source along avoiding severe environmental impacts.

2.10.1 Regulator

To avoid overloading the grid, a regulator needs to control the power flow. A simple model of the inputs and outputs of a regulator is displayed in figure 2.10. This section is written in collaboration with Master student Karoline Ingebrigtsen, but the models are not identical as the systems considered for our theses are somewhat different. There are many electrical configurations available for regulating the power flow, but the description of the methods are out of scope for this thesis. It was an agreement together with Troms Kraft to rather present a simple overview of the regulators operation by a simple model.

The operating tasks of the regulator is to analyse the solar and wind resources

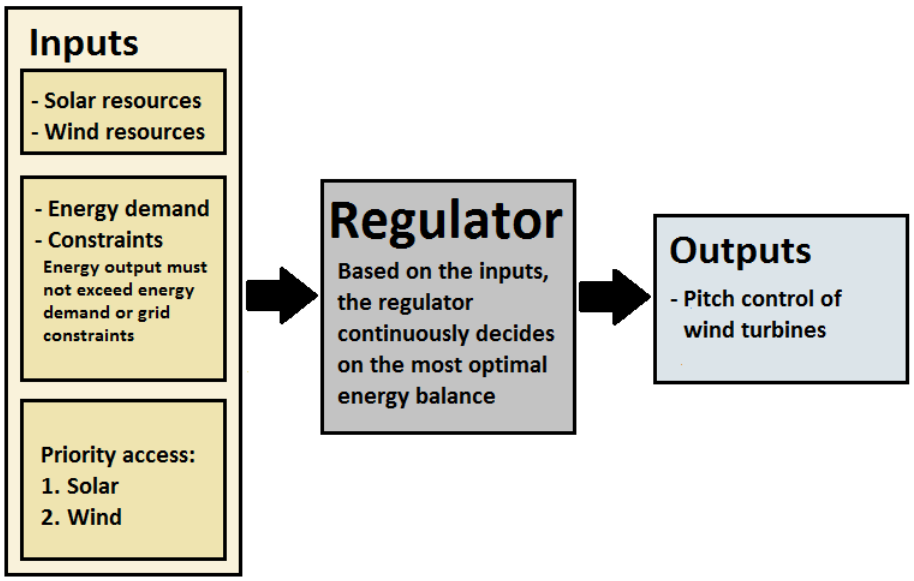

Figure 2.10: Regulator

continuously and compare them to the constraints of the electricity grid. At most times will the total power from the wind and solar production come short in producing 54 MW and the regulator will decide to fed the grid with all the power produced at site. If, however the production exceeds the capacity constraints, the production should be limited if not a storage unit is connected. The ideal case would be if the regulator could communicate directly with the turbine control system to regulate the pitch. If a storage device is added to the system, the regulator will decide, based on the grid demand and the power production, if the storage unit should add power of extract power from the system. If the power produced is higher than the grid constraints, the storage device should be charged before the turbine blades are pitched.

2.10.2 Storage Solutions

Storage is mostly applied to stand-alone microgrid systems. For large scale systems, these storage opportunities might become costly. From figures 1.3 and 1.4, it can be seen that the average consumption in Troms Kraft concession area is 15-20 times higher than the wind farm produces on average. Most of

the power supply is therefore from hydropower, which provides a simple and economical way of storing power since no additional construction is needed. Weitemeyer et al. discovered in 2015, that over 50% of the German electricity demand can be covered by a combination of wind and solar without both curtailment and storage devices. The only requirement is that the rest of the electricity demand is produced by flexible sources [43]. Hydropower might be the most flexible power source available as it has short response time and the production is easily regulated in addition of serving as a highly efficient way of storing large amounts of energy. The high amount of hydropower in Troms Kraft's concession area ensures that the energy security is kept intact even without a adding a new storage unit at Fakken, which would likely be a very costly utility.

3

Methodology and Data Sources

The first part of this chapter concerns the collection of data applied in the simulations and the correlation analysis, focusing on the solar resource data collection. This comprises short descriptions of the pyranometer and the WRF model. The next section concerns the cost of the system components. A section to how *HOMER* operates is also included. The last part of this chapter covers the simulation strategy and a description of how the financial feasibility of the scenarios are evaluated.

3.1 Solar, wind and temperature resources at Fakken

Solar radiation is a very site specific quantity, and it was decided to measure the radiation at Fakken directly by installing a SP- 230 all season pyranometer from Apogee Instruments. The installation date was 24.01.2017, just in time to record the first traces of sunlight at Fakken after the polar night. *HOMER* needs a whole year of global solar radiation data in order to conduct a simulation. To solve this, the WRF model is used for simulating the solar radiation at Fakken for 2016. The simulation is also conducted for Holt, where an existing

pyranometer has measured the global solar radiation continuously for many years. All solar radiation data from Holt used in this thesis is retrieved from *Landbruksmetrologisk tjeneste* [82]. The WRF simulation data for Holt is compared to the actual measured values at the same location. The validity of the WRF simulation at Fakken is evaluated based on this comparison. The mean global solar radiation on a horizontal surface at Holt during 2007-2015 was $6.58 W/m^2$ while it was $6.56 W/m^2$ for 2016. 2016 was therefore a year with quite normal radiation levels, and is thus an appropriate choice for evaluating the the solar resources at Holt.

The WRF simulation could potentially be simulated for 2017 so that a direct comparison of the irradiance at Fakken could be conducted between the simulated and observed data. But since only a few months of observed data would be available, was 2016 chosen so that a whole year observed data could be applied in the evaluation of the model. The downside to this method lies in the uncertainty of how similarly the model will simulate the radiation at Holt and at Fakken. The climatic conditions at the two locations can fortunately be assumed to be similar to each other, which increases the reliability in this comparison analysis.

The existing wind farm is simulated in a hybrid system together with a PV installation. The wind speed data is received from Troms Kraft, measured using a Vaisala anemometer WAA 151. The wind speed time series for 2016 is imported to *HOMER* based on the recordings of this anemometer. Temperature data provided by Troms Kraft for each hour of 2016 are also imported to *HOMER*. The hourly temperature data is plotted in figure 3.1. The temperature sensor is placed on a turbine's nacelle. The measurements might be affected of the heat from the nacelle especially on less windy days. The average temperature at Fakken for 2016 was $5.78°C$

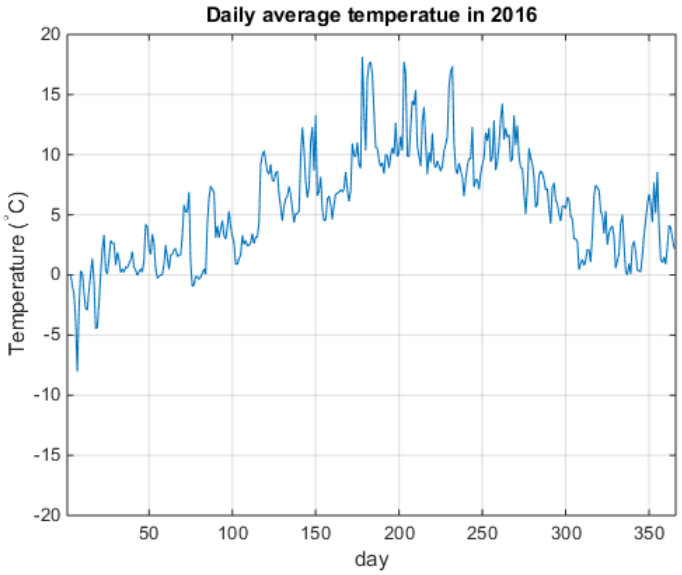

Figure 3.1: Ambient temperature measured at Fakken during 2016

3.1.1 Sp-230 All season pyranometer from Apogee

The SP- 230 All- season Pyranometer uses a silicon sensor for measuring the global solar radiaton on a horizontal surface. When the silicon is exposed to sunlight, the photovoltaic effect provides an electrical signal corresponding to the amount of radiation absorbed by the material [28]. Silicon based pyranometers are therefore reliable for PV applications since they will have similar response pattern to solar cells [28].

Since the radiation recieved will depend on the relative position of the earth, the pyranometer conducts a calibration in which it corrects for the difference in incident angle. This is carried out for the elevation angle (cosine correction), and for the azimuth angle [28]. The Sp- 230 All- Season Pyranometer has an accuracy of ±5%, when the zenith angle is 75° and an accuracy of ±1% when the zenith angle is 45° [25].

The pyranometer is installed on a pre existing station at Fakken, in a mount. The signals from the solar sensor will be transmitted using a data logger. The pyranometer will take measurements every 10th second, and the data logger will transmit the average of these measurements once for each ten-minute interval. A big mast will be shadowing the pyranometer when the sun is positioned northwards, but since this is during the night times, it should not affect the measurements too much. A picture of the pyranometer can be seen in

figure 3.2. PV- panels installed with optimized angles will absorb more radiation than horizontal panels as described in section 2.8.

Figure 3.2: Sensor attached to the mount

Plotted in figures 3.3, 3.4 and 3.5 are the solar radiation at Fakken for February, March and April 2017 recorded with the Apogee pyranometer on an hourly time scale.

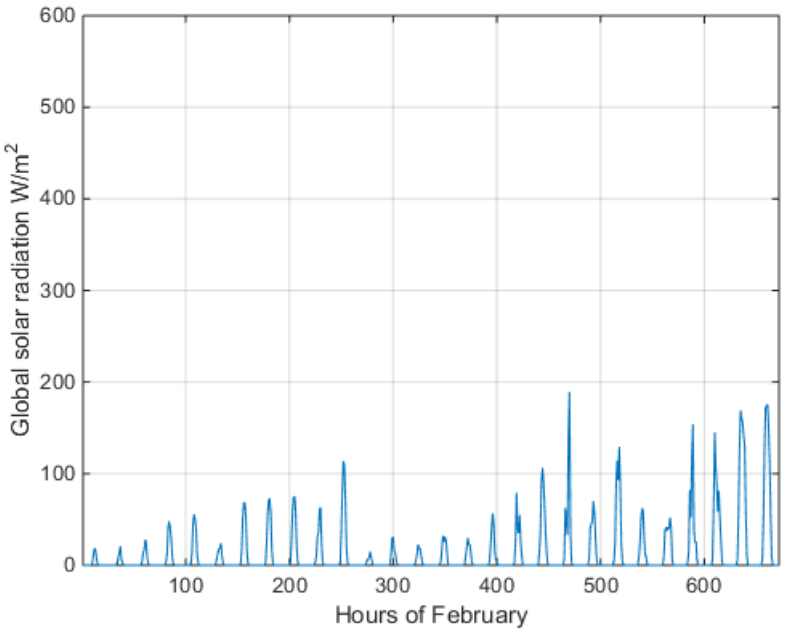

Figure 3.3: Observed global radiation at Fakken during February

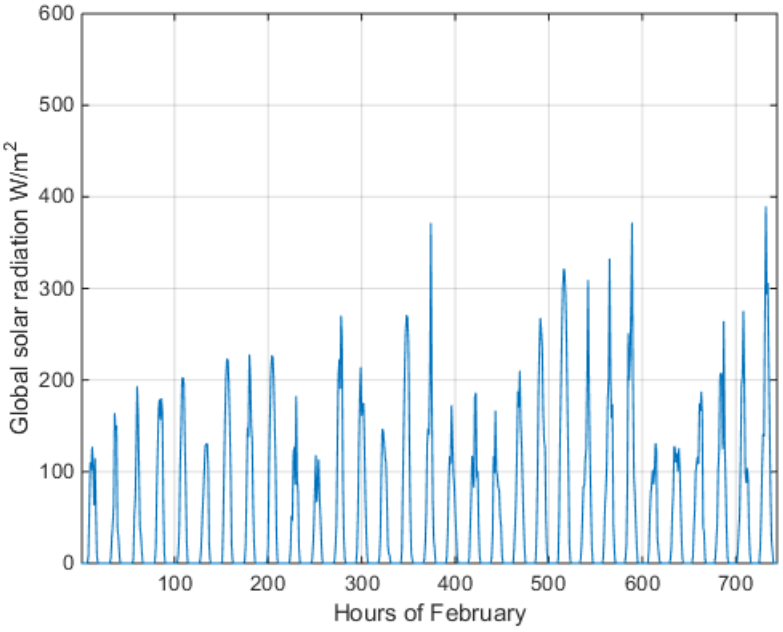

Figure 3.4: Observed global radiation at Fakken during March

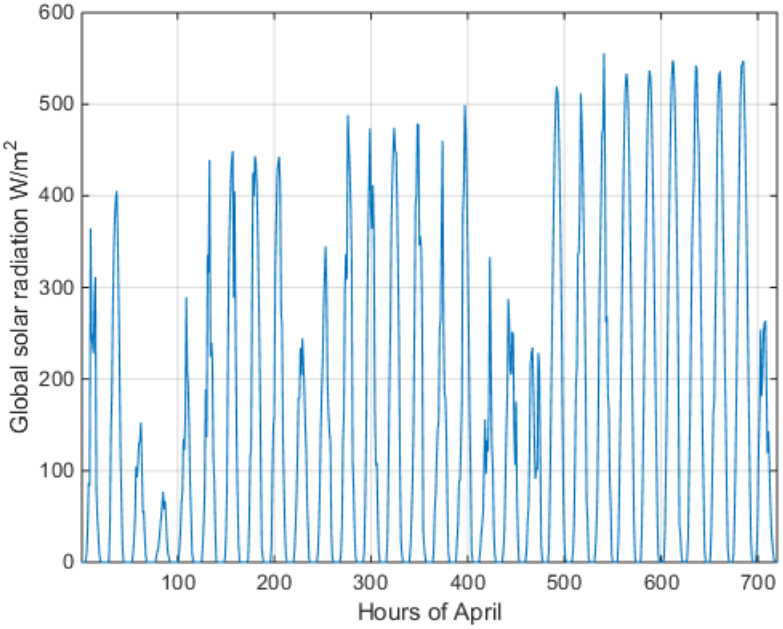

Figure 3.5: Observed global radiation at Fakken during April

3.1.2 The WRF model

The solar radiation input to Homer will be simulated in with The Weather Research and Forecasting (WRF) program , version WRF3.7.1. This is a tool for numerically simulating and predicting mesoscale weather conditions. Contributors to the WRF-model are National Center of Atmospheric Research's (NCAR), Mesoscale and Microscale Meteorology Division (MMM), National Centers of Oceanic and Atmospheric Administrations (NOAA), National Centers for Environmental Prediction (NCEP) and others [65]. As the program requires over 25 TB in memory space and contains over 150 variables, the simulation is carried out by the supercomputer *Stallo* at UiT- the Arctic University of Norway [12].

The WRF simulation is conducted in two phases, namely the WPS step (WRF prepocessing system) and the ARW (Advanced Research WRF) dynamical solver step [65]. In the preprocessing phase, the model uses terrestrial and meteorological data input to decide on boundary and initial conditions for the WRF simulation. This phase utilizes three programs, namely *geogrid*, *ungrib* and *metgrid*. These programs uses paramenters defined in the *namelist.wps*-file, and the results from the *ungrib* and *geogrid* are fed into *metgrid*, so that the meteorological data preocessed in the unigrib is horizontally connected to the geographical data [65].

The simulation domains are implemented in the *namelist.wps* file. First, the user defines a coarse domain, called the parent domain. A finer resolution domain can be defined inside the parent domain and this is called a child domain. A new child domain can also be defined inside the first child domain, or the child domain can have sliblings. This process is called *nesting*, and can be repeated multiple times until the desired resulution is obtained [12] [65]. The nesting options are illustrated in figure 3.6 When a child domain is defined, the simulation results from the parent domain serves as boundary and initial conditions [65].

The meteorological input data implemented to the unigrib are GRIB-files, in which time dependent data is presented in a binary form and are standardized by the World Meteorological Organization [12]. These files are usually based on historically observed weather conditions. The geographical input file defines and creates the static landscape profile in the spatial domain defined in the namelist file. The output from the *metgrid* is a three dimensional field (the horizontal directions and the time dimension) [65] containing temperature, humidity and the horizontal components of momentum.

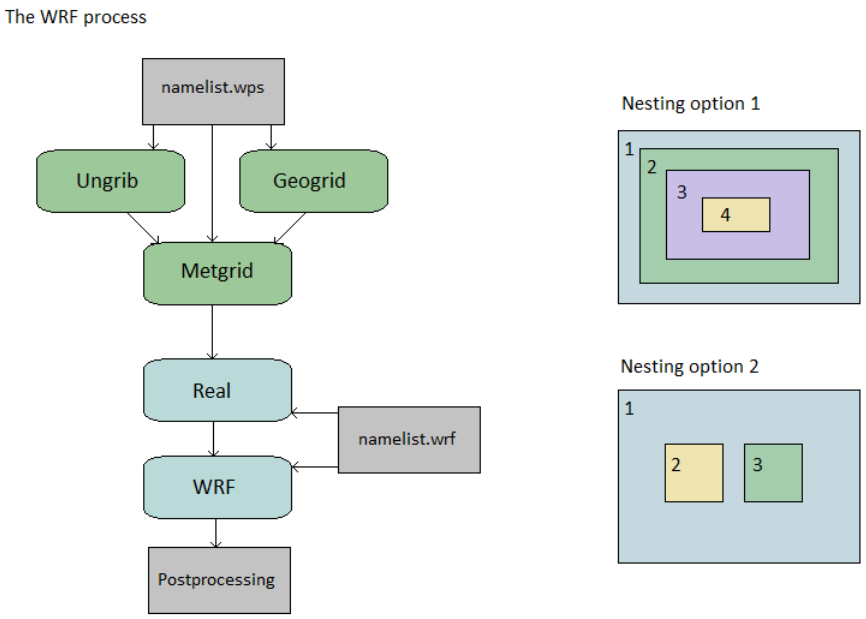

Figure 3.6: Model of the WRF process inspired by [12] and [65] and the two nesting options available

When the *metgrid* program has finished processing is it time for the ARW phase. This phase consists of two main steps, namely the *Real* program, and the *WRF*. A *namelist.wrf* - file needs to be implemented to the program. This file contains a detailed list of physical parameters and options [12]. Some of these options are microphysics schemes, cumulus parametrization, radiation scheme and others [12]. Both the *namelist.wps* and the *namelist.wrf* files are included in the apendix. *Real* starts by taking the horizontally interpolated 3 dimensional fields from the *metgrid* and interpolates it into a 4 dimensional meteorological field in the specified domain [12]. The dimensions consists of the three spatial dimensions in addition to the time dimension. When *real* has finished its job, the program is ready to conduct the actual WRF-simulation.

The validity of the simulation will be decided upon by comparing the simulated global radiation at Holt with the measured values at the same location. The comparison will be done by calculating the bias, the root mean square error (RMS error) and Pearson's correlation coefficient for the WRF-simulated data set at Holt and the observed values at the same location for 2016. These calculations are conducted on 60 minute, 24 hour, weekly and monthly intervals

over the whole year, and on a 60 minutes and 24 hours interval over each month of the year. When calculating the weekly correlation, bias and RMSE are the two last days of 2016 are omitted to obtain exactly 52 weeks. This is assumed to have almost no effect on the results as these are days with almost no radiation at all. The first week starts at January 1st regardless of the weekday. The comparison will also contain an analysis of the total sum of the radiation on an annual basis for the simulated radiation at Fakken and the simulated and measured radiation at Holt. The same will be done for the three months when there are measured radiation at Holt available. This analysis will help in determining how much the *WRF* model overestimates or underestimates the radiation. Based on this, will it be determined if the radiation should be scaled up or down to better fit the assumed weather conditions at Fakken.

A description of Pearson's correlation coefficient, bias and root mean square error follows. Based on the results from the comparison of the observed and simulated data will it be decided if the radiation needs to be scaled up or down to obtain more reliable radiation levels. This is assumed appropriate since the climatic conditions at Fakken and Holt is quite similar. The *HOMER* simulations will be highly dependent on the results from this analysis.

Pearson's correlation coefficient

This is a simple method for detecting the linear dependence between two data sets, and is widely applied [40]. The general equation is displayed in figure 3.1.

$$r = \frac{\sum_{i=1}^{n}(x_i - \overline{x})(y_i - \overline{y})}{\sqrt{\sum_{i=1}^{n}(x_i - \overline{x})^2}\sqrt{\sum_{i=1}^{n}(y_i - \overline{y})^2}} \tag{3.1}$$

$\overline{x}$ and $\overline{y}$ are the sample means of the variables x and y respectively, and n is the sample size [45]. The correlation coefficient will always be a value between -1 and 1. A correlation coefficient close to 1 indicates that the data samples correlate well, a value of 0 indicates that the data sets has no correlation at all, and coefficient close to -1 shows that the data samples has completely opposite natures, such that when one data sample is high the other sample will be low.

When calculating the correlation between the simulated and observed global solar radiation will $x_i = x_{i,wrf}$ represent the simulated radiation at time step i, and $y_i = x_{i,obs}$ represents the observed radiation at time step i. The most desirable output will be a correlation coefficient of 1 since that would indicate that the simulated data perfectly imitates the radiation at Holt during 2016

perfectly. This will result in a high reliability in the simulated data for Fakken, which are used as input in *HOMER*.

Bias

Bias is defined as the mean difference between the observed value and the estimated value for each time step recorded. If the sample size is equal to n, and $x_{i,wrf}$ and $x_{i,obs}$ is the simulated and measured value of the global solar radiation at time step i, respectively, then the bias is calculated according to equation 3.2 [73].

$$bias = \frac{1}{n}\sum_{i=1}^{n}(x_{i,obs} - x_{i,wrf}) \tag{3.2}$$

A low bias would indicate that the simulated and observed data are similar. A positive value indicates that the observed radiation is normally higher than the simulated radiation, while a negative bias indicates the opposite.

Root mean square error

The root mean square error (RMSE) is calculated like equation 3.3 [73].

$$RMSE = \left(\frac{1}{n}\sum_{i=1}^{n}(x_{i,obs} - x_{i,wrf})^2\right)^{\frac{1}{2}} \tag{3.3}$$

A low RMSE indicates that the observed and simulated datasets are similar, and is therefore desirable.

3.2 Correlation Analysis of Wind and Solar Resources

The capacity of the electric power lines from Fakken would be utilized most efficiently if the amount of wind resources always completely complemented the amount of solar energy available for a PV-plant to harvest. This is important since both wind and solar are energy sources that are hard to predict. Perfect anti-correlation will obviously be far from reality in most cases, and a regulator

must be connected to control the power flow.

A comprehensive correlation analysis is conducted to decide how the solar radiation at Fakken complements the wind resources on a monthly, daily, hourly and a ten-minutes interval. As intermittent renewables such as wind and solar keeps increasing its shear of the global energy mix, several similar studies has already been done. Monforti et al. [39] refers to several studies that have conducted the same experiment with the conclusion that there is negative correlation between solar radiation and wind speed, especially at longer time scales. However, as Solbakken et al. [40] claims, such studies must be conducted site specifically. Solbakken et al carried out such a study for Tromsø and found negative correlation factor for hourly, daily and monthly time scales, with the monthly time scale correlation being the highest in absolute value (-0.54). The polar nights were omitted in this study, but it is reasonable to believe that including the polar nights could have increased the negative correlation between wind and solar on a monthly basis, simply because wind power is peaking at winter months and direct solar radiation is absent.

The correlation between wind and solar resources at Fakken will be determined by calculating Pearson's correlation coefficient as defined in equation 3.1. The x- values will represent the wind power available per square meter, and y represents the solar power available per square meter. For this case will a correlation coefficient of -1 be the most desirable since it indicates anti correlation [45].

The data for solar radiation is given in W/m^2. The raw wind speed data are therefore converted to the same unit by using that the power in the wind is given by equation 3.4. The wind speed sensor is placed in a mast at 80 m height, same as the hub height of the turbines.

$$P = 0,5\rho AV^3 \tag{3.4}$$

[9]

Wind power per unit area, P_w, is given by equation 3.5.

$$P_w = 0,5\rho V^3 \tag{3.5}$$

For the correlation analysis is the air density is assumed to be $1,246kg/m^3$, corresponding to a temperature of $10°C$ [40]. This choice of density will not affect the resulting correlation factors since the calculation is designed to ignore the absolute sizes of the datasets, but only considers how they relate to

each other relative to their average value.

The correlation coefficient will be calculated with wind speed data and solar radiation data observed at Fakken for February, March and April 2017. This analysis contains correlation at 10 minute, 60 minutes, and daily intervals for each month. Since observed radiation data is only available for a limited number of months, will a correlation analysis also be conducted for 2016 using observed wind data and simulated solar radiation data. In this analysis will the correlation coefficient be calculated on a 10 minute 60 minute, 24 hour and 7 days interval for the whole year, and for each month separately. The reliability of this analysis for the simulated solar data will be highest for the high time scales since the *WRF* has a limited resolution and thus low viability on small time scales.

3.3 Cost of PV systems

This section concerns the argumentation and estimation process concerning the estimation of the cost of a PV system.

The capital cost is the initial purchase price of a PV installation and consists of PV- panel costs and system costs. PV-panel costs are those associated with material, manufacturing and module assembly costs. System costs are the structural system costs, electrical systems costs and software system costs. There will also be operation and maintenance costs associated with the plant during its lifetime [55].

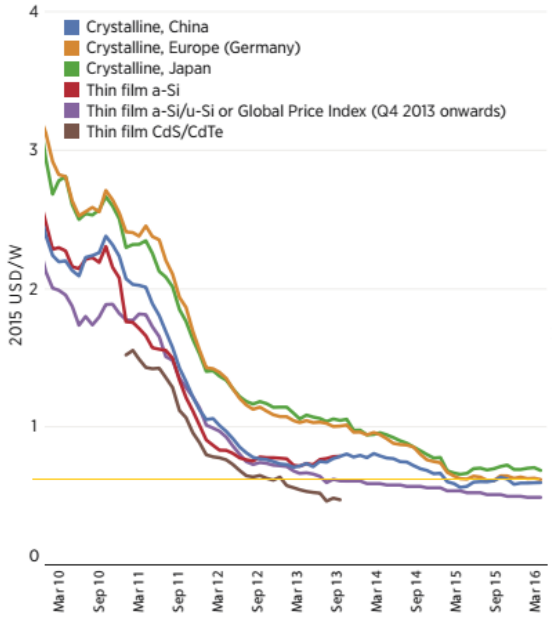

Figure 3.7: Module cost developmet from March 2010 to March 2016 [59]

IRENA [55] reported in 2015 that the cost reduction in PV was so strong that decision makers and the public had a hard time keeping track of the development. The general PV module cost in 2014 was only one quarter of the module cost in 2009. The cost reduction in panels will gradually slow down, and further price reduction should be due to development of the BoS. The report emphasizes that using cost analysis from even 6 months back can potentially overestimate the real cost of PV modules. The high learning rate (18 – 20%) is due to the increased efficiency, more competitive markets and optimization processes [55]. The strong module cost reductions during the recent years are illustrated in figure 3.7. The cost is, however highly technology and site dependent. For instance is the capital cost of a PV system in Norway up to 40% higher than the same installation in Germany [57]. This has nothing to do with the choice of technology, but is rather a result of low solar installation volumes in Norway which increases transportation and installation costs [57]. It is likely that the costs of installation in Norway will decrease when the installation volumes grows. The cumulated grid connected installed capacity of PV in Norway is modest to say the least, but had an enormous growth during 2016 compared to earlier years as can be seen in figure 3.8.

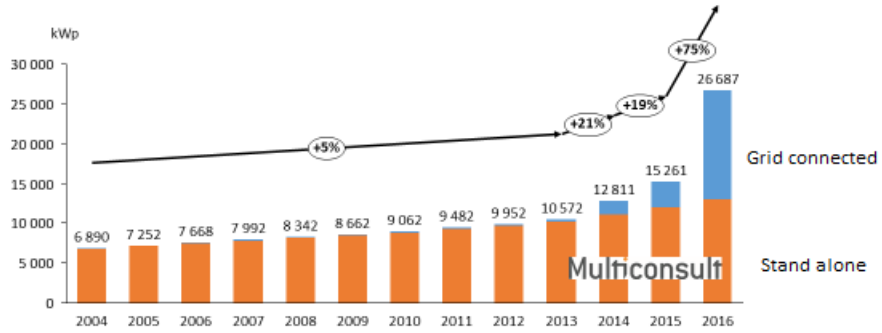

Figure 3.8: Accumulated installed effect of PV in Norway in recent years merely modified from [62]

Finding some reports on cost estimates for large scale PV systems in Norway has proven to be very difficult. In lack of better alternatives is this cost analysis partly based on cost values for PV systems in the range of 10-100kW fetched from [61] as represented in figure 3.9. The installed effect for the system considered in this thesis will be 20 MW (This will be explaied in section 3.5), in other words 200 to 20000 times bigger than the systems described in figure 3.9, and thus the price per kW installed effect will probably be greatly reduced compared to the prices suggested in this figure. It is seen that a system size in the range of 10-100 kW installed effect has a capital cost of 14,000 NOK/kW including an inverter cost around 1,200 NOK/kW. *Solbes* evaluates a cost between 5,000 NOK/kW and 10,000 as appropriate to assume for a PV system of 20 MW. Based on these two sources is a capital cost estimate of approximately 7,500 NOK/kW for the PV system considered approprate. If the same cost reduction due to large systems size can be expected for the inverter, will its cost be reduced to approximately 700 NOK/kW. The annual operation and maintenance cost is assumed by the rule of thumb to be around 2% of the total capital cost for systems sizes between $10 - 100kW$ including the maintenance cost of the

inverter [61]. If the PV capital cost is 7,500 NOK/kW will the annual O&M cost for the PV become 150 NOK/kW and the annual O&M cost for the inverter become 14 NOK/kW.

Due to the uncertainty in the cost estimates is it necessary to examine the systems profitability also under alternative cost regimes. Scenarios with a PV capital cost of 10,000 and 5,000 NOK/kW will be considered, corresponding to an increase and decrease in capital costs of around 30 %. This will also involve changes in operation and maintenance costs accordingly. By allowing the inverter cost to change by the same percentage as the PV capital cost changes, will inverter costs of 933 and 467 NOK/kW be evaluated. Installation and mounting costs are included in these numbers. The warranty of a PV module is usually around 25 years, while the inverter lifetime is around 15 years. Even though the the warranty of the PV modules expires after approximately 25 years is it likely that the system can operate for several years after this time. The replacement cost of the inverter is assumed to be equal to its capital cost, but will be discounted by *HOMER*.

By following the cost assumptions above will the total nominal O&M costs of the system correspond to 1/3 of the project costs while the capital cost is the rest 2/3. The argumentation is shown by the equations below.

If the capital cost per kW is C, the annual operation and maintenance cost per kW, Y, is 2% of C, and the lifetime is 25 years, the annual maintenance cost per kW will be

$$Y = 0.02 \cdot C$$

The total maintenance cost Y_{tot} will be

$$Y_{tot} = 25 \cdot Y = 25 \cdot 0.02 \cdot X = 0.5 \cdot C$$

Hence, the total O&M cost over the lifetime of the project corresponds to one third of the lifetime costs, L. The capital is the rest of the lifetime cost per kW :

$$C = L - Y_{tot} \quad \rightarrow C + 0.5C = L \rightarrow L = 1,5C$$

The total investment cost in Norway is assumed to be reduced by about 30−40% by the year of 2030[61]. These factors might cause PV installations to be more favourable in the future.

3.3.1 Electricity prices

One of the major obstacles for PV installations on mainland Norway, together with high installation costs and modest solar radiation, are the low electricity

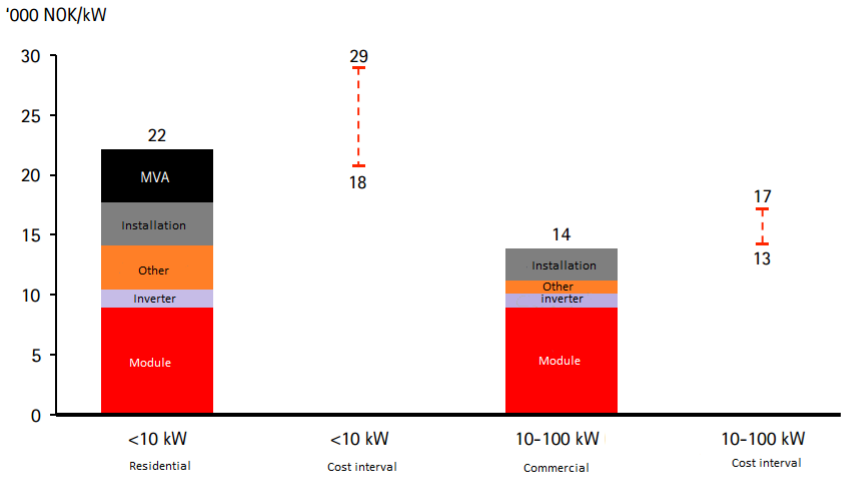

Figure 3.9: System costs for PV installations in Norway. Slightly modified from [61]

prices. For comparison are the electricity prices in Denmark approximately twice as high as in Norway [84] For instance has solar power been proved to be cost efficient at Svalbard were electricity prices are higher than for the rest of Norway, although the yearly solar radiation is modest.

3.4 ArcGis' Area solar radiation

A geoprocessing tool in *ArcGis* is applied to give an indication of the optimal locations for panel installation at Fakken. The geoprocessing tool is called *Area solar radiation*. It takes as input a digital elevation model (DEM) for the area in question, and produces a floating raster image of the area. The raster image represents the solar radiation at each point in Wh/m^2. The energy received by surface areas is calculated by multiplying the user defined transmittance by extraterrestrial solar radiation. The transmittance is defined as the average transmittance for the solar radiation wavelength spectrum. A transmittance of 0.5 is chosen to imitate a generally clear sky. The user defines the dates that the program should simulate for. Multiple days can be simulated at once, but the operation is very time consuming. To limit the calculation time, only three days will be modelled for each operation. The chosen days are the 14th-16th of May, June, July, August, September and October. The latitude of the concerning area needs to be implemented, and from this can the *ArcGis* tool calculate parameters such as the declination angle and the solar position. The user can define how many directions the horizon angles should be calculated

from. Calculations from 32 directions are used for these images, which is recommended for areas with complex topography [75]. This analysis is only meant as a guide for the citing of the solar panels, and no quantitative measures will be considered. The images will show that certain areas are more exposed to sunlight than others.

3.5 Homer Energy

The large number of options that needs to be evaluated in a process of installing a hybrid renewable energy system is overwhelming and the use of *HOMER* will simplify this process by presenting the technologically and economically optimized option and carry out complicated calculations that otherwise would be nearly impossible for the scope of this thesis [54]. *HOMER* is short for 'Hybrid Optimization Model for Multiple Energy Resources'. The program is developed by the National Renewable Energy Laboratory (NREL) [69].

The user defines the technological options relevant for a hybrid system and implements them into a scheme. Load and grid sale prices also needs to be defined. For each hour of a year will *HOMER* conduct an energy balance calculation (Comparing the energy demand to the energy supply from the system in that hour). The energy flow through each of the components are identified by the program. The system feasibility and the cost of installation and operation are calculated for all possible configurations.

Sensitivity analysis can be carried out to examine how the system will respond to changes in factors that affect the power production or the cost effectiveness of the system. The sensitivity analysis in this thesis will be conducted manually by letting *HOMER* calculate outputs at different specified scenarios were the system's sensitivity to different variables are evaluated one by one.

Based on the geographical location, azimuth and slope angles of the panels, the albedo, the time zone and the horizontal global radiation time series data, will *HOMER* conduct comprehensive calculations to find the radiation on the specified angle and tilt of the solar panels. *HOMER* transforms the solar radiation data measured in civil time to solar time using the equation of time. By calculating the horizontal extraterrestrial radiation and comparing it to the measured horizontal global radiation at the surface, *Homer* are able to calculate the clearness index and hence to distinguish the direct radiation from the diffuse radiation. The *HOMER* calculations also take diffuse radiation being stronger in the horizon (horizon brighting) and the additional diffuse radiation in the direction of the sun (circumsolar radiation) into consideration. The global radiation on the tilted panel is eventually calculated based on

this together with adding the effect of the albedo [54]. A presentation of the calculation techniques for calculating the radiation on the PV array and the solar cell temperature based on the *Homer help manual* ([54]) is added to the appendix.

The wind power output is calculated based on the imported wind speed time series obsered at Fakken for 2016 on a ten minute interval, and the reported hub height of the anemometer in addition to the power curve recieved by Troms Kraft. Based on this, *Homer* can calculate the wind speed on the hub height of the turbines. Since the anemometer is located at the same height as the hub heigh of the turbines will the power production be calculated without having to correct for height differences. The power output of the turbines will be based on the wind speed and the power curve under standard conditions and pressure [54]. Troms Kraft reports an overall loss factor of 0.8 % for the turbines at Fakken although it might be a somewhat higher. The power curve received from Troms Kraft does is not specified for the average air density at Fakken. *HOMER* does provide the possibility of using temperature data and correct the standardised power curve for temperature effects. When this alternative was chosen was it discovered that the production actually exceeded the rated power of the turbines occasionally, which is not the case in reality. It was therefore considered to be safer to ignore temperature effects. The average density at Fakken is $1.240 kg/m^3$ while the standard density applied in the power curve is $1.225 kg/m^3$. If it was known to me before the simulations were conducted that Troms Kraft possessed power curves specified for the average air density at Fakken, I would have requested it. I assumed that they only used the standard curve since this was the received when the power curve was inquired.

The nominal power capacity of the PV can be implemented in the search space. The capacity size of the system can also be decided by letting Homer find the optimal amount inside a user defined range. This approach can not be applied if the the Multi- Year module is applied, as it will be in the work of this thesis in order to count for varying electricity prices.

Both the PV system, the inverter and Wind turbine systems contains cost boxes.

The cost boxes contains:

- **Capital cost per kW:** The initial purchase price. For the PV system will this need to include the price of the PV-panels, mounting hardware, wiring and installation costs.

- **Replacement cost per kW:** The cost of replacing the equipment after its lifetime has passed.

- **Operation and maintenance per kW:** The annual cost of operating and maintaining the equipment per kW.

HOMER assumes that the cost varies linearly with size. This is chosen because a nearly fixed system size is applied in nearly all simulations. All costs for the wind power system are set to zero since the wind facility is pre existing. For the PV system and the inverter, the boxes will be implemented according to section 3.3.

Ground reflectance, panel slope and azimuth angle can be specified as well as different types of tracking strategies. An azimuth angle of 0° corresponds to the panels facing south and an angle of 90° corresponds to west facing panels. A slope angle of 0° models horizontal panels, while a 90° slope simulates vertical panels. The efficiency of the PV cells under STC, the cell temperature under NOCT, the derating factor and the temperature coefficient all needs to be added in the design of the system, if not a default PV module type is chosen. Parameters for the inverter will also be necessary to specify.

Generic turbines and modules can be modelled with user defined parameters. Some of the default settings will be contained while other will be modified.

Grid and load model

Homer is a program mainly developed for using in microgrid applications. To simulate a grid with varying electricity prices can the advanced grid module be applied in the simulation. The electricity prices can be real time or scheduled. For this thesis, real time grid prices will be used. A historical hourly electricity price- time series for 2016 downloaded from *Nord pool* [64] is imported to *Homer*. The sale capacity will be defined as the grid capacity constraint of 54 MW. The load is defined as the average power consumption of all of the wind turbines combined, namely 48.47 kW/h like calculated in section 1.2. This value is chosen because no time series is available for the load during 2016 and this value is assumed to be reliable since it is the average over several years. Since this load is highly variable, a 100% variability is chosen for the load. The average load is still 48.47 kW/h.

In the multi year module, future electricity prices for the next 25 years are implemented as a multiplier of the electricity price in year 1. 2016 is set to be year 1 since this is the only year with a complete resource dataset. This unable *HOMER* to perform optimization processes.

The hybrid system as modelled in Homer is presented in figure 3.10.

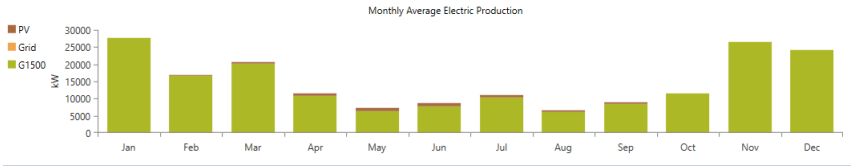

Figure 3.11: Hybrid system with 5 MW installed PV capacity

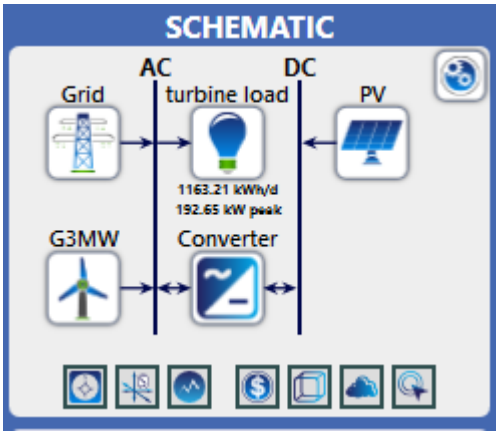

Figure 3.10: Model of the hybrid system in *Homer*

The first strategy formed was to let *HOMER* decide the appropriate sizing of the PV system. Not only was this impossible when the *multi year* module was enabled, but *HOMER* always decided that the smallest system size is the most economically feasible when trial simulations without the multi year module. The lesson learned from this was simply that the system is likely to result in negative NPV. The strategy was modified to have a fixed size, and rather evaluate and compare the outcomes from different scenarios when employing a fixed capacity of 20 MW. This size was chosen based on the objective of increasing production during times when the wind farm comes short in covering the grid capacity. Several smaller sizes were tested, but the PV power contribution appeared almost insignificant, and was considered to not respond well to the motive behind this thesis. An example of the monthly production for the hybrid system if a PV capacity of 5 MW is added is viewed in figure 3.11.

In order to have MPPT on the module the PV production will be connected to a DC-bus. A DC-AC inverter will serve as a bridge between the DC bus and the AC bus connected to the wind turbines, the load and the grid. As already discussed is the limit on the AC grid set to 54 MW. The inverter is at all times obliged to adjust to the further restriction on the AC bus due to the wind power

production that fills the line to a certain degree depending on the time step in question. The converter size is defined as the maximum output power the inverter can pass to the grid. It also holds a certain efficiency, which in most cases is assumed to be 95 %. This number is based on Fedkin and Dutton [79], although higher efficiencies have been demonstrated [80].

By trying different converter sizes, *Homer* finds a converter capacity of 13,000 kW as the optimal size when the PV capacity is set to 20 MW. This will restrict the PV power output and cause losses although it leads to lower capital cost. Solbes informs that the standard strategy is to use inverter capacities that are able to absorb 100 % of the power produced by the panels based on the fact that the cost of inverters are a smaller part of the system costs. If the panels never produced more than their rated power would an inverter capacity of 19 MW be adequate for all scenarios. The power output can occasionally be even higher than 20 MW if the incident radiation is high and the temperature is very low. Applying tracking strategies will increase the system's risk of producing more than the rated power. For other scenarios will the output never even approach 20 MW (due to low efficiency/ radiation and so on), and having an inverter of 19 mW will be a waste and reduce the cost efficiency of the system. The strategy for this thesis eventually became to use trial simulations for all scenarios, and based on the maximum power production from the PV array in year one, will the inverter be scaled to be able to absorb this power. The size is scaled up to be the nearest integer value in MW. This will to a some degree count for the fact that radiation varies over the lifetime of the project depending on how close the maximum output is to the nearest integer inverter capacity. *HOMER* assumes that the radiation is constant over the lifetime of the project and if the inverter is able to absorb the maximum amount during year one, will it be able to do the same for the rest of the lifetime due to degradation of the panels. It can not be guaranteed that this will be the case in reality since radiation levels varies from year to year. By customizing the inverter capacity to the scenarios will all the power produced get entrance to the grid while still not wasting resources on capacities that are not fully exploited. There might still be restrictions on the AC bus caused by wind power production filling the line as already discussed.

3.6 Economic feasibility of PV installations

To evaluate the financial viability of the project, will the net present value (NPV) and the leveliced cost of energy (LCOE) be evaluated. NPV is defined as

[51]:

$$NPV = \sum_{t=1}^{N} \frac{R_t - C_t}{(1+i)^t} - I_0 \tag{3.6}$$

R_t and C_t are the revenue and cost in year number t respectively, i is the discount rate and I_0 represent the initial investment equivalent to the capital cost. *HOMER* does not calculate the net present cost for each energy source individually, so the NPV for the PV utility needs to be calculated manually.

The levelized cost of energy (LCOE) can be calculated like 3.7. The unit of LCOE is NOK/kWh and it represents what the price of electricity needs to be for the project revenue to equal the project costs.

$$LCOE = \frac{\sum_{t=0}^{N} \frac{(I_t+O_t)}{(1+i)^t}}{\sum_{t=0}^{N} \frac{S_t(1-d)^t}{(1+i)^t}} \tag{3.7}$$

I_t and O_t represents the investment cost and the O&M cost of the system in year t, respectively. S_t is the power output of the PV inverter for year t. This number is assumed constant by *HOMER*. This is analogous to assume that the yearly global radiation do not change over the lifetime of the project. By multiplying the rated PV power output in year t by $(i-d)^t$ is the degradation factor counted for. This equation is simplified from Branker et al. [76], by excluding the interest expenditures.

The hybrid system might occasionally produce more than 54 MW resulting in excess power. Excess power can not be sold to the grid, and must not be included in the LCOE or NPV calculations. Since the wind power utility is unable to produce excess power alone, all the excess power produced will count as excess energy produced by the solar utility simply because the solar installation needs to be adapted to the pre existing wind farm. When calculating the LCOE and NPV of the PV utulity only the production sold to the grid from the PV should be included. Because of the efficiency limitations of the inverter and the restrictions of the AC bus must the PV power production be defined as the inverter output in these calculations. For the NPV will the calculation be complicated since *HOMER* does not distinguish between grid sales from the wind farm and grid sales from the solar utility. This is problematic since the revenue from an energy unit is depending on the electricity price at the time step in question. The PV system can be simulated alone, but this will fail giving realistic results for the grid sale. This is because the excess energy that appears

in the hybrid system must be counted for. To find the approximate grid sales from the PV utility isolated from the wind, the excess power from the simulated hybrid system is subtracted from the grid sales in the simulation with the PV system exclusively. The revenue from grid sales for the PV simulation will be reduced by the same percentage as the excess electricity represents. Since the revenue obtained by selling the electricity to the grid is time dependent will the revenue stream calculated be an approximation with unknown uncertainty. For instance is the economical losses of excess energy higher if the energy is produced at a time period accompanied by high electricity prices than if it is at a time with low electricity prices. The error by using this method is still considered to be more reliable than using grid sales from the hybrid system since solar and wind power has such different natures. For instance is solar being absent at night and during the polar night when wind power is high.

If R_{PV} represents the grid sales in NOK from the exclusive PV plant in one year, the annual hybrid revenue stream from the PV unit, R_h becomes:

$$R_h = \left(\frac{E_h}{E_{PV}}\right) \cdot R_{PV} \tag{3.8}$$

Where E_{PV} is the annual inverter energy output from the system with solar energy exclusively and E_h is the annual inverter output in the hybrid system.

The NPV equation can be adapted to fit the needs for these circumstances.

$$NPV = \sum_{t=0}^{N} \frac{R_h - (I_t + O_t)}{(1-i)^t} \tag{3.9}$$

The term $S_t(1-d)^t$ in the LCOE calculations should be replaced by the actual inverter output for each year if the system typically produces a high amount of unsold power. The inverter output for each year of the lifetime of the project is provided by *HOMER*.

To calculate NPV's and LCOE's correctly will demand two simulations for each case and manually implementing three arrays into a matlab code. This is process with a high risk of typing errors.

Solar parameters	
Capacity	20 MW
Azimuth angle	0° (south)
temperature coefficient	$-0.500\%/^{\circ}C$
Consider temperature effects	yes
Electrical bus	DC
Derating factor	90%
Nominal operating cell temperature	$47.00^{\circ}C$
Lifetime	25 years
Wind parameters	
Hub height	80 meters
Anemometer height	80 meters
Anemometer heigh over sea level	57 meters [71]
Overall loss factor	0.8 %
lifetime	20 years
Number of turbines	18
Electrical bus	AC
Consider temperature effects	no
Surface roughness length	0.01 m (rough pasture)
Inverter	
Capital cost	700 NOK/kW
O&M cost	14 NOK/kW
Replacement cost	700 NOK/kW
Lifetime	15 years
Efficiency	95 %
Grid settings	
Annual purchase capacity	unlimited
Sale capacity	54,000 MW
Rate setting	Real time rates
Include grid in all simulations	yes
Sellback rate	Imported time series (see section 3.5)
Load Settings	
Load	48.47 kW/h
Scaled annual average	1,163.28 kWh/d
Random variability:	time step 1, Day to day 100 %
System settings	
Discount factor	5%
inflation rate	0%
Annual capacity shortage (to meet the load)	100%
Project lifetime	25 years

Table 3.1: Parameters and settings that are identical in all simulation cases

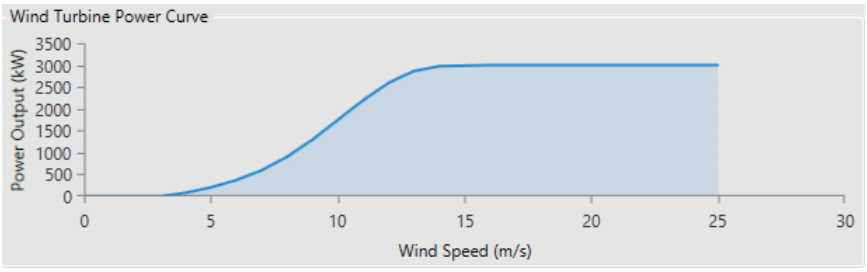

Figure 3.12: Wind power curve implemented to *Homer*

3.6.1 Simulation Strategy

The unchanged parameters implemented to *Homer* includes those displayed in table 3.1. In addition to these are the sensitivity variables presented in table 3.2 fed to the program to test different scenarios. Sensitivity analysis are conducted for the efficiency levels, panel slopes, capital and maintenance costs, and the albedo as shown in the table. The albedo at Fakken can be assumed to be roughly 0.25 for most parts of the year. This is the albedo corresponding to summer grass. The albedo for dry grass is some percentage points higher, but the surrounding water and rocks will reduce the overall albedo. *seNorge.no* reports that there are 25-50 days of snow at Fakken each year [71]. The days with snow cover are likely to occur on time periods with low radiation such as December, January and February. The periodically high albedo is therefore assumed to have low impact on the annual solar power production. Since one of the focus areas of this thesis is to determine if Fakken is an appropriate location for solar power installations, different albedo factors will be tested to obtain a basis for comparing Fakken to sites with different climatic conditions. Apart from the albedo sensitivity analysis will the albedo be set to be 0.25 since this best represents the Fakken surroundings.

The most common approach is to install stationary panels facing south at a slope equal to the latitude of the specific location. This will be considered to be the ultimate base case of the simulation together with an efficiency of 20 % and an albedo of 0.25. A module efficiency of 20 % is chosen as a rough estimate based on several factors as discussed in section 2.3. The best performing multicrystalline cells in 2017 had an efficiency of 22-25 % and commercial cells had an efficiency of 17-18.5 % in 2013 (slightly higher for mono-crystalline cells). The commercial solar cell efficiency has most likely improved since 2013. If PV panels were installed at Fakken, would it probably take some years before the installation date, and the efficiency should have improved further for commercial cells. The module efficiency should be lower than the cell efficiency, and therefore was the value of 20 % chosen. To count for the uncertainty in this value will a sensitivity analysis be conducted on

the efficiency. The radiation will also be adjusted according to the findings in the WRF analysis. Sensitivity analysis will be conducted on some of the most important variables affecting the solar power performance. Some of the sensitivity variables are given while others can be controlled and customized to the predetermined conditions.

On the stationary panels will the sensitivity of the following technical and/or physical variables be tested:

- PV Efficiency
- Radiation
- Inverter efficiency
- Slope
- Albedo

The following economical sensitivity variables will be tested:

- discount rate
- electricity prices
- System costs

Tracking strategies are also tested. These are

- Horizontal axis tracking, continuous adjustment.
- Vertical axis tracking, continuous adjustment
- Two axis tracking, continuous adjustment.

The project profitability response to higher revenue stream can be tested by increasing the grid sales by multiplying the grid sales for each year by a factor bigger than one. This will be an indication of how the system responds to higher electricity prices, which will increase the income of the project. It is reported in [84] that Denmark has roughly twice as high electricity prices as Norway, and hence are the multipliers of the grid sale income in the range of 1-2.

The horizontal axis tracking will be tested with different radiations and albedo

factors and the two axis tracking strategy is tested with different PV module efficiencies and solar radiations. The vertical axis topology is tested with a variety of slopes, albedo factors and radiation levels. The sensitivity variables for the different tracking scenarios are chosen based on their appeared significance on the amount of generated electricity. Ideally would every sensitivity variable be tested on all of the scenarios, but this would occupy more space than what is considered appropriate in the scope of this thesis.

The first part of the simulation result section will contain sensitivity analysis of the physical parameters. The solar radiation is considered the most crucial sensitivity variable due partly due to the findings that are presented in section 4.1.1. Other sensitivity parameters will be tested for different radiations. As the sensitivity analysis is conducted will some cases appear more relevant for further investigation than others. The cells that are marked in the tables represents cases that seems relevant for further investigations. This can either be because they appear to perform better at the most realistic and relevant conditions at Fakken, or because the topologies are widely applied. Based on these chosen scenarios will a economic feasibility analysis be conducted. Stationary panels are generally viewed as more relevant than the tracking scenarios because they are more widely used, more realistic for large scale installations and they are the foundation for the cost estimates in this thesis. Some basic tracking scenarios are examined based on the same cost estimate, but these numbers are not realistic. Solbes guesses that tracking systems can increase the cost of the PV system by 40-80 %. Great uncertainty is associated with these numbers so the main focus is to look at how the NPV and LCOE could change if tracking topologies had the same cost as the stationary panels and how it varies if the cost increased by 40% and 80 %. By comparing the NPV's and LCOE's for the different cases, will the approximate cost rise that the tracking scenarios can have while still being as profitable as the stationary panels be estimated. The most relevant stationary panels are those that generates most electricity over the lifetime of the project under the assumed radiation.

Settings	**Base Case**	**Sensitivity cases**
PV efficiency	20%	17%, 23% and 30%
Inverter efficiency	95%	99%
Panel slopes	70.1° (latitude)	40°, 50°, 60° , 80° and 90°
PV capital costs	7,500 NOK/kW	10,000 NOK/kW and 5,000 NOK/kW
PV O&M cost	150 NOK/kW	100 NOK/kW and 200 NOK/kW
Inverter capital cost	700 NOK/kW	467 NOK/kW and 933 NOK/kW
Inverter O&M cost	14 NOK/kW	9.47 NOK/kW and 18.7 NOK/kW
Albedo	0.25 (grass)	0.10 (bare rocks) and 0.9 (fresh snow)
Discount rate	5 %	2-8 %%

Table 3.2: Solar sensitivity parameters in the case of stationary panels

3.6.2 Bifacial panels

Bifacial panels can not be simulated in *HOMER*, so an experimental method is tried out for simulating bifacial panels. This is done by doubling the PV capacity and placing half of them with opposite tilt and azimuth angle. The panels that faces north simulates the rear side of the panels and has a lower efficiency since this is a normal feature of bifacial panels.

3.6.3 Future scenario

A "future scenario" will be tested. This scenario is tested as an attempt on getting insight in if a PV installation could be profitable under technical and economical conditions that are unrealistic today. A low cost scenario is tested on PV modules with a 30 % efficiency and with inverter efficiencies of 99 %. The slope will be decided in the sensitivity analysis for the slope.

3.6.4 Correcting for azimuth angle

Less than 24 hours before the submission of this thesis was it discovered that some of the errors in the *WRF* model could be corrected for to some extent by optimizing the azimuth angle for higher power output. Since this was discovered right before the submission was it impossible to correct for this error for all the simulations conducted. It was chosen to simulate two more cases were this effect was counted for and compare them to the other results achieved. For all simulations except for these two cases are the azimuth angle set to be $0°C$, which is the convention at the Northern hemisphere.

4

Results and Discussion

4.1 Analysis of solar and wind data

4.1.1 The *WRF* model simulations

Table 4.1, 4.2 and 4.3 displays how the observed global solar radiation at Holt correlates with the WRF simulated global solar radiation. All tables show that there is a positive Pearson correlation between the datasets, meaning that the two curves are likely to have approximately the same shape. This means that if the WRF model predicted a higher than average radiation at one particular time step, it is likely that the recorded radiation at that time step was higher than average as well. The same will also be true for radiations at all levels. It can be seen from table 4.1 that Pearson's correlation coefficient increased when the time step increased and had almost perfect correlation at monthly and weekly time scales. The same trend is not seen from table 4.2 and 4.3. In fact were the correlation factors higher for the 60 minute interval for 6 out of 11 months (Matlab fails in calculating a coefficient for December, as the radiation is 0 at most time steps). A clear trend in the correlation coefficients for each month are not identifiable. In figure 4.1, 4.2 and 4.3 are the measured and simulated values plotted together on different time steps. The correlation is maybe best viewed through figure 4.3. By investigating these figures, it appears that the WRF model overestimates the radiation in most time steps, and the highest degree during summer. This hypothesis is supported by the bias calculations. The biases are slightly positive during the winter months but decreases heavily when summer approaches, and has its minimum for June, where the observed

values are on average only 57 % of the simulated values. For May and July is the observed values 74 and 71 % of the simulated values. For the rest of the months (omitting January, November and December) are the observed values around 70-88 % of the *WRF* simulated radiation. Figures 4.5 and 4.6 displays the average hourly radiation for each month of 2016. Also here is it evident that the model overestimates most parts of the year with the only exceptions being January and December when the radiation is insignificant anyway. Table 4.1 shows that the root mean square error increases with decreasing time steps. The same is true when comparing the RMSE's of table 4.2 and 4.3. The RMS errors are also a lot higher for the summer months compared to winter months. This is not surprising as the bias holds the same trends like already discussed.

Another important finding is that the simulated radiation seems to have a rather unfortunate offset compared to the recorded radiation. While this factor might not have a catastrophic outcome on the total radiation during a day, it might certainly disturb the calculations carried out by Homer. It is also likely that the biases, RMS values and especially Pearson's correlation coefficients would have improved if the simulation did not possess this offset. When investigating the file containing the *WRF* simulated data set and comparing it to the Pyranometer recorded values, was no clear trend observed. While the *WRF* model on average is shifted forward, is this far from the case every day. To correct for this error is therefore not considered to be a viable option. When investigating the plots for May, June and July in figure 4.5 is it seen that correcting for the error will create another error on the other end of the radiation plot.

When Homer calculates the clearness index it will rely on the average radiation for one day. Now, when the radiation simulated is largely overestimated (especially during summer) in addition of being displaced by several hours, it will calculate the clearness index based on wrong presumptions. The suspicion is confirmed by *HOMER*'s presentation of the monthly average clearness index generated as shown in figure 4.4. The most striking results are that the clearness index is zero at June and higher than unity for May and July. A clearness index of zero indicates that no radiation manage to penetrate the atmosphere and directly beam the surface of earth. Although the weather might be extremely cloudy occasionally, it is highly unlikely that this will be the case during an entire month at once. A clearness index above unity is not only highly unlikely, but in fact impossible based on *HOMER*'s own definition of the variable. This indicates that the direct radiation observed at earth's surface is higher than the extraterrestrial radiation. *HOMER* does not provide the user with the clearness indexes except for the monthly average. This fact makes it impossible to examine the problem further.

In other words is the model better at predicting the radiation at times with

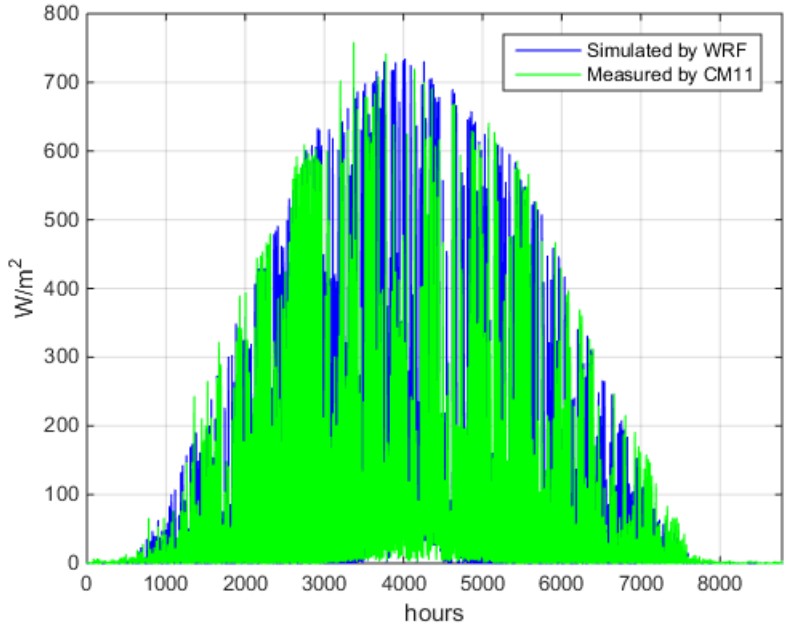

Figure 4.1: Hourly simulated and measured global radiation at Holt during 2016

modest irradiance. This is evident also from the mean values that the WRF model on average overestimates the radiation, and especially during sunny months. Table 4.1 confirms this by showing negative biases for all time steps, and that the mean of the recorded values on average are 70 – 72% of the WRF simulated values over the year. It is reasonable to assume that the WRF model also overestimates the radiation at Fakken to a similar degree, since the climatic conditions are similar at the two locations.

The WRF models main failure concerns its overestimation of the radiation at summer months together with the offset errors and the simulation results from *Homer* needs to be examined with this in mind. Especially since the overestimations are more conspicuous for the most significant time periods.

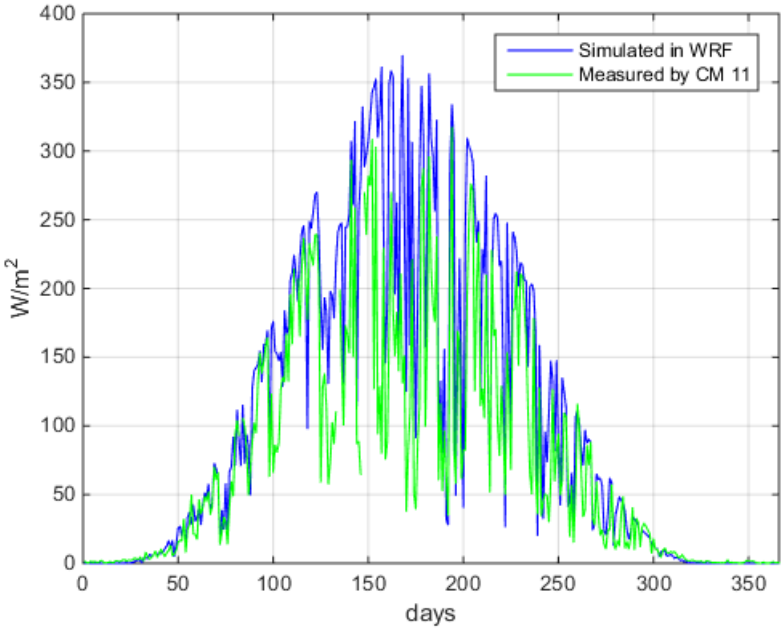

Figure 4.2: Daily average simulated and measured global radiation at Holt during 2016

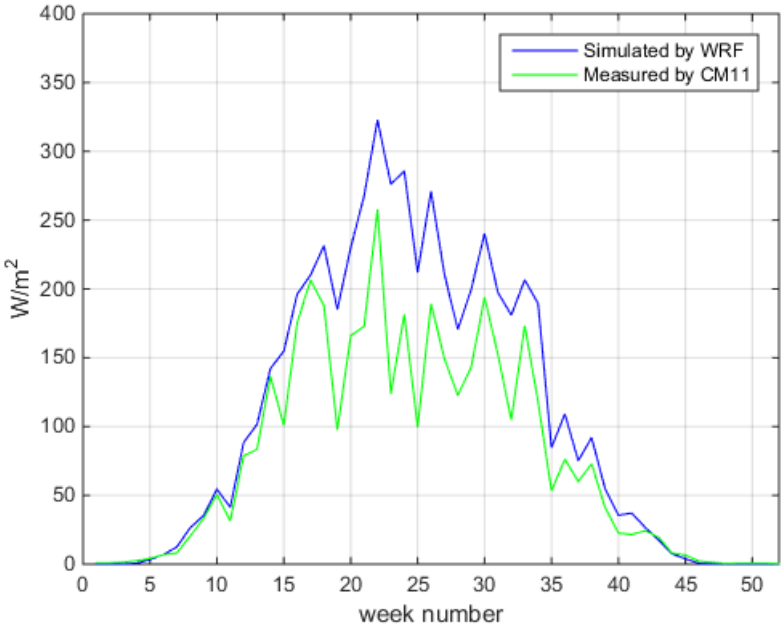

Figure 4.3: Weekly average simulated and measured global radiation at Holt during 2016. The two last days of the year is omitted

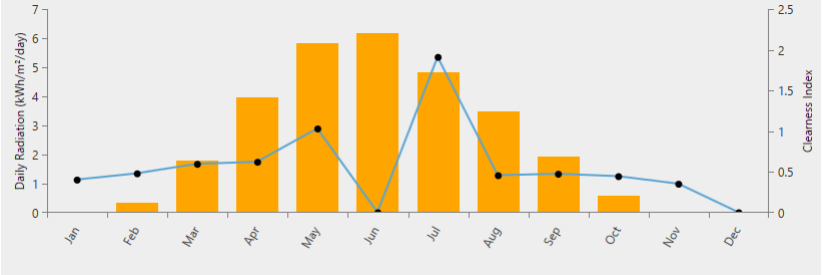

Figure 4.4: Global radiation and *HOMER*'s calculated clearness index

Time step	Time period	Mean Pyranometer W/m^2	Mean *WRF* W/m^2	Pearson	Bias	RMSE
60 mins	2016	76.2	105.1	0.8460	-28.9	97.7
24 hours	2016	76.3	105.1	0.9005	-28.8	58.1
7 days	2016	76.7	105.7	0.96	-28.9	46.6
monthly	2016	76.7	105.7	0.97	-28.8	45.0

Table 4.1: Overview of the comparison of the simulated and measured global solar radiation data on different time scales over a whole year at Holt

Time period	Time step	Mean Pyranometer W/m^2	Mean WRF W/m^2	Pearson	Bias	RMSE
January	60 minutes	1.6103	0.3188	0.6834	1.2916	2.4127
February	60 minutes	12.9175	16.3077	0.7590	-3.3901	23.5741
March	60 minutes	59.0996	68.1324	0.8256	-9.1245	59.4120
April	60 minutes	159.1989	180.6861	0.8894	-21.7384	91.8242
May	60 minutes	171.0915	240.6305	0.8233	-69.9245	142.8621
June	60 minutes	152.8707	267.1054	0.7108	-114.2349	166.4309
July	60 minutes	152.0753	205.3372	0.7893	-53.2618	139.9856
August	60 minutes	120.2983	170.5140	0.7946	-50.2158	129.1052
September	60 minutes	59.8994	81.7748	0.7935	-21.8753	74.3596
October	60 minutes	20.4007	26.7065	0.7416	-6.3059	34.8358
November	60 minutes	3.3499	1.7082	0.7525	1.6416	6.6442
December	60 minutes	0.6454	0	NaN	0.6454	1.0239

Table 4.2: Comparison of the simulated and measured global solar radiation for every month of 2016

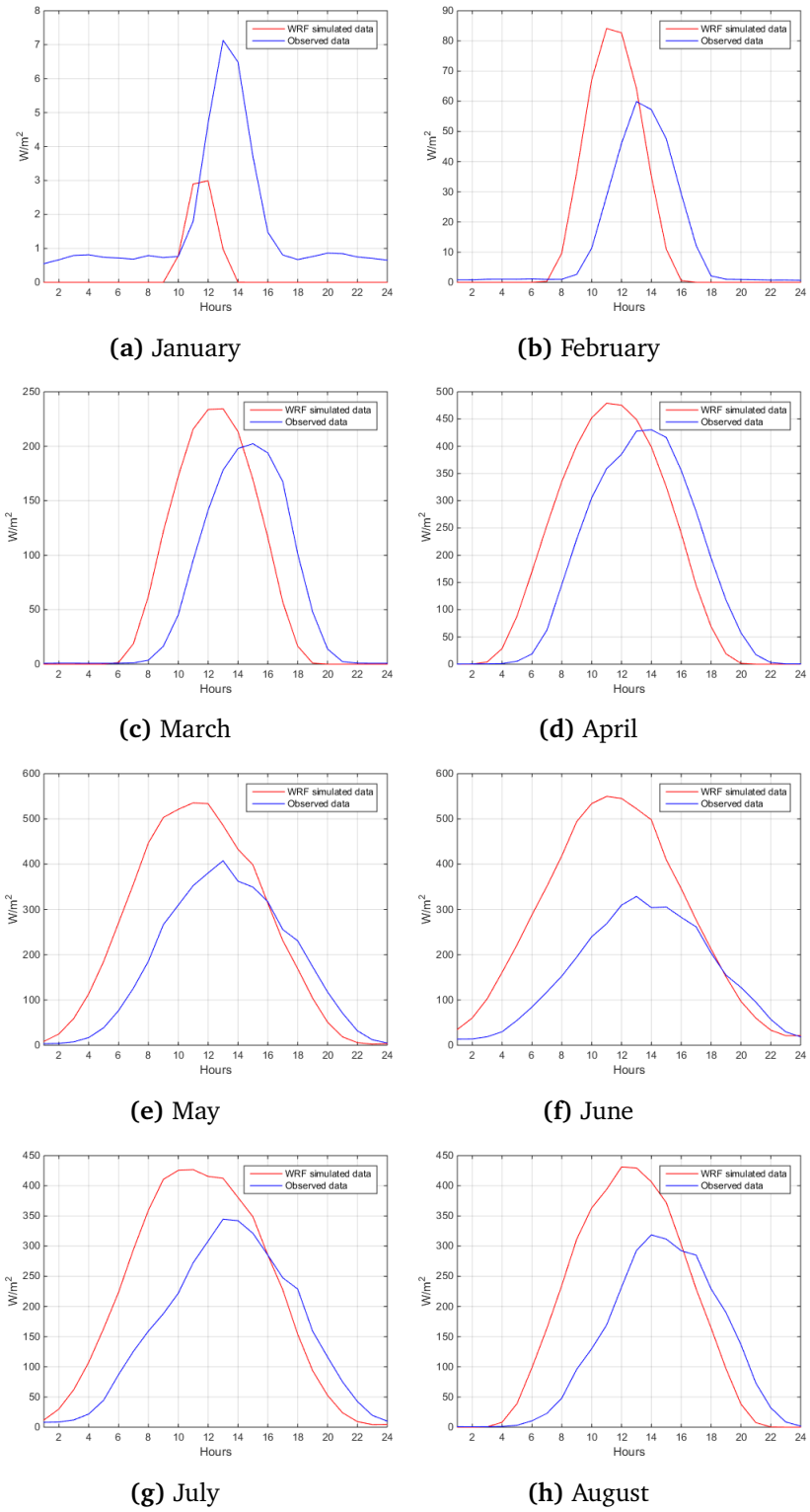

(a) January **(b)** February

(c) March **(d)** April

(e) May **(f)** June

(g) July **(h)** August

Figure 4.5: Simulated and observed global solar radiation at Holt for January-August 2016

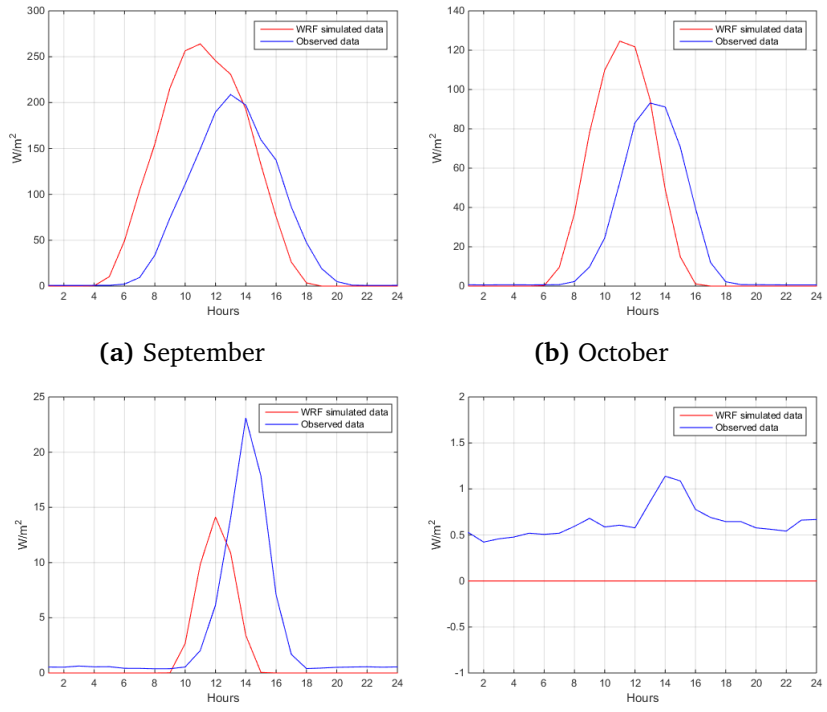

(a) September **(b)** October

(c) November **(d)** December

Figure 4.6: Daily profiles of the simulated and observed global solar radiation at Holt for September-December 2016. Note that the y-axis is differently scaled for each month.

Solar resources

The solar resources at Holt and Fakken are tested with the available data sources to compare the total energy exposure at each location with simulated and measured data sources. Table 4.4 shows that Fakken receives less energy than Holt according the the *WRF* model, both at a three month basis and for the complete year of 2016. The pyranometer at Holt records that for February, March and April was the radiation in total somewhat higher in 2016. It is discovered that the observed radiation at Fakken the during February, March and April in 2017 are 81.8 % of the simulated radiation at Fakken for the same months in 2016, corresponding to a relative difference of approximately 22 %. Since the radiation at Holt was slightly higher in 2016, can it be reasonable to assume that this is true at Fakken as well. If that is the case, might the real overestimation by the *WRF* model be lower than a relative change of ~ 22 %. The observed radiation at Holt on the three month basis is 87,2 % of the simulated data in the same period, while on a yearly basis is it already discovered that the *WRF* model overestimated the radiation by around 38

Time period	Time step	mean CM11	Mean WRF	Pearson	Bias	RMS error
January	24 hours	1.61	0.32	0.75	1.29	1.48
February	24 hours	12.92	16.31	0.78	-3.39	8.21
March	24 hours	59.1	68.13	0.83	-9.05	20.55
April	24 hours	159.20	180.69	0.74	-21.39	40.62
May	24 hours	171.09	240.63	0.81	-69.33	83.49
June	24 hours	152.87	267.11	0.57	-114.23	136.64
July	24 hours	152.07	205.34	0.79	-53.26	79.79
August	24 hours	120.30	170.51	0.74	-50.22	70.09
September	24 hours	59.90	81.77	0.66	-21.88	35.64
October	24 hours	20.40	26.71	0.60	-6.31	13.78
November	24 hours	3.35	1.71	0.95	1.64	1.94
December	24 hours	0.65	0	NaN	0.65	0.87

Table 4.3: Comparison of the daily correlation between the measured global solar radiation and the simulated data for each month of 2016

% in relative change, but the overestimation was clearly more severe during summer months. It is likely that this trend is relevant for Fakken too, such that the overestimation will be a lot higher during summer also for Fakken. It is therefore assumed that the radiation at Fakken will be largely overestimated and a value of 30 % reduction seems appropriate. There lies a lot of uncertainty in this approximation since the overestimation is more severe during some parts of the year than others. Leap day is included when the calculations are made for the whole year of 2016.

In the simulations will therefore a radiation scaled down to 70 % of the original simulated radiation be tested alongside a 100 % radiation. Both radiations are used because there lies uncertainty in how much the radiation actually differs from the simulated values.

The WRF model has not succeeded to a satisfactory degree in simulating the global solar radiation at Holt. But in lack of better alternatives are the the WRF simulated data for Fakken still implemented to *Homer*. It was considered to use the observed solar radiation at Holt instead of the simulated data because of these fatal errors, but the whole point of this thesis is to evaluate Fakken as a site for solar installation, while master student Karoline Ingebrigtsen evaluates Skibotn for the same applications. If the same data was used in both theses would the main aim of the simulations vanish. I can also be noted that the possibility of there being an measurement error on the pyranometer at Holt can not be eliminated, but this is assumed to be highly unlikely.

Data source	Time period	Location	Solar resources
WRF simulated	2016	Fakken	885.17 kWh/m^2
WRF simulated	2016	Holt	923.33 kWh/m^2
Pyranometer	2016	Holt	669.42kWh/m^2
Pyranometer	Feb, Mar Apr 2016	Holt	166.86 kWh/m^2
WRF simulated	Feb, Mar, Apr 2016	Fakken	184.23 kWh/m^2
WRF simulated	Feb, Mar, Apr 2016	Holt	191.33 kWh/m^2
Pyranometer	Feb, Mar, Apr 2017	Fakken	150.71 kWh/m^2
Pyranometer	Feb, Mar, Apr 2017	Holt	154.95 kWh/m^2

Table 4.4: Solar resources

4.1.2 Correlation analysis between wind and solar resources

Observed Wind and Solar Resources at Fakken

Pearson's correlation coefficient is calculated for February, March and April on daily, hourly and 10 minute intervals as displayed in table 4.5. Correlation coefficients close to -1 would be preferable as discussed in section 3.2. The results in 4.5 show that this is not the case for any of the months on any time scale. The lowest coefficient was obtained in April on a 24 hour time step, and the highest coefficient was obtained in February on a 10 minute time step. The correlation factor seems to generally decrease both when summer approaches and for increasing time steps. It might be reasonable to expect this trend to persist, meaning that the correlation will be closest to -1 for June, and then start to diminish again in July. It also appears from the figures 4.7, 4.8 and 4.9, that the solar and wind resources varies quite randomly on a daily basis. The results from this analysis does not give an optimistic view on the correlation at Fakken. However, this is a study over three months, and the overall impression could improve if a whole year of datasets were available. Note that the scales on the figures are different for each month. This is done to better observe how the wind and solar resources correlate every month. The wind power per square meter is plotted with a density that differs somewhat to the actual average density. Both wind and solar resources are plotted without any losses. The solar resources are measured on a horizontal surface, and the power exposure on a tilted surface will be a lot higher than the figure shows. How to calculate the irradiance on a tilted surface as a function of the irradiance on a horizontal surface is displayed in section 2.2.5.

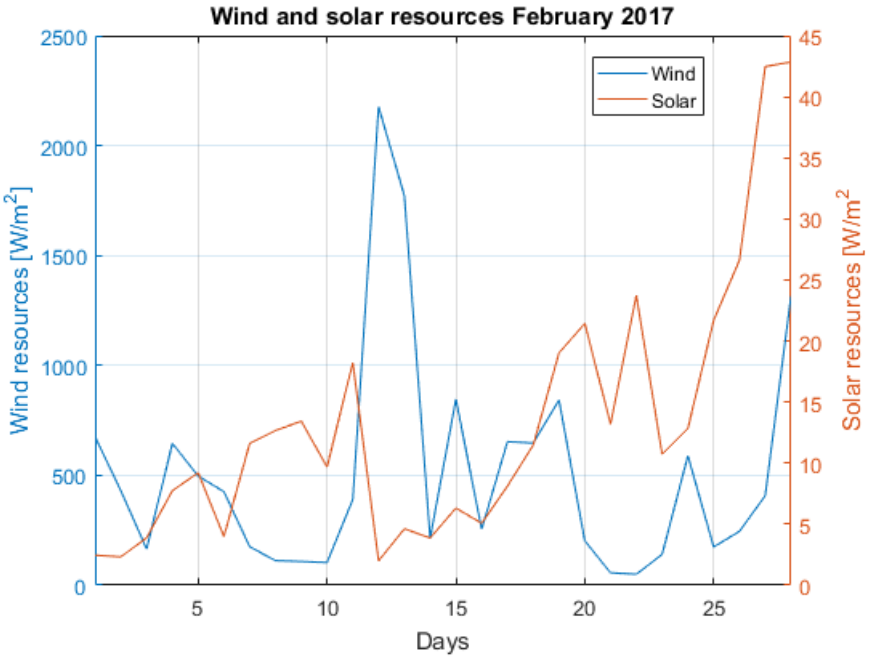

Figure 4.7: Daily profile of solar and wind resources at Fakken during February 2017

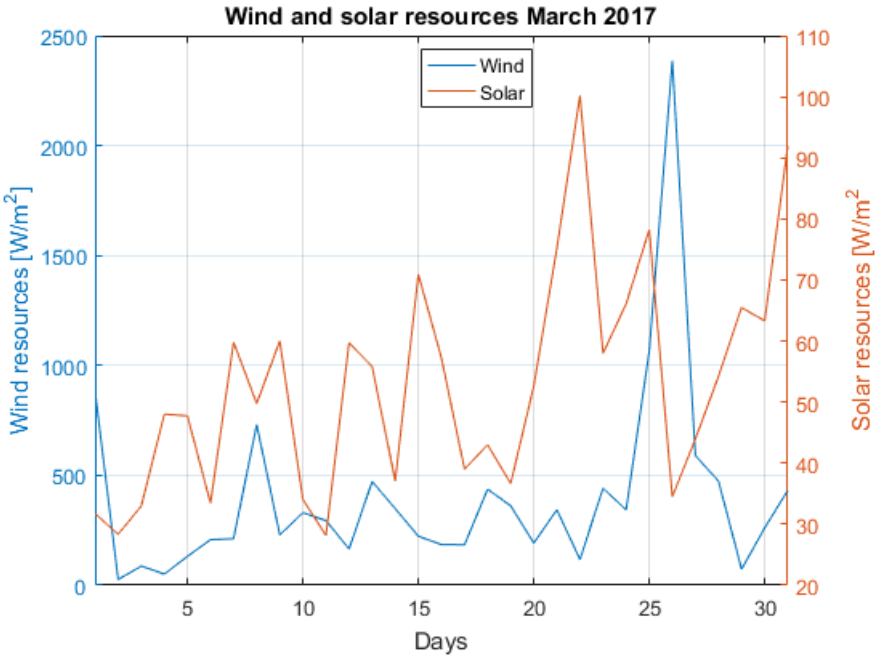

Figure 4.8: Daily profile of solar and wind resources at Fakken during March 2017

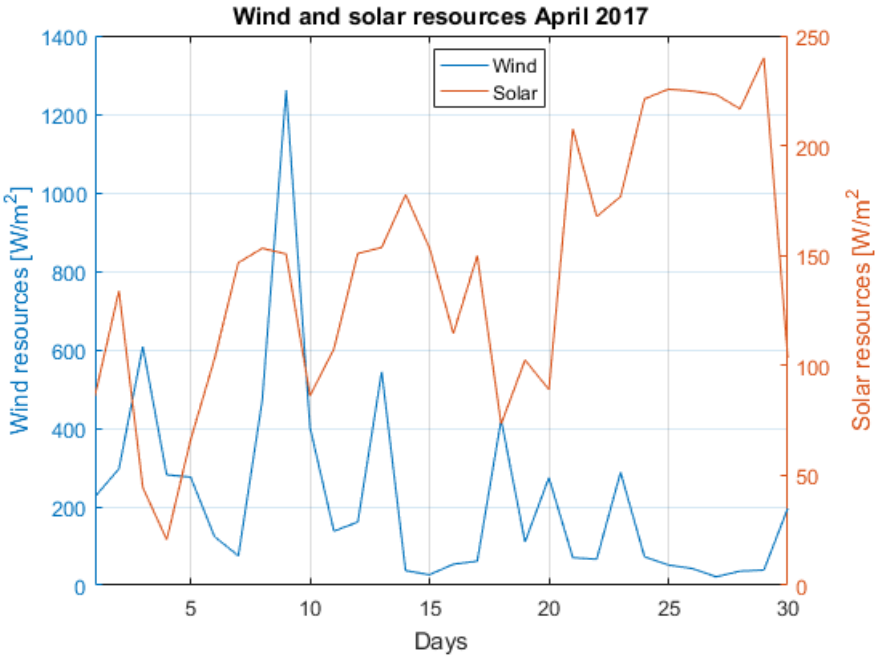

Figure 4.9: Daily profile of solar and wind resources at Fakken during April 2017

year	Time Period	time step	Pearson Correlation Coefficient
2017	February	10 minutes	0.8811
2017	February	60 minutes	-0.0354
2017	February	24 hours	-0.0951
2017	March	10 minutes	-0.0605
2017	March	60 minutes	-0.0696
2017	March	24 hours	-0.1243
2017	April	10 minutes	-0.1250
2017	April	60 minutes	-0.1259
2017	April	24 hour	-0.3569

Table 4.5: Correlation between wind and solar resources at Fakken 2017 at a 10 minute interval

Simulated solar radiation and observed wind speed data at Fakken

Tables 4.6 and 4.7 shows that there are almost zero correlations between the WRF simulated solar radiation and recorded wind speed at Fakken on 10 minutes and 60 minutes time steps. This is true both when the correlation coefficient is calculated over the whole year and over each month separately.

For 24 hours time steps are the correlation coefficients more negative for some of the months and also when calculated over the whole year, but still not considered close enough to -1 to be of significance. The correlation coefficient is more ideal on weekly and monthly time steps, especially the latter. This means that the solar radiation is likely to be high during moths of low average wind speeds and vise versa. It can be argued that a negative correlation is more important on long time scales since the objective is to increase production during summer season. June is actually the month with best correlation factor on a 24 hour time step. This might be a result of high solar overestimation in this period. This is one of the most significant months for solar power production. On smaller time scales is the correlation rather random for all months.

The correlation factors for each month does not show an increasing trend like it did for the observed solar and wind data for 2017 for the same months. This might be due to natural climate variability from year to year, but it might as well be due to the inaccuracy and in the simulated radiation data. The correlation coefficient does anyhow decrease to some degree for June and July.

The comparison of the correlations coefficients between the wind resources and the observed and the simulated solar resources suggests that the correlation coefficients have more ideal values for the measured data. This might be due to the fact that the WRF simulations has limited resolution and unable to detect small scale weather events like clouds, which are often accompanied by windy conditions in reality. This makes the uncertainty higher for the correlation analysis on small time scales. If it is assumed that the simulated and observed solar radiation at Holt and Fakken differs similarly and taken into account that the correlation between the simulated and observed solar radiation at Holt was generally high, could it be assumed that the correlation factors between simulated and measured solar radiation for Fakken for the same year also would be high. High correlation factors indicates that the datasets will fluctuate similarly even if the simulated data overestimates the radiation. Based on this argumentation can it be assumed that the correlation values between the simulated values and the observed wind speed might be quite reliable and that the differences between the the correlation coefficients in table 4.5 and table 4.7 are due to differences in weather conditions for 2016 and 2017, but there is no guarantee for these claims.

Time Period	Time Step	Pearson Correlation Coefficient
2016	10 minutes	-0.1539
2016	60 minutes	-0.1595
2016	24 hours	-0.3362
2016	7 days	-0.6385
2016	months	-0.8619

Table 4.6: Correlation analysis of simulated solar radiation and recorded wind speed at Fakken for 2016

Time Period	time step	Pearson Correlation Coefficient
January	10 minutes	-0.0210
January	60 minutes	-0.0210
January	24 hours	0.0686
February	10 minutes	-0.0232
February	60 minutes	-0.0236
February	24 hours	-0.0268
March	10 minutes	-0.0113
March	60 minutes	-0.0136
March	24 hours	-0.1020
April	10 minutes	-0.0146
April	60 minutes	-0.0153
April	24 hours	0.0431
May	10 minutes	-0.0207
May	60 minutes	-0.0201
May	24 hours	-0.2260
June	10 minutes	-0.0246
June	60 minutes	-0.0280
June	24 hours	-0.2923
July	10 minutes	-0.1241
July	60 minutes	-0.1281
July	24 hours	-0.1531
August	10 minutes	-0.0662
August	60 minutes	-0.0692
August	24 hours	-0.1221
September	10 minutes	0.0564
September	60 minutes	0.0571
September	24 hours	-0.2283
October	10 minutes	0.0646
October	60 minutes	0.0657
October	24 hours	-0.1205
November	10 minutes	-0.0554
November	60 minutes	-0.0581
November	24 hours	-0.2639
December	10 minutes	NaN
December	60 minutes	NaN
December	24 hours	NaN

Table 4.7: Correlation analysis for each month of 2016 with simulated solar radiation and recorded wind speed at Fakken

4.2 Simulation results

Correction of the *WRF* data

As a result of the findings in section 4.1.1 are the *HOMER* simulations conducted on two radiation levels, namely 70 % and 100 % of the *WRF* simulated data. The 70 % radiation is considered to be more realistic, but since there is uncertainty in how much the actual radiation levels at Fakken differs from the simulated data, is still the 100 % radiation regarded as relevant for some analyses. 70 % radiation was selected because it seemed reasonable based on the findings in section 4.1.1. It was discovered that the observed radiations for all months except May, June, July and August were between above 74 - 88 % of the *WRF* simulated radiation (In May was the observed radiation 71 % of the simulated values). But since May, June July and and August are the most significant months for solar power production must the radiation be scaled further down to count for this. 70 % was considered to strike the balance of the overestimation in overall power production for all of the months together. The power output from the simulations might thus be underestimated for all months except June, where it will be overestimated. By scaling down the radiation will *HOMER* assume that the surface is less exposed to radiation, and the amount of diffuse radiation is assumed to increase at the expense of the direct radiation. But the clearness index is also affected by the offset. The offset error is difficult to presume the impact and uncertainty for. It introduces several issues for the reliability in the simulations. One is the clearness index, in which the error was discussed in section 4.1.1. *HOMER* does not allow the user to investigate or change how the calculations are conducted, and the clearness index can therefore not be modified. *HOMER* compares the input radiation to a pre calculated extraterrestrial solar radiation, and decides the clearness index based on this. When the input radiation is shifted in time will it look like the radiation at earth is a lot higher or lower than it actually is, and *HOMER* will fail in calculating a realistic clearness index. This will affect the power production in all the simulations and affect the result when deciding on the best slope of the panels. How *HOMER* calculates the clearness index and the radiation on the panels are briefly described in section 3.5, and a detailed presentation is included in the appendix.

The offset will also affect the power production directly because the radiation strength will not correspond to the calculated position of the sun conducted by *HOMER*. The power output might be bigger at some slopes and azimuth angles than other simply because the radiation is "measured" to peak at a time step that does not correspond to solar noon calculated by *HOMER*. The vertical and two axis tracking strategies will not be affected by the error in azimuth angle, and the horizontal axis tracking and two axis tracking will not be affected by the error in slope. The only error is that they will receive more power at

	Stationary panels	Horizontal axis tracking
Inverter capacity [MW]	14	16
Inverter output [MWh]	13,612,853	15,045,961
PV output [MWh]	8.40	15,974,446
Grid sales [kWh]	142,011,289	132,800,098
PV penetration [%]	10.25	11.91
Excess electricity [kWh]	386,956	136,591.8
Yield [MWh/MW_p]	736	799
NPV [NOK]	-168.93	-
LCOE NOK/kWh	1.1310	-

Table 4.8: Electrical output for azimuth angle of 300°

other times of the day than they would if the offset error did not exist. The uncertainty in the tilt angles have been given a lot of attention in this thesis by conducting sensitivity analysis on them. The problem with the azimuth angle was unfortunately discovered less than 24 hours before the submission, which limited the possibilities of reducing this uncertainty throughout the analysis.

As already discussed is it impossible take measures in correcting for the offset only by shifting the simulated data, since that will incur other errors to the data. However, the optimal azimuth angle can be found by sensitivity analyses. If this appears to be optimal for the panels to face directions far from the standard strategy of letting the panels face southwards will it be an indication of the offset to impact the results to a high degree, and creating an even higher uncertainty than first assumed.

Table 4.8 presents the outputs from a stationary and horizontal axis tracking system at 70 % radiation and an albedo of 0.25 when the optimal azimuth angle is used. The stationary panels has a tilt angle of 40°, which will be proven in this section to be the optimal tilt at a 70 % radiation and an albedo of 0.25. The results from this analysis will be discussed at the end of this chapter. For the rest of the analyses will the optimal azimuth angle not be counted for because of time limitations. However, the error should be held in mind during the reading of this chapter. The errors are discussed in the end of the chapter.

By including the 100 % radiation will the systems sensitivity to radiation become apparent. The base cases are defined as stationary panels at a 70.1° tilt angle at both a 100 % and 70 % radiation. The results from the simulations needs to be evaluated with the errors of the input data in mind. Most of the technical/ physical sensitivity variables will be tested on both 70 % and 100 % radiation in order to investigate how the system responds to different

radiations.

In the tables in the sensitivity cases are only the results from year 1 displayed for convenience. Because of the degradation of the solar panels will the power output be reduced over the years as demonstrated in tables 4.9 and 4.10. This means that all variables viewed in the tables (except the inverter capacity), will decline as the project lifetime proceeds.

Comparing different tracking strategies and stationary panels

The results from stationary panels, horizontal axis tracking, vertical axis tracking and two axis tracking all at 100% radiation are shown in tables 4.9 and 4.10. The slope of the stationary panels and the vertical axis tracking panels are also 70.1°. The efficiency is 20 % and the albedo is 0.25 for all scenarios. The table shows some of the physical differences between the stationary and various tracking scenarios and the effects of the PV degradation for all of them. It is seen that the output from the vertical axis tracking scenario is a lot higher than the horizontal axis tracking scenario. It is also seen that the output from the vertical axis tracking does not differ notably from the output from the two axis tracking topology. And the vertical axis tracking strategy might even be optimized further by changing the tilt angle. It is sensible to assume that a two axis tracking system will be significantly more expensive than a one axis tracking system and hence can it be expected that the NPV of the vertical axis tracking system should be lower than the NPV of the two axis tracking scenario. With 70 % radiations will probably the effects of tracking be lower than table 4.9 and 4.10 suggests. The further analysis will focus on optimizing these scenarios to obtain higher power production and to investigate how they respond to different physical variations.

Electrical Parameters	Output			
	Stationary		Horizontal axis tracking	
	Year 1	Year 25	Year 1	Year 25
Inverter capacity [MW]	19	19	19	19
PV Capacity factor [%]	11.88	10.53	14.27	12.65
PV power produced [kWh/yr]	20,813,749	18,454,584	24,999,853	22,166,208
Energy output inverter [kWh/yr]	18,948,449	16,852,323	22,834,620	20,305,900
Converter capacity factor [%]	11.38	10.13	13.72	12.20
Converter losses [kWh/yr]	997,286	886,964	1,201,822	1,068,732
PV penetration [%]	13.91	12.53	16.25	14.68
Excess power produced [kWh/yr]	868,013	715,297.4	963,412	791,577
Mean inverter output [kW]	2,163	1,924	2,607	2,318
Hours of operation [h/yr]	4,256	4,256	4,256	4,256
Energy available for grid sale[kWh]	147722892	145626765	151609063	149080343

Table 4.9: Results for base case stationary panels and horizontal axis tracking at 100 % radiation

Electrical Parameters	Output			
	Vertical axis tracking		Two axis tracking	
	Year 1	Year 25	Year 1	Year 25
Inverter capacity [MW]	22	22	23	23
PV Capacity factor [%]	17.78	15.76	17.95	15.92
PV power produced [kWh/yr]	31,142,930	27,612,988	31,450,048	27,885,295
Energy output from inverter [kWh/yr]	28,309,308	25,187,016	28,585,318	25,433,011
Converter capacity factor [%]	16.97	15.13	17.13	15.28
Converter losses [kWh/yr]	1,486,478	1,325,613.75	1,500,776	1,338,551
PV penetration [%]	19.47	17.65	19.62	17.79
Excess power produced [kWh/yr]	1,413,373	1100714	1,434,533	1,114,283
Mean inverter output [kWh/yr]	3,224.10	2,875.19	3,255	2,903
Hours of operation [h]	4,256.00	4,256.00	4,256	4,256
Energy available for grid sale [kWh/yr]	157017523	153961105	157289182	154206905

Table 4.10: Results from two axis tracking and vertical axis tracking at 100 % radiation

Sensitivity case: slope and albedo for vertical axis tracking and stationary panels

In this sensitivity analysis are the stationary and the vertical axis tracking panels tested at different slopes and albedos both at a radiation of 70 % and 100 %. The most relevant results are displayed in tables 4.11, 4.12,4.13, and 4.14. The stationary panels will be discussed first. As shown in table table 4.11 is a

50° slope preferable under albedos of 0.1 and 0.25 at a radiation of 100%. Only with the very high albedo of 0.9 would a slope of 70.1° be optimal. At the 0.25 albedo would the panels with a slope of 50° generate approximately 4 % more electricity during year 1 compared to the base case, and it also produces less excess electricity which reduces the pressure on the dump load. This indicates that using a slope of 70.1° makes the panels absorb very high amounts of power for short time periods, and thus demanding a bigger converter, while a the production during most time periods are modest. With a less steep slope will the power production be more evenly distributed over time. The yield at at a 50° slope is $1077.2 MWh/MW_p$ for year 1 under an albedo of 0.25. This result is very good, but makes the radiation implemented appear unrealistically high.

For a radiation of 70 % did a slope of 40° produce most power at albedos of 0.1 and 0.25, while on an albedo of 0.9 did a 80° slope angle perform best. The low tilt angle being optimal at the reduced radiation indicates that a lower global radiation decreases the clearness index and results in high fracture of diffuse radiation. At an albedo of 0.9 did the 100 % radiation scenario perform best a tilt angle less steep than the radiation at 70 %, indicating that the albedo gives high radiation in the vertical that counts more for the low radiation scenario compared to the high radiation case. These results confirms that the diffuse radiation is best captured with lower tilt angles. The relative difference between power output between a 40° tilt angle and the base case is 6 % at an albedo of 0.25. In other words is there more relative power to loose by installing the panels at a 70.1° when the radiation is low compared to when it is high. The yield for 70 % radiation at 0.25 albedo at optimal tilt angle is $660.3 MWh/MW_p$, which is 61 % of the yield under a 100 % radiation at optimal angle.

These simulations indicates low clearness indexes large parts of the year. At least for time periods of highest radiation. This might be a consequence of the clearness index being zero in June, which is the sunniest month of the year. But the clearness index is larger than 1 for May and July, which could be argued to influence the results in the opposite direction. It could also be claimed that the offset error in the *WRF* simulations would affect the slope because the radiation might seems highest at time periods of the day when the solar position is low and vice versa. If observed radiation data were available is it likely that the results might turn out somewhat differently and that a slightly higher slope than 40° would appear to be optimal.

An albedo of 0.9 corresponds to fresh snow, which can only be expected occasionally. The slope chosen should not only depend on the total electricity production during the year as a whole, but should also review at what time periods there are most desirable to extract power. As discussed in section 2.8.1

will a steeper tilt angle optimize production during winter while a low slope optimizes the production at summer. Figure 4.12 displays the excess energy produced for the base case with stationary panels with a slope of 70.1°. It shows a high amount of excess energy during March and April. These are usually months with large wind resources and possibly snow providing a high albedo. The main motivation of installing solar panels at Fakken is the advantage of exploiting the existing grid's capacity during summer. The installation should therefore focus on optimizing the production for summer times. As seen by figure 4.12, is the excess power production during summer modest. All other factors being equal, is still the scenario with a 50° degree slope under the influence of an albedo of 0.25 enabling the system to sell more power to the grid and produce less excess power if the radiation is equal to the *WRF* simulated data, while a slope of 40° is optimal if the radiation is closer to 70 % of the radiation. Since 40° was the lowest tilt angle tested and this performed best of them all, was also a slope of 30° tested. This scenario had a slightly lower inverter output than the scenario of 40° slope and will therefore not be considered further.

Table 4.11 and 4.12 confirms that high albedos yields higher power outputs regardless of the slope. Both tables together with figure 4.10 shows that the tilt angles are crucial for the power output and that the steepest angles has highest variations in power output depending on the albedo. For instance is the power output at an albedo of 0.1 and a slope angle of 40° 6.4% lower in relative change than the power output at an albedo of 0.9 at the same slope angle while the corresponding relative difference is over 34 % for a slope of 90° at 100 % radiation. At a 70% radiation is the relative difference at the high and low albedo at a tilt angle of 40° around 8% and for a slope of 90° is the relative difference 43 %. This shows that under low radiation is finding the optimal angle customized for the site specific conditions of elevated importance compared to sites with high radiation levels. The power production could have been improved if Fakken had more days of the year with snow cover.

Locations with similar radiation (70 %) and more snow cover could generate between roughly 6.3 % - 19 % more PV power if the albedo was 0.9 during the whole year, compared to if the albedo is 0.25 during the whole year, which is assumed in this thesis. However, even locations with snow cover large parts of the year will most likely be snow-free during the most significant months for solar power. The yield could be improved from $660.3 MWh/MW_p$ to $739.2 MWh/MW_p$, which corresponds to a relative increase of 12 %.

When it comes to the vertical axis tracking systems did the optimal tilt angle appear to be 60° both at a 70 % and a 100 % radiation as shown in tables 4.13 and 4.14. The differences between the power output for the same slope at different albedos were not quite as strong as for stationary panels. The

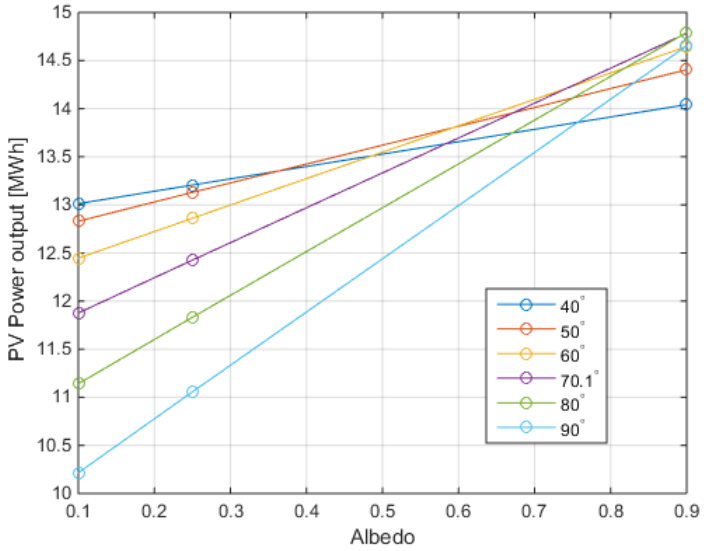

(a) Sensitivity analysis of albedo and slope for 70 % radiation

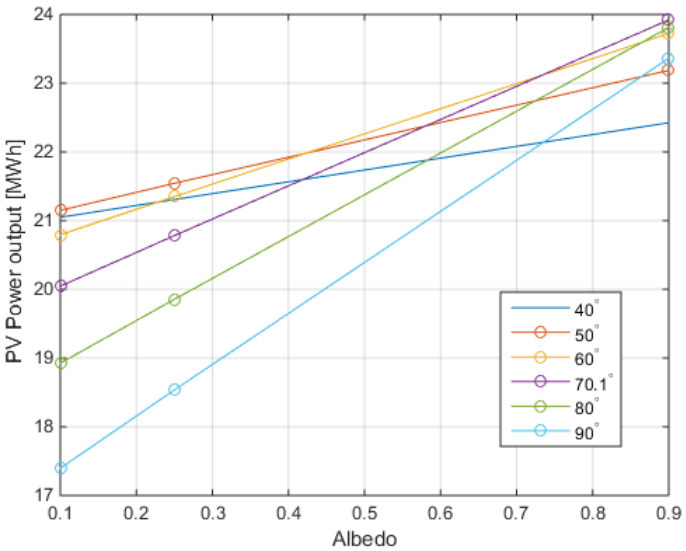

(b) Sensitivity analysis of albedo and slope for 100 % radiation

Figure 4.10: Slope and albedo analysis for 70% and 100% radiation. Note that the axis are not identical for the two plots.

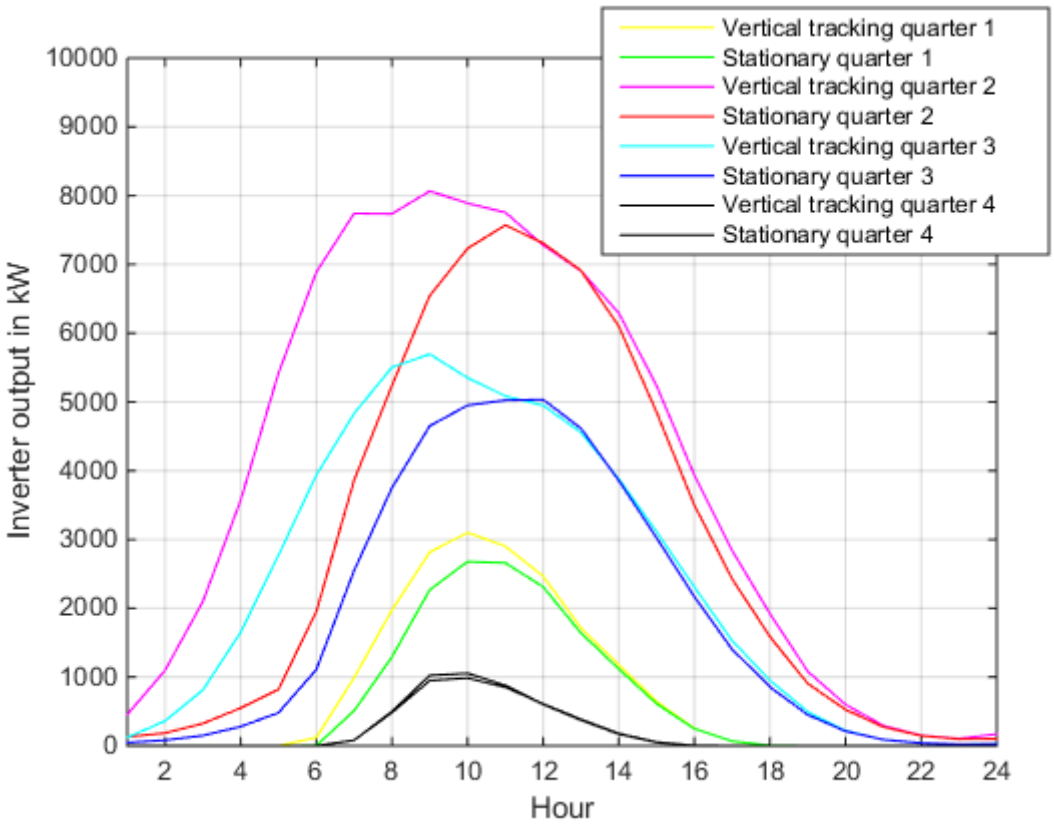

Figure 4.11: Stationary panels and Vertical axis tracking system, daily profile for each quarter of the year

difference in power output at a slope of 90° for albedos between 0.1 and 0.9 is 19 % under a 100 % radiation and 28 % for a 70 % radiation. The fact that the tracking system will be able to produce high amounts of power during larger parts of the day is probably the main contributor to this difference in optimal slope for the stationary and vertical axis tracking scenarios. It is seen by comparing the outputs from stationary and vertical axis tracking systems at the same radiation levels that for a 100 % radiation did the vertical axis tracking system produce 44 % more power than the stationary panels when both is simulated at their optimal angle. For a 70 % radiation was the relative increase 32 % by replacing the stationary panels with a vertical tracking system. This confirms that tracking is more beneficial at locations with high radiation. The yield of the vertical axis tracking system under a 70% illumination and an albedo of 0.25 is $874 MWh/MW_p$ and under a 100 % radiation is the yield $1417 MWh/MW_p$.

When it comes to how the albedo affects the benefits of tracking is no clear trend observed. If the optimal angles are chosen for each scenario at 70 % radiation was it a 31 % increase in power output for using tracking at a 0.1 albedo factor, 32 % increase at 0.25 albedo and 32.6 % increase at an albedo of 0.9. Since the tracking method *HOMER* uses are astronomical calculations of the sun's position rather than sensor tracking, will the simulated tracking face the sun even if the radiation is mostly diffuse so that the panels actually should be facing a more horizontal angle or when the albedo is high, might the absorption be higher if the panels has a steeper tilt angle. None of these factors are counted for when using astronomical tracking. The effects of using tracking might therefore be higher if sensor tracking is applied. The summaries of the findings in this sensitivity analysis at an albedo of 0.25 is included in the appendix.

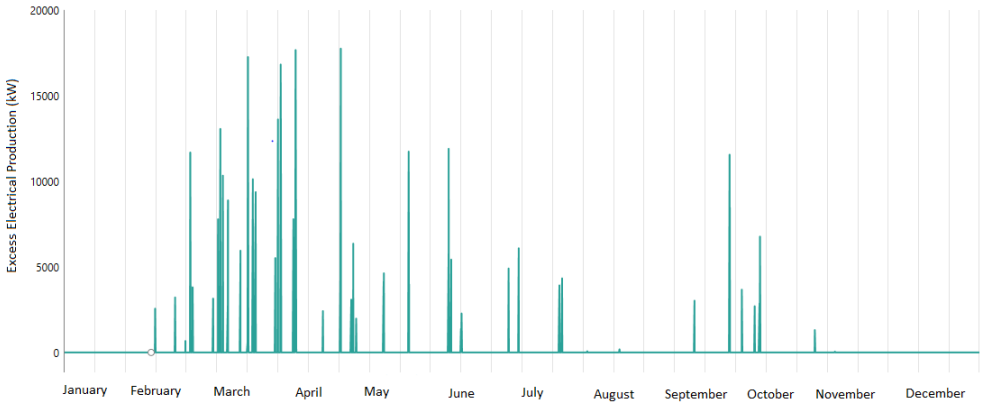

Figure 4.12: Excess energy produced in year 1 for stationary panels at 100 % radiation at a 70.1

Slope ↓		Albedo ⟶		
		0.1 (Bare rock)	**0.25** (Grass)	**0.9** (Fresh snow)
40°	**Inverter Capacity [MW]**	18	18	19
	Inverter output [MWh]:	19,245	19,480	20,488
	PV output [MWh] :	21,048	21,307	22,424
	PV capacity factor [%]	12.01	12.16	12.80
	Grid sales [kWh]	147,644,412	147,878,660	148,886,845
	PV penetration [%]	14.04	14.19	14.83
	Excess energy [kWh]	789,886.4	802,197.3	857,433.9
50°	**Inverter capacity [MW]**	18	18	19
	Inverter output	19,300	19,657	21,187
	PV output [MWh]	21,149	21,544	23,241
	Capacity factor [%]	12.07	12.30	13.27
	Grid sales [kWh]	147,699,406	148,055,670	149,584,666
	PV penetration [%]	14.10	14.33	15.28
	Excess energy [kWh]	832,679.8	852,252.1	939,660.0
60°	**Inverter capacity [MW]**	18	19	20
	Inverter output [MWh]	18,950	19,452	21,592
	PV output [MWh]	20,795	21,349	23,723
	Capacity factor [%]	11.87	12.19	13.54
	Grid sales [kWh]	147,349,442	147,850,318	149,990,060
	PV penetration [%]	13.90	14.22	15.55
	Excess energy [kWh]	847,594.4	873,901.7	994,169.2
70.1°	**Inverter capacity [MW]**	19	19	19
	Inverter output [MWh]	18,253	18,920	21,754
	PV output [MWh]	20,047	20,781	23,920
	Capacity factor [%]	11.44	11.86	12.83
	Grid sales [kWh]	146,653,068	147,319,187	148,854,972
	PV penetration [%]	13.47	13.89	14.86
	Excess energy [kWh]	832,175.0	865,539.3	1,021,104.8
80°	**Inverter capacity [MW]**	19	19	20
	Inverter output [MWh]	17,229	18,074	21,649
	PV output [MWh]	18,926	19,855	23,809
	Capacity factor [%]	10.80	11.33	13.59
	Grid sales [kWh]	145,628,158	146,473,032	150,047,156
	PV penetration [%]	12.81	13.35	15.60
	Excess energy [kWh]	790,362.0	829,664.1	1,019,677.6
90°	**Inverter capacity [MW]**	18	18	20
	Inverter output [MWh]	15,840	16,878	21,253
	PV output [MWh]	17,397	18,535	23,362
	Capacity factor [%]	9.93	10.58	13.33
	Grid sales [kWh]	144,239,903	145,277,258	149,650,887
	PV penetration [%]	11.90	12.58	15.35
	Excess energy [kWh]	722,605.7	768,456.0	990,162.0

Table 4.11: Albedo and slope analysis of stationary panels at 100 % radiation. The orange is the best performing case under an albedo of 0.25.

Slope ↓		Albedo ⟶		
		0.1 (Bare rock)	**0.25** (Grass)	**0.9** (Fresh snow)
40°	**Inverter Capacity [MW]**	12	12	12
	Inverter output [MWh]:	12,046	12,224	12,990
	PV output [MWh] :	13,013	13,206	14,042
	PV capacity factor [%]	7.43	7.54	8.02
	Grid sales [kWh]	140,445,838	140,623,276	141,389,064
	Excess energy [kWh]	332,159.9	338,770.6	368,225.1
50°	**Inverter capacity [MW]**	12	13	13
	Inverter output	11,871	12,142	13,311
	PV output [MWh]	12,834	13,130	14,405
	Capacity factor [%]	7.33	7.49	8.22
	Grid sales [kWh]	140,270,558	140,541,615	141,709,848
	Excess energy [kWh]	338,853.7	348,981.0	393,692.5
60°	**Inverter capacity [MW]**	12	12	13
	Inverter output [MWh]	11,505	11,886	13,522
	PV output [MWh]	12,446	12,861	14,646
	Capacity factor [%]	7.10	7.34	8.36
	Grid sales [kWh]	139,904,788	140,285,438	141,920,811
	Excess energy [kWh]	335,923.1	349,679.0	412,314.3
70.1°	**Inverter capacity [MW]**	12	12	13
	Inverter output [MWh]	10,975	11,480	13,641
	PV output [MWh]	11,876	12,427	14,783
	Capacity factor [%]	6.78	7.09	8.44
	Grid sales [kWh]	139,374,783	139,879,337	142,039,704
	Excess energy [kWh]	324,004.8	341,538.2	424,003.0
80°	**Inverter capacity [MW]**	12	12	13
	Inverter output [MWh]	10,294	10,931	13,646
	PV output [MWh]	11,140	11,831	14,792
	Capacity factor [%]	6.36	6.75	8.44
	Grid sales [kWh]	138,694,300	139,330,584	142,044,661
	Excess energy [kWh]	304,273.5	325,077.5	427,382.4
90°	**Inverter capacity [MW]**	12	12	13
	Inverter output [MWh]	9,442	10,218	13,519
	PV output [MWh]	10,215	11,057	14,652
	Capacity factor [%]	5.83	6.31	8.36
	Grid sales [kWh]	137,842,182	138,617,831	141,917,459
	Excess energy [kWh]	276,394.1	300,639.7	421,514.1

Table 4.12: Albedo and slope analysis on stationary panels at a 70 % radiation. The gray is the base case

Slope ↓	Albedo →			
		0.1 (Bare rock)	**0.25** (Grass)	**0.9** (Fresh snow)
40°	**Inverter capacity [MW]**	19	19	19
	Inverter output [MWh]	26,662	26,884	27,839
	PV output [MWh]	29,208	29,456	30,523
	PV CF [%]	16.67	16.81	17.42
	Grid sales [kWh/yr]	155,060,029	155,281,786	156,235,896
	PV penetration	18.48	18.61	19.16
	Excess electricity	1,156,580.1	1,142,486.4	1,218,846.2
50°	**Inverter capacity [MW]**	20	20	21
	Inverter output [MWh]	27,573	27,907	29,342
	PV output [MWh]	30,267	30,641	32,249
	PV CF [%]	17.28	17.49	18.41
	Grid sale [kWh/yr]	155,970,254	156,304,528	157,739,083
	PV penetration	19.03	19.22	20.02
	Excess energy	1,242,863.8	1,265,232.8	1,362,813.5
60°	**Inverter output**	21	22	22
	Inverter output [MWh]	27,886	28,352	30,345
	PV output [MWh]	30,648	31,170	33,404
	PV CF [%]	17.49	17.79	19.07
	Grid sale [kWh/yr]	156,283,634	156,749,481	158,742,538
	PV penetration	19.22	19.48	20.59
	Excess energy	1,294,680.4	1,326,111.7	1,461,678.9
70.1°	**Inverter capacity [MW]**	22	22	23
	Inverter output [MWh]	27,645	28,262	30,886
	PV output [MWh]	30,399	31,089	34,031
	PV CF [%]	17.35	17.74	19.42
	Grid sale [kWh/yr]	156,042,870	156,659,510	159,283,357
	PV penetration	19.09	19.44	20.90
	Excess energy	1,299,095.7	1,339,871.7	1,519,314.7
80°	**Inverter size [%]**	22	23	23
	Inverter output [MWh]	26,888	27,668	30,971
	PV output [MWh]	29,564	30,435	34,135
	PV CF [%]	16.87	17.37	19.48
	Grid sale [kWh/yr]	155,286,844	156,066,642	159,368,561
	PV penetration	18.67	19.11	20.95
	Excess energy	1,260,213.5	1,310,431.8	1,534,161.0
90°	**Inverter capacity [MW]**	22	22	23
	Inverter output [MWh]	25,609	26,568	30,609
	PV output [MWh]	28,137	29,205	33,725
	PV CF [%]	16.06	16.67	19.25
	Grid sale [kWh/yr]	154,007,480	154,966,462	159,006,150
	PV penetration	17.93	18.48	20.75
	Excess energy	1,179,999.7	1,238,729.0	1,505,826.2

Table 4.13: Sensitivity analysis of slopes of vertical axis tracking under 100% radiation. The orange cell marks the best performing case for an albedo of 0.25

Slope ↓		Albedo →		
		0.1 (Bare rock)	**0.25** (Grass)	**0.9** (Fresh snow)
40°	**Inverter capacity [MW]**	14	15	14
	Inverter output [MWh]	15,611	15,784	16,532
	PV output [MWh]	16,896	17,086	17,907
	PV CF [%]	9.64	9.75	10.22
	Grid sales [kWh/yr]	144,009,064	144,182,400	144,930,454
	Excess electricity	463,800.3	471,317.0	504,303.6
50°	**Inverter capacity [MW]**	15	15	15
	Inverter output [MWh]	15,827	16,091	17,228
	PV output [MWh]	17,148	17,437	18,685
	PV CF [%]	9.79	9.95	10.66
	Grid sale [kWh/yr]	144,225,087	144,489,103	145,626,168
	Excess energy	487,849.5	499,315.4	549,787.8
60°	**Inverter capacity [MW]**	15	16	16
	Inverter output [MWh]	15,760,157.63	16,130	17,717
	PV output [MWh]	17,085,256.50	17,490	19,233
	PV CF [%]	9.75	9.98	10.98
	Grid sale [kWh/yr]	144,158,626	144,528,176	146,115,395
	Excess energy	495,616.9	511,583.5	582,843.2
70.1°	**Inverter capacity [MW]**	16	16	17
	Inverter output [MWh]	15,426	15,915	18,008
	PV output [MWh]	16,727	17,263	19,561
	PV CF [%]	9.55	9.85	11.16
	Grid sale [kWh/yr]	143,824,707	144,313,397	146,406,424
	Excess energy	489,191.6	510,100.1	604,343.7
80°	**Inverter size [%]**	16	16	17
	Inverter output [MWh]	14,852	15,468	18,096
	PV output [MWh]	16,104	16,778	19,662
	PV CF [%]	9.19	9.58	11.22
	Grid sale [kWh/yr]	143,251,196	143,867,100	146,494,406
	Excess energy	470,461.0	495,503.6	612,855.7
90°	**Inverter capacity [MW]**	16	16	17
	Inverter output [MWh]	14,032	14,784	17,979
	PV output [MWh]	15,211	16,031	19,533
	PV CF [%]	8.68	9.15	11.15
	Grid sale [kWh/yr]	142,430,920	143,182,641	146,376,868
	Excess energy	440,462.1	469,022.9	608,209.0

Table 4.14: Sensitivity analysis of slopes of vertical axis tracking under 70% radiation. The orange cell marks the best performing slope under an albedo of 0.25

Sensitivity case: Albedo and radiation for horizontal axis tracking systems

The horizontal axis tracking system essentially changes the slope according to the elevation movement of the sun. As discussed did the stationary panels at a 70% radiation at its best performing slope produce $\sim 12200MWh$. The horizontal axis tracking system yields $\sim 13650MWh$ at the same radiation and albedo. This is a relative increase of 9.4 %. For a 100% radiation with a 0.25 albedo scenario will the stationary panels at their optimal angle produce $\sim 19,700MWh$, while the horizontal tracking system produce approximately 22, 830MWh. This corresponds to a relative increase of 16 %. The benefits for using horizontal tracking systems seems to increase with increasing radiation. This is not surprising given that *HOMER* assumes that when radiation increases will the direct radiation rise, while the diffuse radiation diminishes. The benefits of having the panels in the direction of the sun will increase when a larger part of the radiation is actually directed towards the panels as opposed to a scenario with high amounts of diffuse radiation were the radiation is spread in all directions. The yield under a radiation of 70 % an albedo of 0.25 is $738.40MWh/MW_p$, while for a radiation of 100 % will it be$1250MWh/MW_P$. For a 130 % radiation becomes the yield $1548MWh/MW_p$.

To sum up the tracking strategies did the horizontal axis tracking give a relative increase in power output of 9.4 % compared to stationary panels, while the vertical axis tracking gave an increase of 32 % under 70% radiation. The reason for the relative poor performance of the horizontal axis tracking system might have something to do with the latitude at Fakken. The sun has rarely a very high elevation which cancels some the benefits of horizontal axis tracking. If the horizontal axis tracking had used sensors to track the lightest spot on the sky, could maybe the horizontal axis tracking be more favourable, especially regarding that quite low tilt angle proved to be favourable for stationary panels. The high performance of vertical axis tracking is perhaps the most favourable of the two since the sun shines at highly varying azimuth angles at high latitudes, and it enables the system to benefit from the high amount of solar hours during summer and spring.

Supposed that the cost difference between horizontal axis tracking installations and vertical axis tracking installations are negligible, will the vertical axis tracking system be by far the most favourable. The horizontal axis tracking system will therefore be disregarded from the further investigations.

Global solar ↓ radiation	Albedo →	0.1 (Bare rock)	0.25 (Grass)	0.9 (Fresh snow)
70%	**Inverter capacity [MW]**	12	12	13
	Inverter output [MWh]	13,375	13,657	14,872
	PV output [MWh]	14,458	14,768	16,107
	PV CF [%]	8.25	8.43	9.19
	Grid sales [MWh/yr]	141,773,884	142,056,067	143,269,637
	PV penetration[%]	10.09	10.28	11.11
	Excess electrical [kWh]	378,764.0	392,071.7	452,581.9
100%	**Inverter capacity [MW]**	19	19	20
	Inverter output [MWh]	22,471	22,835	24,397
	PV output [MWh]	24,591	24,999	26,754
	PV CF [%]	14.04	14.27	15.27
	Grid sales [kWh/yr]	150,868,603	151,232,512	152,793,933
	PV penetration[%]	16.03	16.25	17.20
	Excess electrical [kWh]	938,202.6	963,411.6	1,074,018.8
130%	**Inverter capacity [MW]**	22	22	23
	Inverter output [MWh]	27,695	28,106	29,861
	PV output [MWh]	30,501	30,964	32,949
	PV CF [%]	17.41	17.67	18.81
	Grid sales [kWh/yr]	156,093,022	156,502,971	158,257,959
	PV penetration[%]	19.14	19.38	20.37
	Excess electrical [kWh]	1,347,846.7	1,379,221.8	1,516,598.9

Table 4.15: Horizontal axis tracking sensitivity analysis for albedo and solar radiation

Sensitivity case: Inverter and PV module efficiency

In the efficiency analysis has the different PV and inverter efficiencies been tested at 70% radiation both for stationary panels and for a two axis tracking scenario. An inverter efficiency of 99 % is also tested for stationary and vertical axis tracking panels at 100% and 70% radiation.

The yields for 17 %, 20 %, 23 % and 30 % efficient modules are 659, 660, 662, 664 MWh/WW_p, respectively. The yields are therefore quite low, even for Scandinavia. The yields do not differ significantly when the efficiency of the modules increases. Table 4.16 sum up the most important findings for stationary panels when increasing the PV module efficiency. The relative elevation in inverter output by switching from PV modules with a 17 % efficient to modules with 30 % efficiency is 76 % in relative gain, corresponding to 7,912 MWh with an inverter effiiency of 95 %. If the inverter efficiency is 99 % is the difference in inverter output for 17 % and 30 % efficient panels 8,235 MWh, also

corresponding to a relative difference of 76 %. 8,235 MWh is the approximate energy consumption of 407 households in 2012 [83]. The results shows that the power output benefits of investing in very high efficient solar panels and inverters are good if the cost rise of installing high efficient components is modest. Figure 4.13 shows how the inverter output varies with increasing PV module efficiency for inverters of 95 % and 99 % efficiencies. The outputs are seen to have a linear growth, where the 99 % efficient inverter has a slightly steeper absolute growth rate. At a PV module efficiency of 30 % is the power output difference almost 1 MWh/yr while for 17 % efficient panels is the difference approximately 0.5 MWh/yr when 95 % and a 99 % efficient inverters are applied. The figure also confirms that increasing the PV module efficiency by a couple percentage points is more advantageous than increasing the inverter efficiency by 5 percentage points.

When two axis tracking systems are applied are the absolute differences of replacing 17 % efficient panels with 30 % efficient panels 10,475 MWh and 10,897 MWh for inverter efficiencies of 95 % and 99 % respectively. Both these inverter output growths corresponds to a relative difference of 76 %, exactly like in the stationary panel scenario.

The yields for two axis tracking systems under 17 %, 20 %, 23 % and 30 % efficiencies are 874, 876, 878, 884 MWh/MW_p respectively. These are yields that are considered to be acceptable in Scandinavia.

The increased efficiencies in inverters and PV modules boosts the grid sales, but produces slightly more excess energy. This is caused by the limitations on the electricity grid which will occur when wind power production is sufficient in covering the electricity line capacity resulting in that only limited PV power production can access the grid. When the PV output increases will the excess electricity increase too. If very efficient systems are used, should the system size be reduced to be more cost efficient.

There is generally more power gain in increasing the efficiency of the PV modules rather than increasing the inverter efficiency. However, the highest efficiency recorded for silicon a PV cell is 26.3 % [81], while inverter efficiencies approaching 99 % (98.2 %) are already commersially available [80]. In section 2.9 was different solar integration to grid configurations described, were some are more efficient than others. The use of very efficient grid connection strategies will increase the system cost. The standard for large scale PV systems are to use centralized converters. The results in this thesis is that there is more to gain in increasing the PV module efficiency than to use a very sophisticated inverter strategy, which would also increase the maintenance requirements for the system. However, increasing the efficiency of the centralized inverter can be a physical opportunity that is not far from reality today. Highly efficient panels

are likely to be more costly than panels with low efficiency panel. The use of high efficient panels will also demand bigger inverter capacities, and thus increase the system cost. In this thesis are all inverter capacities scaled up to the closest integer in MW to partly count for the fact that radiation will vary from year to year. If the PV utility was to be installed should a more careful analysis on the best fitting inverter capacity be conducted, and bigger dissimilarities would appear between the scenarios with different efficiencies.

An efficiency of 23 % on the panels should be realistically achievable. Compared to the 20 % efficient panels will they increase the output by 1,826 MWh corresponding a relative increase of almost 15 % if the inverter efficiency is 95 %. If the inverter capacity is also increased to 99 % will the gain be of almost 20 %, or 2,407 MWh. This equals the annual energy demand of 119 Norwegian households [83].

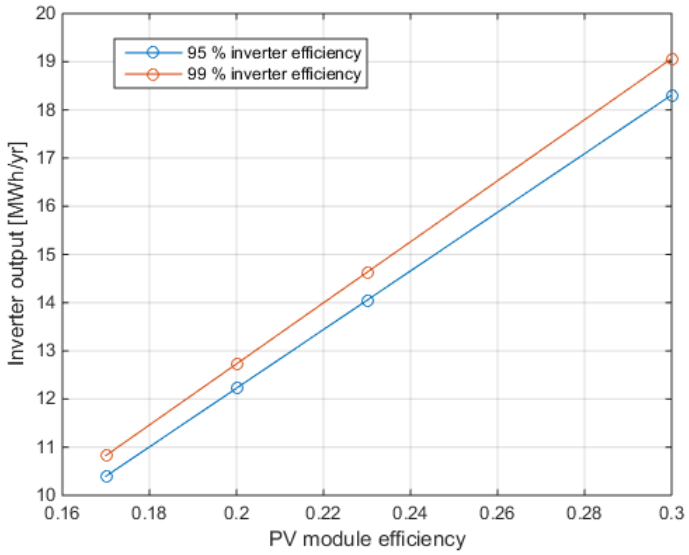

Figure 4.13: Sensitivity of inverter and PV module efficiency

Figure 4.14 and table 4.18 presents the electrical output of stationary panels and vertical axis tracking configuration when the inverter efficiency is 99 % at different radiations. Figure 4.14 confirms that the benefits when it comes to absolute power production of using a high-efficient inverter is somewhat more prominent if the PV array can absorb high amounts of power, such as when the radiation is high and/or tracking is applied to the system. The results in table 4.18 can be compared to similar simulated cases in section 4.2 and

PV ↓ Efficiency	Inverter efficiency →	95 %	99 %
17%	Inverter capacity [MW]	10	10
	Inverter output [MWh]	10,398	10,829
	PV output [MWh]	11,204	11,204
	PV capacity factor [%]	7.52	7.52
	Grid sales [kWh]	138,797,460	139,228,203
	PV penetration [%]	8.00	8.00
	Excess energy [KWh]	258,599.5	265,580.4
20%	Inverter capacity [MW]	12	17
	Inverter output [MWh]	12,224	12,729
	PV output [MWh]	13,206	13,206
	PV capacity factor [%]	7.54	7.54
	Grid sales [kWh]	140,623,276	141,129,518
	PV penetration [%]	9.30	9.30
	Excess energy [KWh]	338,770.6	348.196.6
23%	Inverter capacity k[MW]	13.100	14
	Inverter output [MWh]	14,050	14,631
	PV output [MWh]	15,217	15,217
	PV capacity factor [%]	7.55	7.55
	Grid sales [kWh]	142,449,005	143,029,385
	PV penetration [%]	10.56	10.56
	Excess energy [KWh]	426,968.9	438,183.0
30%	Inverter capacity k[MW]	17.200	18
	Inverter output [MWh]	18,309	19,063
	PV output [MWh]	19,938	19,938
	PV capacity factor [%]	7.59	7.59
	Grid sales [kWh]	146,707,582	147,461,470
	PV penetration [%]	13.40	13.40
	Excess energy [KWh]	665,270.3	682,373.8

Table 4.16: Stationary panels efficiency and radiation

PV Efficiency ↓	Inverter efficiency →		
		95 %	**99 %**
17%	**Needed inverter size [MW]**	14	14
	Inverter output [MWh]	13,738	14,307
	PV output [MWh]	14,858	14,858
	PV CF [%]	9.98	9.98
	Grid sales [kWh/yr]	142,137,743	142,705,756
	PV penetration [%]	10.34	10.34
	Excess electrical [kWh/yr]	396,678.7	407,123.3
20%	**Needed inverter size [MW]**	16	17
	Inverter output [MWh]	16,156	16,823
	PV output [MWh]	17,525	17,525
	PV CF [%]	10.00	10.00
	Grid sales [kWh/yr]	144,554,370	145,221,589
	PV penetration [%]	11.97	11.97
	Excess electrical [kWh/yr]	519,099.2	532,131.3
23%	**Needed inverter size [MW]**	20	20
	Inverter output [MWh]	18,574	19,338
	PV output [MWh]	20,205	20,205
	PV CF [%]	10.03	10.03
	Grid sales [kWh]	146,971,997	147,736,734
	PV penetration [%]	13.56	13.56
	Excess electrical [kWh]	654,247.1	671,630.9
30%	**Needed inverter size [MW]**	25	26
	Inverter output [MWh]	24,213	25,204
	PV output [MWh]	26,514	26,514
	PV CF [%]	10.09	10.09
	Grid sales [kWh]	152,611,097	153,601,632
	PV penetration [%]	17.07	17.07
	Excess electrical [kWh/yr]	1,026,122.1	1,055,302.8

Table 4.17: Two axis tracking, albedo 25, converter sizes: efficiency and radiation

Stationary panels 70% radiation 40° slope	**Needed inverter size [MW]**	12
	Inverter output [MWh]	12,729
	PV output [MWh]	13,206
	PV CF [%]	7.54
	Grid sales [MWh]	141,128
	PV penetration [%]	9.30
	Excess electrical [kWh/yr]	348,196
Stationary panels 100 % radiation 50° slope	**Needed inverter size [MW]**	19
	Inverter output [MWh]	20,489
	PV output [MWh]	21,576
	PV CF [%]	12.32
	Grid sales [MWh/yr]	148,887
	PV penetration [%]	14.35
	Excess electrical [kWh/yr]	880,235
Vertical axis tracing system 70 % radiation 60° slope	**Needed inverter size [MW]**	17
	Inverter output [MWh]	16,796
	PV output [MWh]	17,490
	PV CF [%]	9.98
	Grid sales [MWh/yr]	145,194,195
	PV penetration [%]	11.95
	Excess electrical [kWh/yr]	524,757.1
Vertical axis tracing system 100% radiation 60° slope	**Needed inverter size [MW]**	22
	Inverter output [MWh]	29,559
	PV output [MWh]	31,223
	PV CF [%]	17.82
	Grid sales [MWh/yr]	157,956,028
	PV penetration [%]	19.51
	Excess electrical [kWh/yr]	1,366,407.5

Table 4.18: Inverter efficiency: 99%. Output for stationary panels at a 40° tilt angle under different topologies

Bifacial panels

The results turned out to be very unrealistic, and not worthy of presenting in this thesis. It is saved for the section on further work (section 5.3.

4.2.1 Summary of the technical sensitivity analysis

Until now has the sensitivity analysis concerned the examination of how different physical and technological parameters will affect the power output of the

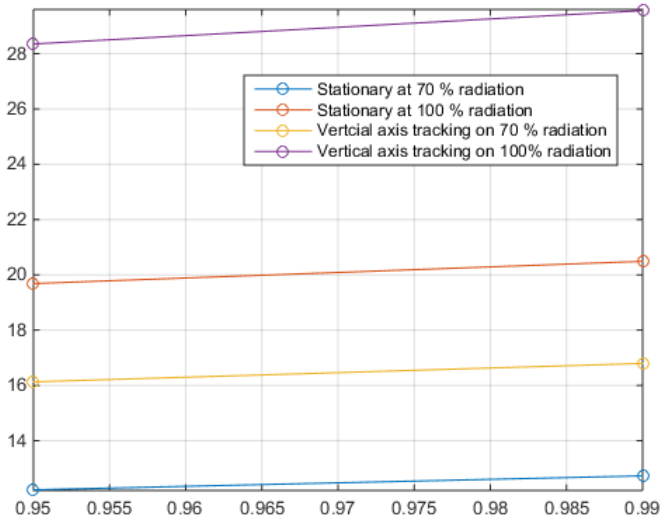

Figure 4.14: Sensitivity analysis of inverter efficiency

system. These analysis has enabled the selection of the most relevant systems for further investigations. The albedo is set at a constant value of 0.25 also in the economical analysis because of reasons already discussed. Since a radiation of 70 % is believed to be more realistic will this be given most focus in the economical analysis. Stationary panels will still be the center of attention, but a simple economical analyses will be conducted on the vertical axis tracking system too. The reasons for why the vertical axis tracking system is given more attention is because it performed significantly better than the horizontal axis tracking system in addition to performing almost as good as the two axis tracking system when the tilt angle was set to 60°. This is demonstrated in figure 4.16. It is assumed that the two axis tracking system is costlier than the vertical axis tracking system and that the vertical axis tracking system will be a more economically viable option.

Figure 4.15 shows the power output for stationary panels facing south with a 40° slope under 70 % radiation. It shows that Solar output contributes to the power generation mostly during the second and third quarters of the year. For the fourth quarter is the solar power production almost absent. The contribution is highest during daytime, which corresponds well with electricity consumption generally. The figures indicate that a solar power installation at Fakken can increase the utilization of the extra grid capacity during summer.

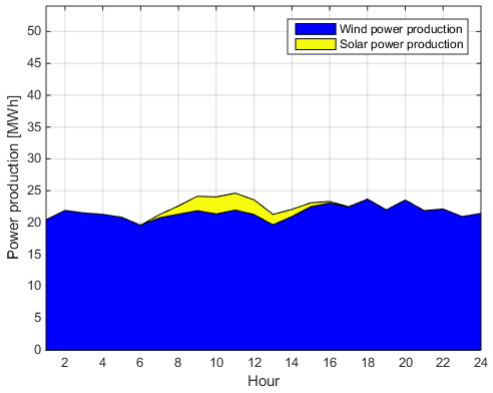

(a) First quarter of 2016

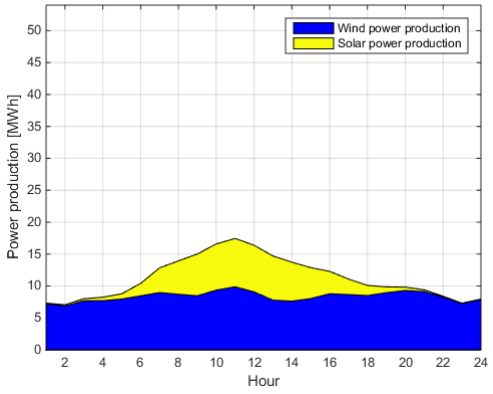

(b) Second quarter of 2016

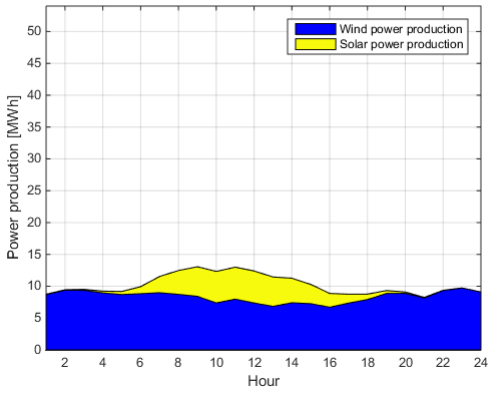

(c) Third quarter of 2016

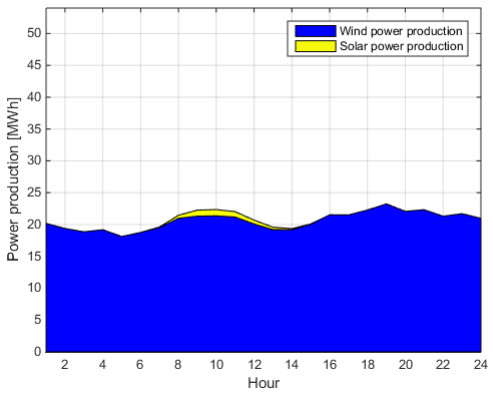

(d) Fourth quarter of 2016

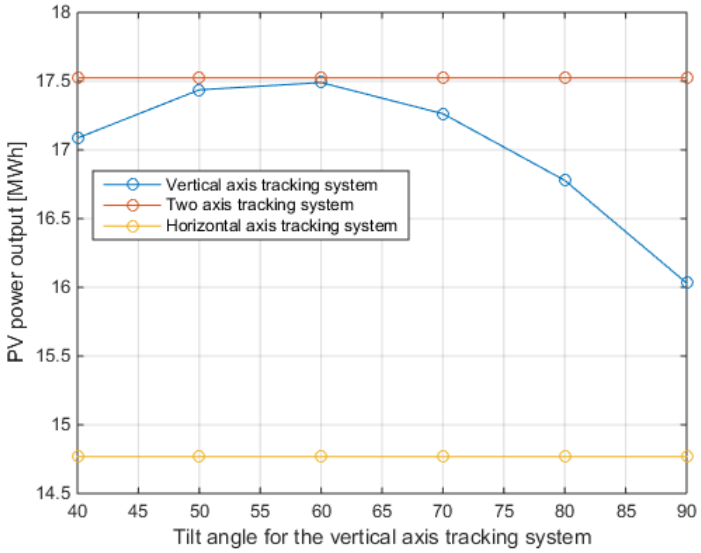

Figure 4.16: Sensitivity between Vertical axis tracking, horizontal axis tracking and two axis tracking

4.2.2 Economic analysis of the most relevant cases

Table 4.19 presents the cost analysis on the most relevant topologies for stationary panels. Both 100 % radiation and 70 % radiation scenarios are included in the table. The best performing scenario at a 70 % radiation is marked in orange because this is the scenarios appears to be the most realistically achievable scenario. This scenario will also lay the basis on some sensitivity analysis on the economic parameters that can affect the system's profitability.

Each technological/ physical scenario is displayed over three rows, where the uppermost row in each case represents the economical parameters when the system cost is equal to the estimated cost as described in section 3.3. These scenarios are marked in blue if the radiation is assumed to be 100 % and in green if the radiation is 70 %. The middle and lowest row represents the economical scenario if the capital cost is 30 % lower and 30 % higher respectively. Table 4.20 presents the economical findings for vertical axis tracking systems at a 60° slope at both radiation levels. Three cost routes are displayed, were the uppermost is the estimated cost for stationary panels, the middle and lowest rows are the cost scenarios if the capital costs increases by 40 % or 80 % respectively, compared to the stationary panels. The inverter cost is assumed not to change when the PV module cost changes. The increased cost compared to the stationary cases at identical radiation are results of higher power production and thus a demand for higher inverter sizes.

Non of the scenarios succeed in obtaining either a positive net present value or low enough LCOE values. The LCOE's should essentially be lower than the average electricity price in Tromsø, this for the installation to be profitable. The average electricity price in Tromsø for 2016 was 0.2326 NOK/kWh.

If the radiation turns out to be closer to 100 % of the WRF simulated data instead of the 70 % estimate and the solar panel tilt angles are adjusted to this fact, can 15.5 millions in net present value be saved compared to the most realistic case marked in orange. If the project proceeded without accounting for the error in the WRF model simulations and the panels were installed at a 50° tilt angle as optimized for a 100 % radiation would the NPV decrease by 100,000 NOK, which is not a significant value in light of the high uncertainty that accompanies both the radiation data and cost estimate. Both scenarios has very high LCOE values and very low NPV values.

If the panels are installed at a 70.1° according to the base case scenarios will the project loose 2.15 millions more if the radiation is 70 % and 3.73 millions if the radiation is 100 %.

Vertical axis tracking profitability

When comparing table 4.19 and table 4.20 is it clear that under the assumptions done in this thesis, are the tracking strategies less economically viable than stationary systems. A trial and error test is conducted in Matlab to investigate how much higher the capital cost of the tracking system can be and still be as economically profitable as the stationary case marked in orange. It is here assumed that the inverter cost is the same as before while the PV module cost will increase by some factor. The discount rate is assumed to be 5 % as usual, and the radiation is 70 % of the *WRF* simulated data. The results of this investigation is that the tracking system can be a multiplying factor of 1.0348 times the best cost estimate for stationary panels and obtain the same NPV. In other words can the cost increase be 3.48 % compared to the stationary panels. The LCOE of this tracking system will be 1.0026 NOK/kWh, which is lower than the LCOE for the stationary system.

Radiation/ Slope/ Efficiency	Cost scenario	Capital cost PV	Capital cost inverter	PV O&M costs	Inverter O&M costs	Grid sales [NOK]	LCOE [NOK/kWh]	NPV [NOK]
Radiation: 100%	**Estimated cost**	150,000,000	1 7,500,000	40,167,742	4,932,881	55.018 mill	0.8406	-159.4 mill
slope: 70.1°	**Low cost**	100,000,000	8,873,000	28,187,889	2,535,923	55.018 mill	0.5604	-87.939 mill
Efficiency: 20%	**High cost**	200,000,000	17,727,000	56,375,778	5,007,579	55.018 mill	1.1208	-230.86 mill
Radiation 100%	**Estimated cost**	150,000,000	12,600,000	42,281,834	3,551,674	57.586 mill	0.8048	-155.67 mill
Slope: 50°	**Low cost**	100,000,000	8,406,000	28,187,889	2,402,454	57.586 mill	0.5366	-84.593 mill
Efficiency: 20 %	**High cost**	200,000,000	16,794,000	56,375,778	4,744,022	57.586 mill	1.0731	-226.74 mill
Radiation: 70%	**Estimated cost**	150,000,000	8,400,000	42,281,834	2,367,783	32.951 mill	1.3353	-173.31 mill
Slope 70, 1°	**Low cost**	100,000,000.00	5,604,000.00	28,187,889	1,601,636	32.951 mill	0.8903	-104.56 mill
Efficiency: 20 %	**High cost**	200,000,000	11,196,000	56,375,778	3,162,681	32.951 mill	1.7804	-242.06 mill
Radiation: 70%	**Estimated cost**	150,000,000	8,400,000	42,281,834	2,367,783	35.105 mill	1.2541	-171.16 mill
Slope: 40°	**Low cost**	100,000,000	5,604,000	28,187,889	1,601,636	32.951 mill	0.8361	102.41 mill
Efficiency: 20%	**High cost**	200,000,000	11,196,000	56,375,778	3,162,681	35.105 mill	1.6720	-239.91 mill
Radiation: 70%	**Estimated cost**	150,000,000	8,400,000	42,281,834	3,748,989	35.001 mill	1.2624	-171.26 mill
Slope: 50°	**Low cost**	100,000,000	5,604,000	28,187,889	1,601,636	35.001 mill	0.8417	102.51 mill
Efficiency: 20%	**High cost**	200,000,000	11,196,000	56,375,778	3,162,681	35.001 mill	1.6832	-240.01 mill

Table 4.19: Economical analysis of stationary panels with different slopes exposed to different radiation levels

System	Cost scenario	Capital cost PV	Capital cost inverter	Inverter O&M costs	PV O&M costs	Grid sales [MWh]	LCOE [NOK/kWh]	NPV [NOK]
Radiation: 100 %	**Base case cost**	150,000,000	15,400,000	42,281,834	4,340,935	83.851	0.5699	-110.99 mill
Efficiency: 20%	**40% increase**	210,000,000	15,400,000	59,194,567	4,340,935	83.851	0.7711	-210.98 mill
Slope: 60°	**80% increase**	270,000,000	15,400,000	76,107,301	4,340,935	83.851	0.9723	-287.89 mill
Radiation:70%	**Base case cost**	150,000,000	11,200,000	42,281,834	3,157,044	46.453	0.9718	-164.47 mill
Efficiency: 20%	**40 % increase**	210,000,000	11,200,000	59,194,567	3,157,044	46.453	1.3261	-241.38 mill
Slope: 60°	**80 % increase**	270,000,000	11,200,000	76,107,30	3,157,044	46.453	1.6805	-318.30 mill

Table 4.20: Economical analysis of Vertical axis tracking strategy if the cost is 40%-80 % higher than the base cases

Discount rate

Figure 4.17 displays how the NPV's and LCOE's will change according to the discount rate. Also here is the case with stationary panels at 70% radiation and tilt angles of 40° used as the basis. Discount rates between 2 % and 8 % are tested. For the estimated and high cost scenario did the NPV grow for increasing discount factor. High discount rates expresses that that the value of money decreases rapidly. The way the NPV values responds to the discount factor indicates that the operation and maintenance costs during the lifetime of the project is higher than the revenue stream from the grid sales. For the low cost scenario is the opposite trend observed. The operation and maintenance costs are set to be depending on the capital costs. Low capital costs will therefore give low maintenance costs. The negative trend indicates that the grid sales exceeds the operation and maintenance cost during the project lifetime such that when the money looses its value fast will it result in more lost value for the system.

For all cost scenarios will the LCOE grow for increasing discount rate. This an expected result since the capital costs of the system is high while the grid sales are more moderate and varies less over the lifetime of the project. A high discount rate makes the capital cost more dominant in the lifetime analysis. Changing the discount factor does not make the system profitable.

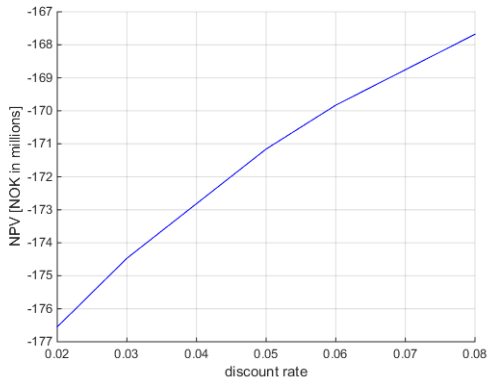

(a) NPV for estimated cost

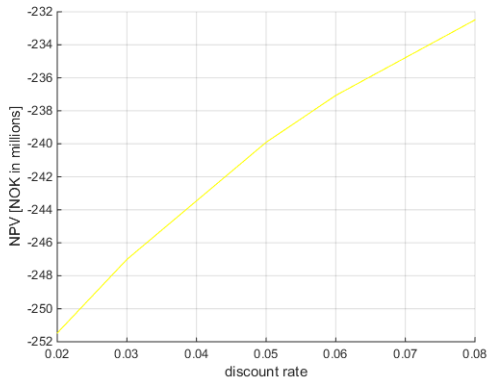

(b) NPV for high cost scenario

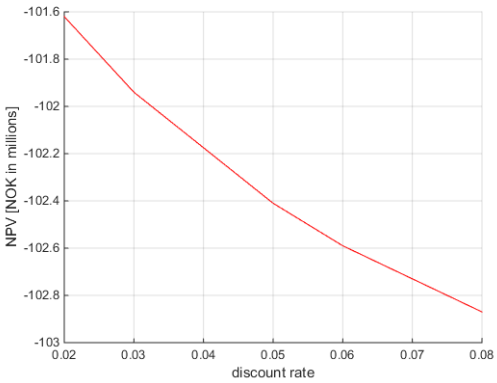

(c) NPV for low cost scenario

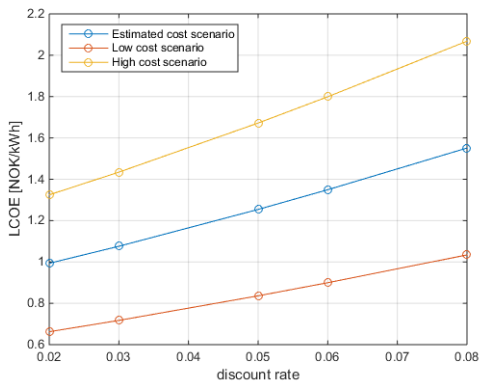

(d) LCOE sensitivity for all cost scenarios

Figure 4.17: Sensitivity of discount rate on NPV and LCOE

Electricity prices

The main obstacles for PV installations in Norway is assumed to be caused by the low electricity prices and the high installation cost in addition to the physical limitation of modest solar radiation. Until now has the solar radiation sensitivity and the cost sensitivity been tested. The NPV response is displayed in figure 4.18. The figure shows that the NPV increases when the electricity price increases, but even when the prices are twice as high as the estimated prices from Nord Pool, will the system still be economically unprofitable and have a negative NPV. If the prices are doubled will the project still have a loss of roughly 137 millions in discounted value.

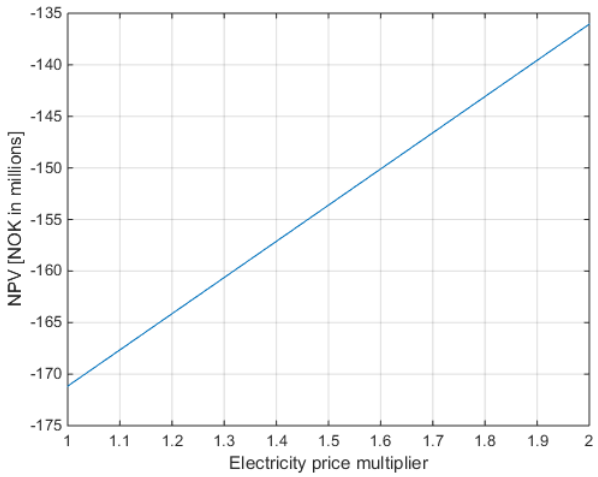

Figure 4.18: NPV sensitivity of electricity prices

Future scenario

An albedo of 0.25 and a radiation of 70 % is assumed as the physical parameters are not expected to change. The system appears to still be economically unprofitable. By trial was it found that the electricity price has to be multiplied by 4 in order to achieve positive NPV. If the capital cost for PV becomes 1,500 NOK /kW and the capital cost of the inverter becomes around 140 NOK/kW will the LCOE reach 0.2412 NOK/kWh. These prices are correspond to 20 % of the best estimated cost of today.

Inverter capacity	18
Capital cost PV	150,000,000.00
Capital cost inverter	14,010,000.00
PV O&M costs	42,281,833.70
Inverter O&M costs	4,004,089.65
Grid sales [NOK]	55.865 mill
LCOE	0.8040
NPV	-150.41 mill

Table 4.21: Future scenarios with 30 % efficiency and low system costs

Discussion of the azimuth angle correction

It was discovered that an azimuth angle of 300° (more eastwards) was optimal and gave 11 % more in inverter output for year 1 for stationary panels than having the panels facing south (0°). For horizontal axis tracking is the inverter output relative difference 8 %. All literature ever read on the subject has recommended an azimuth angle facing south. This result shows that the *WRF* simulations have even more errors than first assumed. Using this angle might give a more realistic view on the potential solar power production at site.

The fact that a slope of 300° is optimal is a result from the offset error in the *WRF* simulations. The azimuth angle differs 60° from the conventional way of installing PV panels, which suggests that the simulated radiation is shifted 4 hours forward from what should be expected by the calculated solar path in *HOMER*. This difference is remarkably high and tells a lot about how much uncertainty there is in the simulations.

For stationary panels are the yield is $736 MWh/MW_p$, and not surprisingly higher than for panels facing south which was $660.3 MWh/MW_p$. The grid sales will therefore improve.

The NPV and LCOE is improved for the system when the azimuth angle is corrected for. For the scenario that is equivalent to this system except for this correction will the relative increase in NPV be 1.32 %. The LCOE will be reduced by 10 %. The absolute difference in NPV is 2.23 million NOK. The absolute change in LCOE is 0.1411 NOK. The profitability of the system is therefore not very much affected by this error.

The difference in output for the sensitivity cases are assumed to have similar variabilities when the azimuth correction is applied. The power output is also assumed to be shifted forward in time since the azimuth angle faces a more eastward direction and will absorb more energy early on a daily basis.

Figure 4.11 shows how the stationary panel starts later on the day in producing power than the vertical axis tracking system, while the daily power production declines at nearly the same time. This is probably due to the offset in the *WRF* model.

4.3 Sources of errors

This section is assigned for a summary of the most significant sources of errors in this thesis. The error sources introduced by the shortcomings of the *WRF* model results have already been discussed at length, while other less complicated sources of errors will only be discussed in this section.

- **The *WRF* model:** The errors in the simulations conducted by the model serves as the most severe source of errors in this thesis. It affects all of the simulations and the impact of the errors can not be directly calculated either. The result is that the simulations are conducted with unknown uncertainties in the most important factor affecting the electrical power output and thus also the economical profitability of the project.

- **Weather and climate variability:** *HOMER* assumes that the radiation will be constant for the whole lifetime of the project. This will not be the case in reality, and the grid sales will differ from year to year.

- **Temperature and PV efficiency:** The temperature time series is might be affected by the heat from the nacelle at which it is located. The temperature might therefore be lower than the temperature implemented to *HOMER*. The program does not count for the cooling effect that wind exerts on the PV panels either. Both these factors makes it reasonable to believe that the cell temperature can be lower than *HOMER* predicts. This will underestimate the power production since low cell temperatures has a positive effect on cell efficiency.

- **Temperature effects in Wind power:** The temperature affects the density, and thus the power output form the turbines. The reasons for why this effect was not considered is explained in section 3.5. The power production from the turbines should therefore be slightly higher. This is not considered to be a serious issue since Troms Kraft reported that the power losses should be set to 0.8 % although it was assumed to be somewhat higher. The lower temperature assumed might count for these losses to some degree, and actually produce a more realistic power output. However, if this is not the case will the PV arrays produce some more excess power than the simulations recorded.

- **Cost and price estimates** The cost estimates in this thesis was based on very limited data even if serious effort was put to the task. The estimate was made on the basis of a conversation with Solbes [96] and on estimates for systems of considerably smaller sizes. There are also high uncertainty in the future electricity prices that are implemented due to the many variables that has impact on this issue.

- **Calculation of NPV** The uncertainties in the NPV calculation is already discussed in section 3.6. The method used is not flawless, but it was assumed to be the best strategy available for achieving the most reliable result as possible. The errors in the method are assumed to be small.

- **Tracking:** The tracking methods used do not exert active tracking. At a location like Fakken, with a low radiation will probably active tracking perform better than passive tracking.

4.4 Comparison with Skiboth

Master student Karoline Ingebrigtsen has performed an analysis similar to this thesis for the feasibility of a large-scale solar, wind and hydro power system in Skibotndalen in Troms. For the most realistic conditions for the site did a yield of Yields of 826 MWh/MW_p and 933 MWh/MW_p was achieved when the offset error was not corrected for and when it was, respectively. Comparing these yields obtained in this thesis of respectively 660 MWh/MW_p and 736 MWh/MW_p was obtained under the most realistic conditions at Fakken. At Skibotn was the daily anti correlation better for all three months with available solar radiation data. The daily correlation coefficients at Fakken is -0.0951, -0.1243 and -0.3569 for February, March and April respectively, while at Skibotn are the corresponding values -0.26, -0.23, and -0.53 respectively. The total solar radiation during these months was in Fakken 151 kWh/m^2 while it was 933 kWh/m^2 during the same time period at Skibotn. It can therefore be concluded that Skiboth is a more optimal location for solar power installations. It is likely that this is has to the colder temperatures, higher radiation, dry climate, albedo together with the higher anti correlation.

5

Conclusion and Further Work

5.1 Summary

The *WRF* model generally overestimates the solar radiation at Fakken such that the observed global radiation is only 70-72 % of the simulated data during one year. The difference is most striking for June, where the observed values on average are 57 % of the simulated radiation. However, the correlation between the observed and simulated data are generally high, especially when the correlation factor is calculated over a whole year. The *WRF* data exposed a very unfortunate offset compared to the observed radiation on average. The findings resulted in scaling down of the *WRF* simulated data by multiplying the radiation with 0.7 for many of the simulations conducted in *HOMER*. It was not discovered until the last 24 hours until the deadline that the offset could be corrected for by optimizing the azimuth angle of the solar panels. The optimal azimuth angle was 300°, which exposes a severe error in the *WRF* simulation. It is assumed to be likely that changing this angle will give a more reliable result than having the panels facing south. The correction was conduced on two simulations in order to obtain a basis for comparing with scenarios were the azimuth was set to 0°. The comparison revealed that stationary panels under a 70 % radiation with optimal tilt would produce 11 % more if the correction was counted for. But the economic impact on the

system was negligible. The yield improved from 660 MWh/MW_p to 736 MWh/MW_p.

The anti correlation analysis of the observed solar and wind resources at Fakken for February, March and April 2017 revealed almost no anti correlation at all. It is assumed that this could have improved if both data sets were available for a whole year to compare. The correlation analysis between the simulated solar data and observed wind data at Fakken were close to zero for time scales smaller than 24 hours. With increasing time scale did the anti correlation improve, but it was only considered to be high for a monthly time scale, were it reached -0.86. The anti correlation could have improved if the offset error were absent.

Several sensitivity analyses were conducted to test the sites vulnerability to variables affecting the feasibility of the system. Since the objective is to increase the production during summer season to obtain higher grid utilization, is it considered most appropriate to install the system such that it is optimized for summer conditions. This means that the system should be optimized at an albedo of approximately 0.25. The best slopes depends on the radiation. A slope of 40° perform best at a 70 % radiation while a slope of 50° was optimal for a radiation of 100 %. However, a system installed at a location with a very high albedo large parts of the year could theoretically produce between 6.3-19 % more power than at Fakken, with everything else being equal.

Horizontal axis tracking systems did not produce nearly as much power as the vertical axis tracking and the two axis tracking. The differences in power output for the vertical axis tracking and two axis tracking was not significant if the vertical axis tracking system had a slope of 60°. Tracking strategies was generally most beneficial under high illuminations. The yields for the tracking strategies under a 70 % radiation and an albedo of 0.25 was 874 MWh/MW_p, 738.4 MWh/MW_p, and 876 MWh/MW_p for the vertical axis, horizontal axis and two axis tracking strategy respectively.

The system appeared to be more sensitive to the efficiency of the PV modules rather than the inverter efficiency. For such a large system as 20 MW is, can large amounts of energy be saved by increasing the efficiency. Higher efficiencies of the components will generally increase the cost of the system.

The economical analysis revealed that non of the systems obtained positive NPV's. Neither changing the electricity prices, increasing the system efficiency, changing the discount rate nor reducing the system cost did

result in a profitable system. The NPV and LCOE was also calculated for the most relevant stationary system when the azimuth angle was optimized. The NPV improved, but was still negative.

A vertical axis tracking system was evaluated to be the most economical tracking configuration for the site, as long as a tilt of 60° was applied. It did not give the system a higher profitability compared to stationary panels unless the two configurations had approximately the same price range.

The future scenario proved that even if the efficiency of both the inverter and the module efficiencies improved would still not the system be profitable. The system cost had to reduce to 20 % of today's best estimated cost or the electricity prices has to be multiplied by four for the system to become profitable. It is assumed that higher efficiency on the PV panels could improve the NPV and LCOE quite substantially.

5.2 Concluding remarks

The technical analysis indicates that it is possible to extract large amounts of PV power at Fakken to improve grid utilization during summer, but will most likely not be profitable yet. Variables that affect the profitability the most appears to be the radiation and the costs. The sources of errors in this thesis has proven to be quite severe. The errors in the technical analysis was mostly due to the errors in the *WRF* model. The uncertainties in the economical analysis was partly because of the uncertainties in the cost estimates and partly because of the uncertainties in the radiation levels.

5.3 Future Work

Acquiring more precise data

Several factors has influenced the reliability in the results presented in this thesis. The further work will mainly concern finding more reliable parameters that affects the performance of the system.

The sensitivity analyses in this thesis clearly exposed how vulnerable the system is to the radiation at site. The first priority should be to wait for the pyranometer at Fakken to record the radiation for a whole year and

make an evaluation based on the results if the project analysis should be proceeded.

This thesis has only looked at PV systems with capacities of around 20 MW. As a result will the system produce some excess electricity than can not be sold to the grid. Care should be taken in finding the most cost efficient size of the PV installation and the appropriate inverter capacity to match the PV capacity. This will require a system precise cost estimate that was not available when this thesis was written. This includes the installation costs and the module and system costs. This was a process aligned a lot of time and effort in, without achieving very precise estimates. The cost estimate should be easier when the installed volumes of PV in Norway has increased.

5.3.1 Bifacial panels

The bifacial PV module technology seems very promising, especially for high latitudes. The vertical axis tracking scenarios yielded very good results, which indicates that the sun's azimuth angle varies a lot, and that is beneficial to exploit. The bifacial panel strategy could potentially be a more cost efficient way of exploiting the surrounding albedo and the varying azimuth angle of the sun. Future work should therefore give attention to bifacial panels and find programming tools that are designed for simulating this.

5.3.2 ArcGis and siting

Another factor that has not been given much attention in this thesis is the optimal and precise siting of a PV installation at Fakken. The satellite images below are meant to expose the solar resources at Fakken compared to the rest of Vannøya. From figures 5.3 and 5.3 is it seen that the cumulative radiation between each area unit can vary quite a lot. The figures shows that certain areas are exposed to more sunlight than others. The south facing hillsides close to the turbines appears to be an appropriate location both for the radiation and the convenience of being close to the existing power system. At Vannøya as a whole are some other locations more exposed to sunlight. These are at the mountain areas, which are areas that are most likely to be less practical to install solar panels at since it will limit the human access and demand more electrical wiring. Further work is necessary in finding the optimal location.

Figure 5.1: Satellite image of Fakken from norgeskart, [2]

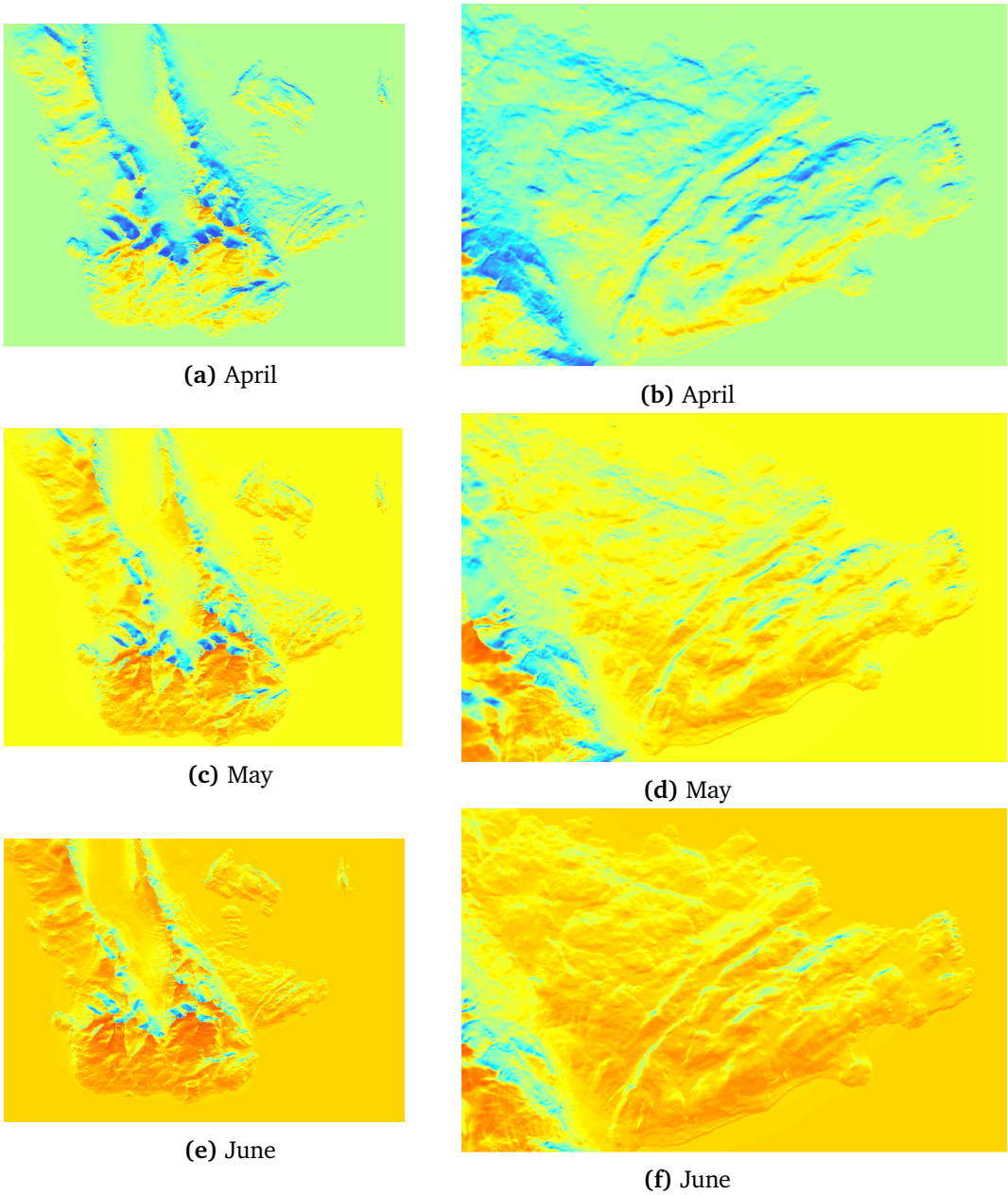

(a) April

(b) April

(c) May

(d) May

(e) June

(f) June

Figure 5.2: ArcGis

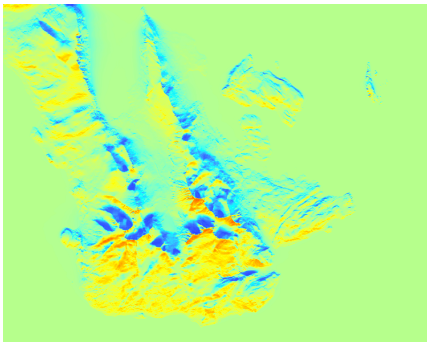

(a) July

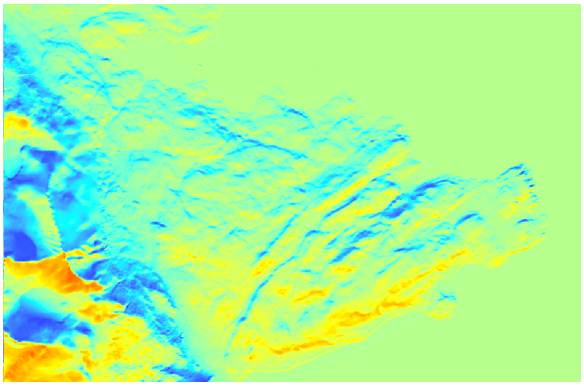

(b) July

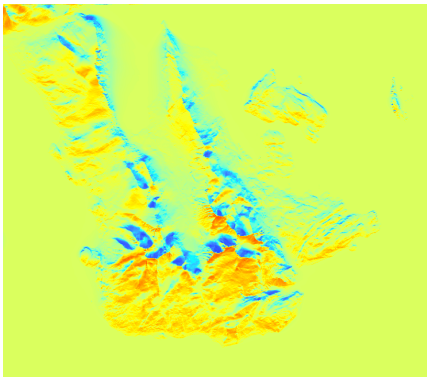

(c) August

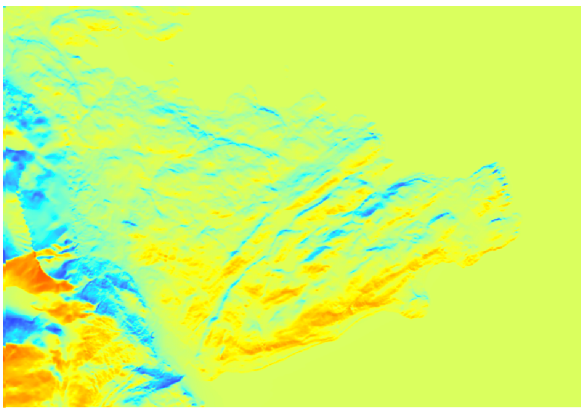

(d) August

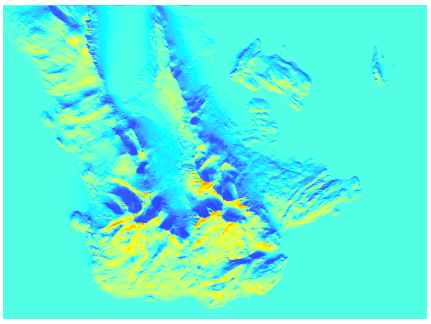

(e) September

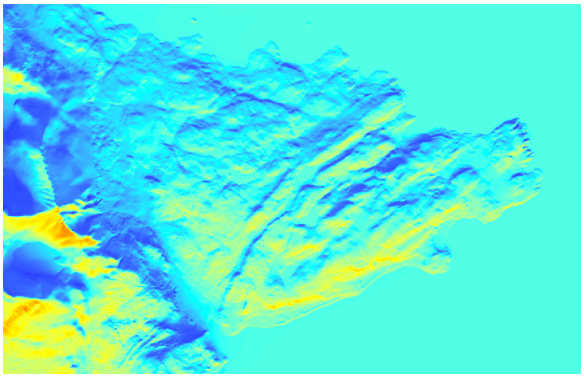

(f) September

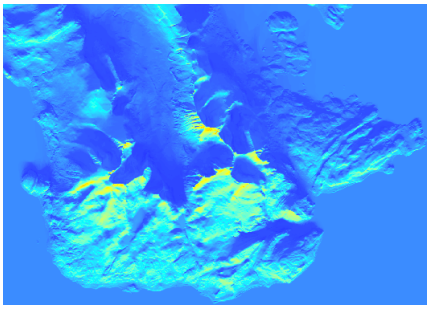

(g) October

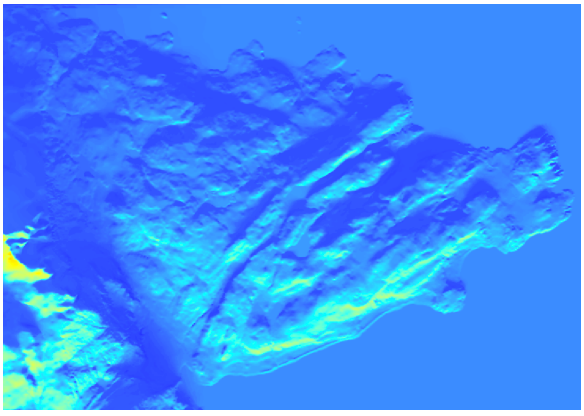

(h) October

Figure 5.3: ArGis Solar area images

??

Appendices

A

Sensitivity results

Slope ↓		Radiation →	
		70%	100%
40°	**inverter capacity [MW]** 14	19	
	Inverter output [MWh	15,784	26,927
	PV output [MWh]	17,086	29,504
	PV CF [%]	9.75	16.84
	Grid sale [kWh/yr]	144,182,400	155,324,801
	PV penetration [%]	11.71	18.64
	Excess energy [kWh]	471,317	1,159,740
50°	**inverter capacity [MW]**	15	20
	Inverter output [MWh	16,091	27,953
	PV output [MWh]	17,437	30,693
	PV CF [%]	9.95	17.52
	Grid sale [kWh/yr]	144,489,103	156,350,115
	PV penetration [%]	11.92	19.24
	Excess energy [kWh]	499,315	1,268,790
60°	**inverter capacity [MW]**	16	22
	Inverter output [MWh	16,130	28,399
	PV output [MWh]	17,490	31,223
	PV CF [%]	9.98	17.82
	Grid sale [kWh/yr]	144,528,176	156,796,539
	PV penetration [%]	11.95	19.51
	Excess energy [kWh]	511,583	1,329,864
70.1°	**inverter capacity [MW]**	16	19
	Inverter output [MWh	15,915	28,309
	PV output [MWh]	17,263	31,143
	PV CF [%]	11.86	17.78
	Grid sale [kWh/yr]	144,313,397	156,707,038
	PV penetration [%]	11.82	19.47
	Excess energy [kWh]	510,100	1,343,658
80°	**inverter capacity [MW]**	16	23
	Inverter output [MWh	15,468	27,716
	PV output [MWh]	16,778	30,489
	PV CF [%]	9.58	17.40
	Grid sale [kWh/yr]	143,867,100	156,113,659
	PV penetration [%]	11.52	19.14
	Excess energy [kWh]	495,503.6	1,314,128
90°	**inverter capacity [MW]**	16	22
	Inverter output [MWh	14,784	26,614
	PV output [MWh]	16,031	29,257
	PV CF [%]	9.15	16.70
	Grid sale [kWh/yr]	143,182,641	155,011,961
	PV penetration [%]	11.07	18.51
	Excess energy [kWh]	469,022.9	1,242,235

Table A.1: Vertical axis tracking: slope and radiation

Slope ↓		Global solar radiation →	
		70%	100%
40°	**Inverter capacity [MW]**	12	18
	Inverter output [MWh]	12,224,033	19,508
	PV output [MWh]	13,206	21,339
	PV CF [%]	7.54	12.18
	Grid sales [MWh/yr]	140,623	147,906
	PV penetration [%]	9.30	14.21
	Excess electricity [kWh]	325,077.5	804,362.2
50°	**Inverter capacity [MW]**	12	18
	Inverter output [MW]	12,142,382	19,685,358
	PV output [MWh]	13,130	21,576
	PV CF [%]	7.49	12.32
	Grid sales [MWh/yr]	140,542	148,084
	PV penetration [%]	9.25	14.35
	Excess electricity [kWh]	348,981.0	854,716.9
60°	**Inverter capacity [MW]**	12	19
	Inverter output [MWh]	11,886	19,480
	PV output [MWh]	12,861	21,382
	PV CF [%]	7.34	12.20
	Grid sales [MWh/yr]	140,285	147,879
	PV penetration [%]	9.08	14.24
	Excess electricity [kWh]	349,679.0	876,426.0
70.1°	**Inverter capacity [MW]**	12	19
	Inverter output [MWh]	11,480	18,948
	PV output [MWh]	12,426	20,814
	PV CF [%]	7.09	11.88
	Grid sales [kWh/yr]	139,879	147,347
	PV penetration [%]	8.80	13.91
	Excess electricity [kWh]	341,538.2	868,013.7
80°	**Inverter capacity [MW]**	12	19
	Inverter output [MWh]	10,931	18,101
	PV output [MWh]	11,832	19,886
	PV CF [%]	6.75	11.35
	Grid sales [MWh/yr]	139,331	146,500
	PV penetration [%]	8.41	13.37
	Excess electricity [kWh]	325,077.5	876,426.0

Table A.2: Slope and solar radiation for stationary panels with an albedo of 0.25

B

Literature Review of Hybrid Renewable Energy Systems

This section is written in collaboration with Master student Karoline Ingebrigtsen, and is therefore identical in the two theses.

The number of large-scale hybrid systems is limited, thus this is also the case for the available documentation on the state-of the-art of such systems. This literature review considers both case studies on and planned and existing large-scale hybrid systems. Many systems in the literature are combinations of both renewable and conventional power sources to ensure that the power demand is met in periods when the renewable source is not sufficient and in addition, some systems also have an energy storage option. Finally, some systems are located on smaller islands and/or only connected to a low or medium voltage grid. In lack of literature on identical hybrid systems to the ones considered in this thesis, such systems are still included in the literature review, as there are some similarities between them.

Kythnos island, Greece

One of the first large-scale hybrid systems was commissioned at the Greek island Kythnos. It is a decentralised system and is not connected to the grid on the mainland, but supplies the medium voltage grid on the island. Before

the hybrid system, diesel generators supplied the island with electricity. In 1982, five 20 kW wind turbines were installed at the island, comprising the first wind park in Europe [88]. These were replaced with five 33 kW turbines from *Aeroman* in 1989. In 1998, a 500 kW *Vestas* turbine was installed. In 1983 a 100 kW Siemens PV system with battery storage was added to the system, and at this time it was the largest hybrid system in the world [89].

In year 2000, a new, fully automatic, control system was installed which controls the power supply according to available renewable energy and electricity demand, in addition to a 500 kW battery storage [89]. This led to a renewable contribution of 50% in off-peak periods and the possibility of 100% renewable penetration in periods of low demand. The battery storage can provide high power with short response time for short time intervals if needed. Connected to the system is also a load control, which consists of a power converter that ensures voltage and frequency stability by cutting off peaks from the wind power converters that are unwanted, as wind gusts is a challenge in the area [89]. The control system consists of an intelligent power system delivered by *SMA*. It is a computer which monitor every component of the system. [89] reports that the system has operated satisfactory and contributed to large fuel savings. A schematic of the system is shown in Figure B.1.

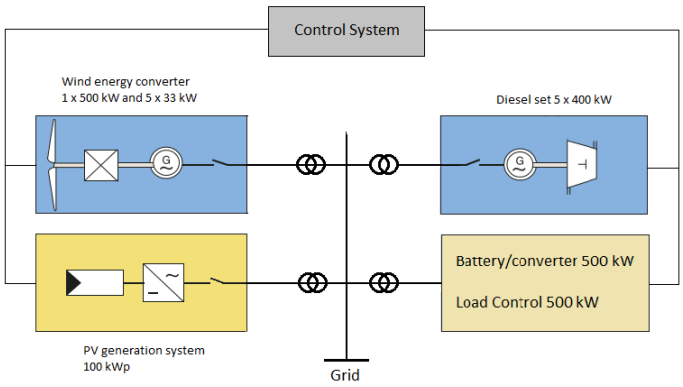

Figure B.1: The arrangement of the hybrid system at Kythnos. Simplified from [88]

Longyangxia hydro and PV hybrid system, China

Today, the world's largest hybrid system is located in China, by the Longyangxia Dam. It consists of PV and hydro power, and is the first commercial large-scale hybrid system with these two power sources. The 1280 MW hydro power plant

was commissioned in 1992 and consists of four 320 MW turbines. In December 2013, a 320 MW PV power plant was commissioned in the same area, and it is connected to the grid through the hydropower plant, via a 330 kV transmission line to one of the hydro power turbines [87]. The PV plant has undergone almost constant expansion, and today, the PV plant has a capacity of 850 MW and covers 27 km^2 [85].

The PV system is one of the world's largest, and on its own it would cause substantial instabilities on the grid due to large variations in the solar resource. The way it is connected via one of the turbines in the hydro power plant, causes it to function as a fifth turbine. The PV output is tracked and the hydro power turbines can compensate for variations with a very short response time as the control system is simultanously controlling the PV and hydro power plant. In addition, the connection between the power plants has enabled a higher capacity factor of the hydro power station in dry periods [87].

In [86], a method for finding the optimum size of a hybrid system between PV and hydro power is formulated and applied to the Longyangxia hybrid system. The article focuses on the flexibility of the system in the short-term, and therefore three daily schemes for operation of the PV and hydro power plants depending on the type of load demand is used in calculations. The method then optimises the size of the system by maximising the net income during the lifetime of the system for each operation scheme while taking into account two factors; the gross output from the hybrid plant should never be larger than the total installed capacity of the hydropower plant and the solar curtailment should be as small as possible to avoid the solar curtailment fee.

The three operating schemes are:

- **All-day lifting scheme**: suitable for areas where the PV output never exceeds the demand and grid constraints.

- **Daytime lifting scheme**: suitable if the load demand is higher during daytime than during night time

- **Peak-load period lifting scheme**: suitable for regions with two peaks in the electricity demand

It is found for the case of Lonyangxia hybrid system that the net revenue increases with PV system size for all schemes, but in the daytime and peak-load period lifting schemes, the gross output constraint limits the size. In the daytime lifting scenario, there is no solar curtailment. Optimum sizes for different hydropower capacities when also considering an expansion of

hydropower is 1030 MW (with 90% hydropower capacity), 2040 MW (with 160% hydropower capacity) and 690 MW (with 105% hydropower capacity), respectively for the three schemes. The article also considers the effect that integrating PV into a hydro power plant has on the water resource allocation of the reservoir used for the Longyangxia system, and concludes that there is a very low degree of adverse effects.

[90] proposes a model that optimises a hybrid system between PV and hydro power. It aims at maximising the amount of generated power and minimising the power output fluctuations by varying the reservoir release. Constraints are the water level in the reservoir, the maximum reservoir release and the maximum capacity of the electricity grid. The model is long-term and results are given for time periods of one year, classified into different categories depending on amount of inflow into the Longyangxia reservoir; extremely wet years, wet years, normal years, dry years and extremely dry years. The model results when applied to Longyangxia showed that the model is adequate and that hydropower and PV power are complementary, with the highest anti-correlation in wet years, when a larger amount of precipitation leads to less solar radiation and more hydro power output.

El Hierro island, Spain

El Hierro is a Canary island with 10,000 inhabitants and with its own isolated grid system [67], [66]. Remote and isolated energy systems depending on fossil fuels are vulnerable to prices and has a high transportation cost of fuels. To mitigate this issue a hybrid system construction consisting of wind power and pumped hydroelectric storage was finalized in 2015 [67]. Five wind turbines with a total capacity of 11.5 MW and a storage capacity of $380,000 m^3$ of water in its upper dam reservoir now provides the island reliable power[66] [67]. Wind power will supply the island with energy directly, and any excess energy will be fed into the hydroelectric facility and pump water from the bottom reservoir to the top reservoir. The top reservoir is in fact a volcanic crater [66]. During times at low wind speed or during peak demand, water from the top reservoir is released and runs a set of Pelton turbines for electricity generation [66]. The hydroelectric plant can respond to the wind production within milliseconds to even out the total power production [67]. The diesel power plant will operate only if the cumulative power from both the wind and hydro systems are insufficient in meeting the demand. By October 2015, the renewable penetration was roughly 50% of the total production, and the goal is for the island to be 100% self supplied with renewable energy. The renewable penetration is assumed to increase when those operating the energy system have gained more experience with the new system [67].

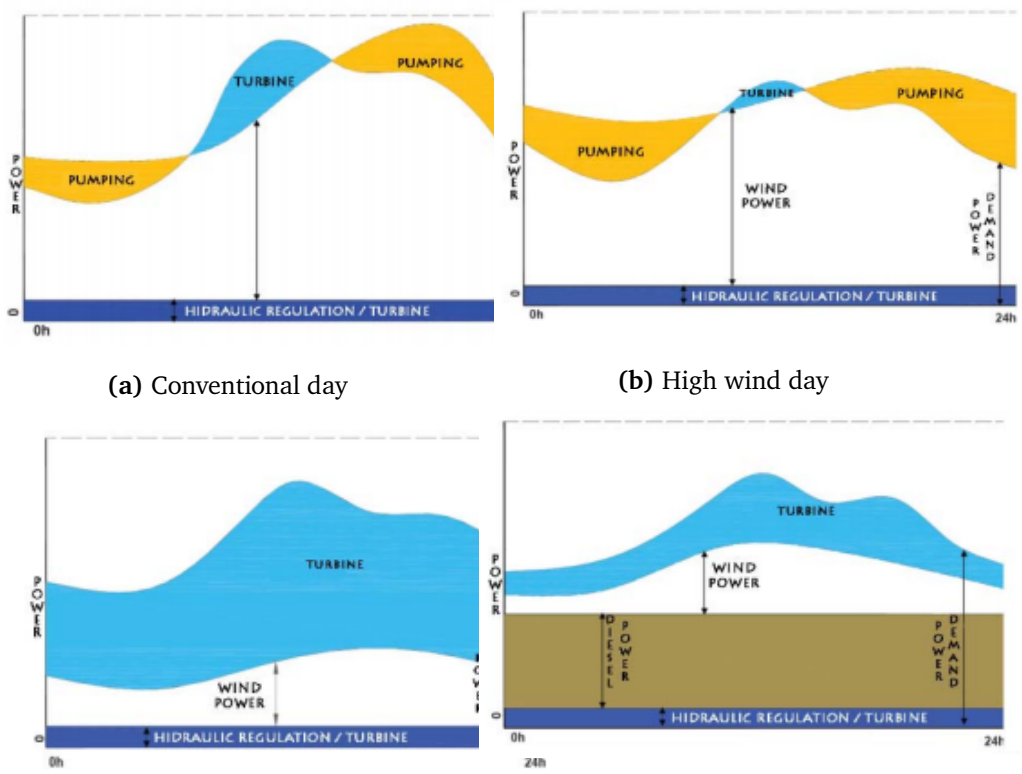

(a) Conventional day

(b) High wind day

(c) Low wind day

(d) Low wind day when upper reservoir is half empty

Figure B.2: Operating scenarios for different wind and reservoir conditions. From [68]

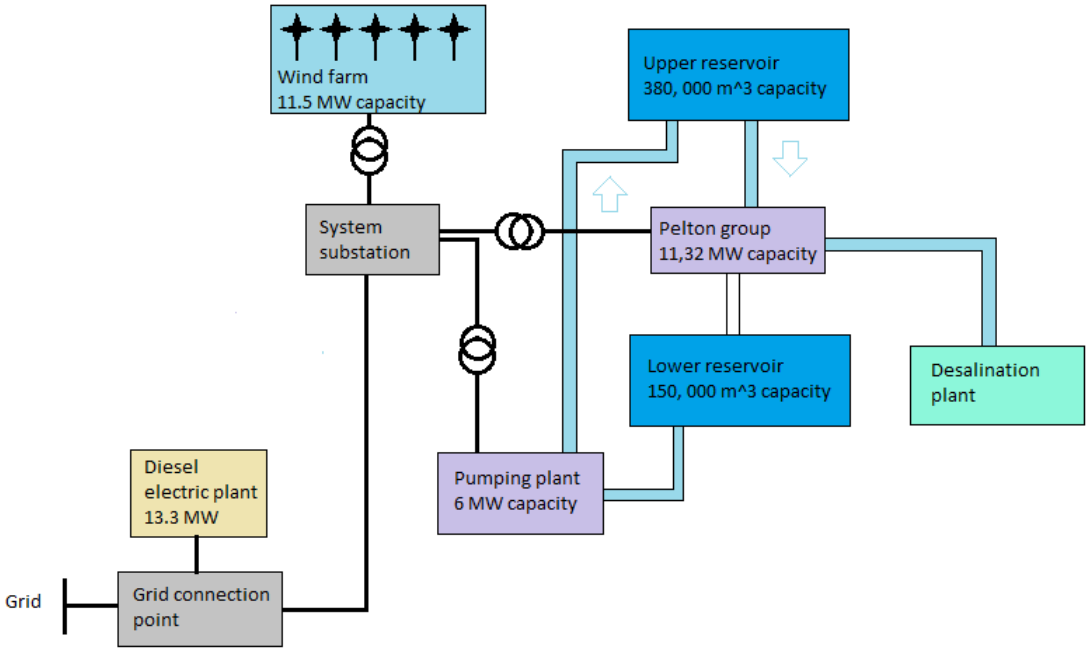

Figure B.3: A diagram showing the hybrid system at El Hierro. Created with information from [66] and [68]

Pellworm island, Germany

Pellworm is an island outside the west coast of northern Germany. The island had 1100 inhabitants in 2013 [91] and its annual electricity consumption is approximately 8 GWh, while the total amount of electricity produced on the island is about 25 GWh. The electricity production at the island comes exclusively from renewable sources; PV, wind and biogas plants. The system on the island also uses batteries as a storage solution [92].

The first PV plant was installed at the island in 1983 and had a capacity of 300 kW. The capacity has since then been increased by another PV plant and wind turbines. The PV modules from 1983 were replaced in 1995 because the inverters had been destructed by lightning [93].

As seen in Figure B.4, the power plants are located quite long distanced between them. There is a hybrid system consisting of a PV power plant (PVP) and a wind power plant (WPP) to the left in the picture, and this has a capacity of 1072 kW (772 kW PV and a 300 kW wind turbine). In 2013, batteries with a storage capacity of 2160 kWh was installed in conjunction with the system

[93].

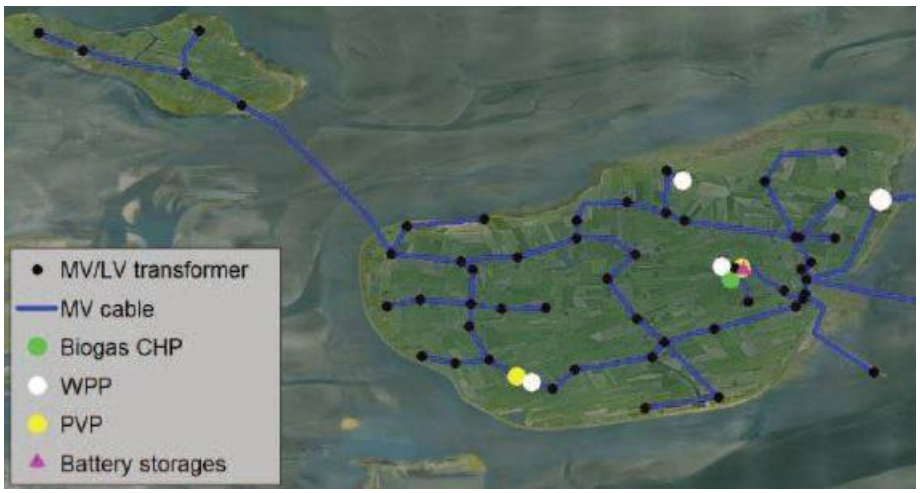

Figure B.4: A map of the power plants and medium voltage grid at Pellworm and its neighboring island. From [92]

The power plants are connected to the island's electricity grid in the medium voltage range and a large number of small-scale PV modules are connected to the grid via a low voltage grid. The grid on Pellworm is connected to the mainland grid to both export and import electricity. [92]. It also covers a small neighbouring island to Pellworm.

Because power losses are large when transmitting electricity over long distances, a smart grid in planned on the island, so that the production and demand can be better correlated. In addition, large storage systems are planned to be installed so that electricity can be stored in periods of high production and hence self-sufficiency of the island can be achieved also in periods of low local electricity production [91].

Linha Sete, Brazil

This section is based on a feasibility study of a grid connected hybrid system consisting of PV, wind and a pumped hydroelectric storage facility together with a diesel generator as a back up source, found in [94]. The hydroelectric plant has a total head of 655 m and a storage volume capacity of $1,510,000 m^3$. The system was simulated using Homer. The PV panels are planned to be installed as a floating structure on the dams in order to reduce evaporation of the water but also to avoid shading of the land area and hence reduce the environmental impacts of the construction. This will increase the PV system

costs by 30% compared to conventional solutions. The wind turbines have a capacity of 1 MW each. Two systems are simulated, one without PV and one containing 10 MW installed capacity.

The hydroelectric plant is simulated as a *Run of the river* connected to a DC bus together with a battery to simulate the pumped storage facility. In order to find the most optimal system size, Homer was asked to simulate a high number of component sizes by implementing different numbers of wind turbines, different capacity sizes of the diesel generator, different converter capacities and different number of batteries. Sensitivity analysis were conduced on the diesel price, the AC load and the wind speed. At least 95% of the load must be provided by renewable sources.

Because of high PV installation costs, the optimal solution was one without PV. However, some of the systems that included PV was not far from the optimal system solution. The study recommends a system consisting of 100 kW in PV, 20 wind turbines, a diesel generator with a capacity of 19,200 kW and the pumped storage unit which gives an energy cost of USD$ 0.408 per kWh. Alternatively, a system excluding the wind turbines but consisting of 10 MW of PV, a diesel generator with a capacity of 30 MW and the pumped storage gives an energy cost of USD $0.609. The first alternative is considered the most stable one, because it has the same amount of energy available in the reservoir at the end of the year as it contained in the beginning.

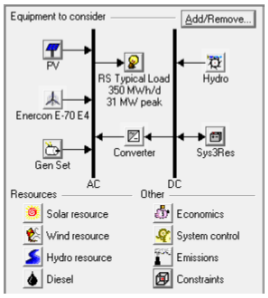

Figure B.5: A diagram showing the hybrid system at in Linha Sete. From [68]

This section is written in collaboration with Master student Karoliene Ingebrigtsen as we both have theses concerning hybrid renewable energy systems.

C

HOMER Calculations

Calculating Radiation on PV array

HOMER finds the radiation on the PV modules by first locating the sun's position by using the same kind of equations described in section 2.2, although they are not completely identical. To calculate the declination angle, *HOMER* uses equation C.1.

$$\delta = 23.45^\circ sin\left(360^\circ \frac{284 + d}{365}\right) \tag{C.1}$$

The hour angle is identical to equation 2.7. To correct for the actual time and the civil time, *HOMER* uses the following equation:

$$LST = LT + \frac{\lambda}{15^\circ/hour} - LSTM + EoT \tag{C.2}$$

The equation of time that *HOMER* applies is very similar to 2.4, but differs slightly. *HOMER*'s equation is shown in the equation below:

$$EoT = 3.82(0.000075+0.001868\cdot cos(B)-0.032077\cdot sin(B)-0.014615\cdot cos(2B)-0.04089\cdot sin(2B)) \tag{C.3}$$

where

$$B = 360^\circ \frac{n-1}{365}$$

HOMER needs the zenith angle in order to calculate the extraterrestrial solar radiation. The extraterrestrial radiation is needed for calculating the clearness index. The zenith angle is calculated from the angle of incident calculation. The angle of incidence θ is defined as the angle between the solar radiation and the normal to the PV panel.

$$\begin{gathered} cos(\theta) = sin(\delta)sin(\phi)cos(\beta) - sin(\delta)cos(\phi)sin(\beta)\cos(a_s) \\ +cos(\delta)cos(\phi)cos(\beta)cos(HRA) + cos(\delta)sin(\phi)sin(\beta)cos(a_s)cos(HRA) \\ +cos(\delta)sin(\phi)sin(a_s)sin(HRA) \end{gathered}$$

If the slope is 0° will the angle of incidence correspond to the zenith angle, θ_z. The zenith angle is defined as the angle between a vertical line and a the line pointing towards the sun. This simplifies the above equation to:

$$cos(\theta_z) = sin(\delta)sin(\phi)cos(\beta) + cos(\delta)cos(\phi)cos(HRA)$$

HOMER goes on calculating the extraterrestrial radiation on a surface normal to the solar beam, G_{on}:

$$G_{on} = Gsc\left(1 + 0.033 \cdot \frac{360d}{365}\right)$$

Where G_{sc} is the solar constant equal to $1.367kW/m^2$.

The extraterrestrial radiation on a horizontal surface, G_0, is :

$$G_0 = G_{on}cos(\theta_z)$$

This is averaged over one time step by integrating over the time step with respect to the hour angle. The average radiation is given by the equation below:

$$\overline{G_0} = \frac{12}{\pi}G_{on}[cos(\phi)cos(\delta)(sin(HRA_2) - sin(HRA_1)) + \frac{\pi(HRA_2 - HRA_1)}{180^\circ}sin(\phi)sin(\delta)]$$

The clearness index is defined as the ratio of the terrestrial radiation on a horizontal surface to the extraterrestrial radiation on a horizontal surface. In *HOMER* is it calculated using equation C.4

$$K_{t_c} = \frac{\overline{G}}{\overline{G_0}} \tag{C.4}$$

where $\overline{G}$ represents the radiation at the surface. In the case of this thesis, this corresponds to the WRF simulated radiation. The clearness index enables *HOMER* to distinguish between the direct and diffuse radiation at the surface.

$$\frac{\overline{G_d}}{\overline{G}} = \begin{cases} 1 - 0.09 \cdot k_{t_c} & k_{t_c} \leq 0.22 \\ 0.9511 - 0.1604 \cdot k_{t_c} + 4.388 \cdot k_{t_c}^2 - 16.638 \cdot k_{t_c}^3 + 12.336 \cdot k_{t_c}^4 & 0.22 < k_{t_c} \leq 0.8 \\ 0.165 & k_{t_c} > 0.8 \end{cases}$$

For *HOMER* to include the isentropic, circumsolar and horizon brightening effects of radiation, three more parameters are needed. Those are the *ratio of beam* in equation C.5, the *Anisotropic index* in equation C.6 and the horizon brightening factor in equation C.7. The ratio of beam is the ratio of the beam radiation on a tilted surface to the beam radiation on a horizontal surface. The anisotriopic index is a measure of the transmittance of solar beam radiation through the atmosphere. The horizon brightening factor is related to the cloudiness of the atmosphere and counts for the diffuse radiation being stronger in the horizon.

$$R_b = \frac{cos\theta}{cos\theta_z} \tag{C.5}$$

$$A_i = \frac{\overline{G_b}}{\overline{G_0}} \tag{C.6}$$

$$f = \sqrt{\frac{\overline{G_b}}{\overline{G}}} \tag{C.7}$$

The radiation on the tilted surface can finally be calculated like equation C.8

$$\overline{G_t} = (\overline{G_b} + \overline{G_d} A_i) R_b + \overline{G_d}(1 - A_i) \left(\frac{1 - cos\beta}{2}\right) \left[1 + f sin^3\left(\frac{\beta}{2}\right)\right] + \overline{G}\sigma \left(\frac{1 - cos\beta}{2}\right) \tag{C.8}$$

Calculating the temperature of the solar cell

It was investigated in section 2.7.2 that cell efficiency is highly dependent on the cell temperature. How *HOMER* calculates the cell temperature is presented in this section. The solar energy absorbed by a PV module will be converted to electricity and thermal energy. The energy balance equation used by *HOMER* is displayed in equation C.9. This section in based on the *Homer help manual*, [54]

$$\tau\epsilon G_t = \eta_c G_t + U_L(T_c - T_a) \tag{C.9}$$

Where τ is the solar transmittance of the cover material of the panels, U_L is the thermal heat transfer coefficient to the surroundings. As in earlier sections will η_c is the module efficiency, and T_c and T_a are the cell temperature and ambient temperature respectively.

This equation can be solved with respect to the cell temperature.

$$T_c = T_a + G_t \left(\frac{\tau\epsilon}{U_L}\right)\left(1 - \frac{\eta_c}{\tau\epsilon}\right) \tag{C.10}$$

The $\frac{\tau\epsilon}{U_L}$ quantity hard to measure. As an alternative, *HOMER* substitute the NOCT conditions to equation C.10 and solve for $\frac{\tau\epsilon}{U_L]}$ as shown in equationC.11

$$\frac{\tau\epsilon}{U_L} = \frac{T_{c,NOTC} - T_{a,NOTC}}{G_{t,NOTC}} \tag{C.11}$$

Substituting the quantity back to equation C.10, equation C.12

$$T_c = T_a + G_t \left(\frac{T_{c,NOTC} - T_{a,NOTC}}{G_{t,NOTC}}\right)\left(1 - \frac{\eta_c}{\tau\epsilon}\right) \tag{C.12}$$

HOMER will always assume that the array operates at its maximum power point with efficiency $\eta_c = \eta_{mp}$. Assuming that this quantity is linearly dependent on the cell temperature like in equation C.13

$$\eta_{mp} = \eta_{mp,STC}[1 + \epsilon_P(T_c - T_{c,STC})] \tag{C.13}$$

where ϵ_P is the power temperature coefficient, $\eta_{mp,STC}$ is the maximum power point efficiency under STC and $T_{c,STC}$ is the cell temperature under STC. *HOMER* will finally insert the equation of η_{mp} into equation C.12 and obtain equation C.14

$$T_c = \frac{Ta + (T_{c,NOCT} - T_{a,NOCT})\left(\frac{G_t}{G_{t,STC}}\right)\left[1 - \frac{\eta_{mp,STC}(1-\epsilon_P T_{c,STC})}{\tau\epsilon}\right]}{1 + (T_{c,NOCT} - T_{a,NOCT})\left(\frac{G_t}{G_{t,NOCT}}\right)\left(\frac{\epsilon_P \eta_{mp,STC}}{\tau\epsilon}\right)} \quad \text{(C.14)}$$

The power output from the PV arrays are calculated according to equation C.15.

$$P_{PV} = P_{PV,STC} \cdot f_{PV} \frac{G_T}{G_{T,STC}}(1 + \mu_p(T_C - T_{C,STC})) \quad \text{(C.15)}$$

Where P_PV is the power output, $P_{PV,STC}$ is the rated power, G_T, is the global radiation at that particular time step and $G_{T,STC}$ is the global radiation at standard testing conditions. μ, is as usual the temperature coefficient, f_{PV} is the derating factor, $T_{C,STC}$ is the cell temperature under standard testing conditions, T_C is the cell temperature.

D

Namelist files

```
start_hour                          = 12,       12,
start_minute                        = 00,       00,
start_second                        = 00,       00,
end_year                            = 2016,     2016,
end_month                           = 07,       07,
end_day                             = 01,       01,
end_hour                            = 00,       00,
end_minute                          = 00,       00,
end_second                          = 00,       00,
interval_seconds                    = 21600,
input_from_file                     = .true.,   .true.,
history_interval                    = 10,       10,
frames_per_outfile                  = 500000,    500000,
restart                             = .false.,
restart_interval                    = 100000,
io_form_history                     = 2,
io_form_restart                     = 2,
io_form_input                       = 2,
io_form_boundary                    = 2,
debug_level                         = 0,

/&domains
time_step                           = 54,
time_step_fract_num                 = 0,
time_step_fract_den                 = 1,
max_dom                             = 2,
e_we                                = 97,       97,
e_sn                                = 97,       97,
e_vert                              = 51,       51,
p_top_requested                     = 1000,
num_metgrid_levels                  = 38,
num_metgrid_soil_levels             = 4,
dx                                  = 9000,     3000,
dy                                  = 9000,     3000,
grid_id                             = 1,        2,
parent_id                           = 1,        1,
i_parent_start                      = 1,       33,
j_parent_start                      = 1,       33,
parent_grid_ratio                   = 1,        3,
parent_time_step_ratio              = 1,        3,
feedback                            = 0,
smooth_option                       = 0,
eta_levels                          = 1.0000, 0.9980, 0.9955, 0.9925, 0.9890, 0.9850, 0.9805, 0.9755,
                                      0.9700, 0.9640, 0.9575, 0.9505, 0.9430, 0.9350, 0.9265, 0.9170,
                                      0.9060, 0.8930, 0.8775, 0.8590, 0.8363, 0.8104, 0.7803, 0.7456,
                                      0.7059, 0.6615, 0.6126, 0.5594, 0.5041, 0.4479, 0.3919, 0.3384,
                                      0.2897, 0.2474, 0.2107, 0.1792, 0.1523, 0.1293, 0.1093, 0.0917,
                                      0.0763, 0.0629, 0.0513, 0.0413, 0.0328, 0.0255, 0.0194, 0.0144,
                                      0.0104, 0.0071, 0.0000,/
```

Figure D.1: *namelist.wrf* part 1

```
&physics
mp_physics                  = 4,        4,
ra_lw_physics               = 5,        5,
ra_sw_physics               = 5,        5,
radt                        = 9,        3,
sf_sfclay_physics           = 2,        2,
sf_surface_physics          = 2,        2,
bl_pbl_physics              = 2,        2,
bldt                        = 0,        0,
cu_physics                  = 2,        2,
cudt                        = 5,        5,
isfflx                      = 1,
ifsnow                      = 1,
icloud                      = 1,
surface_input_source        = 1,
num_soil_layers             = 4,
sf_urban_physics            = 2,        2,/
&fdda                       /
&dynamics
w_damping                   = 0,
diff_opt                    = 1,
km_opt                      = 4,
diff_6th_opt                = 0,        0,
diff_6th_factor             = 0.12,     0.12,
base_temp                   = 290.,
damp_opt                    = 0,
zdamp                       = 5000.,    5000.,
dampcoef                    = 0.2,      0.2,
khdif                       = 0,        0,
kvdif                       = 0,        0,
non_hydrostatic             = .true.,   .true.,
moist_adv_opt               = 1,        1,
scalar_adv_opt              = 1,        1,

/&bdy_control
spec_bdy_width              = 5,
spec_zone                   = 1,
relax_zone                  = 4,
specified                   = .true.,  .false.,
nested                      = .false.,   .true.,
/&grib2
/&namelist_quilt
nio_tasks_per_group         = 0,
nio_groups                  = 1,/
```

Figure D.2: *namelist.wrf* part 2

```
&share wrf_core =
'ARW', max_dom = 2,
start_date = '2016-09-07_12:00:00',
'2016-09-07_12:00:00',
end_date   = '2016-10-01_00:00:00',
 '2016-10-01_00:00:00',
interval_seconds = 21600,
io_form_geogrid = 2,
opt_output_from_geogrid_path = '/home/ynb022/WRF/WRFportal/Domains/Solar2016/',
debug_level = 0,
/&geogrid parent_id         = 1,1,
parent_grid_ratio = 1,3,
i_parent_start    = 1,33,
j_parent_start    = 1,33,
e_we          = 97,97,
e_sn          = 97,97,
geog_data_res = '2m',
'30s', dx = 9000,
dy = 9000, map_proj =  'polar',
ref_lat   = 69.5,
ref_lon   = 20,
truelat1  = 69.5,
truelat2  = 90,
stand_lon = 20,
geog_data_path = '/home/WRF/WPS_GEOG',
opt_geogrid_tbl_path = '/home/ynb022/WRF/WRFportal/Domains/Solar2016/',
ref_x = 48.5,
ref_y = 48.5,
/&ungrib out_format = 'WPS', prefix = 'FILE',
/&metgrid fg_name = 'FILE',
io_form_metgrid = 2,
```

Figure D.3: namelist.wps

```
opt_output_from_metgrid_path = '/home/ynb022/WRF/WRFportal/Domains/Solar2016/',
opt_metgrid_tbl_path = '/home/ynb022/WRF/WRFportal/Domains/Solar2016/',
/&mod_levs press_pa = 201300 , 200100 , 100000 , 95000 ,  90000 ,
 85000 ,  80000 , 75000 ,  70000 ,     65000 ,
60000 , 55000 ,  50000 ,  45000 ,  40000 , 35000 ,
30000 ,  25000 ,  20000 , 15000 ,  10000 , 5000 ,
1000 /&domain_wizard grib_data_path = '/home/ynb022/WRF/GRIBdata',
 grib_vtable = 'Vtable.ERA-interim.pl', dwiz_name    =Solar2016 dwiz_desc
=To run simulations for two master students dwiz_user_rect_x1
=59 dwiz_user_rect_y1 =75 dwiz_user_rect_x2 =168 dwiz_user_rect_y2
=155 dwiz_show_political =true dwiz_center_over_gmt =false dwiz_latlon_space_in_deg
=10 dwiz_latlon_linecolor =-8355712 dwiz_map_scale_pct =12.5 dwiz_map_vert_scrollbar_pos
=0 dwiz_map_horiz_scrollbar_pos =0 dwiz_gridpt_dist_km =9.0 dwiz_mpi_command
= dwiz_tcvitals
=null dwiz_bigmap =Y/
```

Figure D.4: namelist.wps

Bibliography

[1] Troms kraft. [Online]. Available: http://www.tromskraft.no [Accessed March 2017]

[2] Norgeskart. [Online]. Available: https://www.norgeskart.no/. [Accessed May 2017].

[3] J. F Manwell et al. *Wind energy Explained, Theory Design and Applications*, Chichester, England, John Wiley and Sons, LTD, 2008.

[4] V. Yaramasu, Bin Wu, P. C. Sen, S. Kouro and M. Nariman. "High-Power Wind Energy Conversion Systems: State-of-the-Art and Emerging Technologies". *Proceeding of the IEEE*, vol. 22, no. 5, May, 2015, pp. 740-788.

[5] S.Sumathi et al. *Solar PV and Wind Energy Conversion Systems*, Springer International Publishing, 2015.

[6] A. V. da Rosa. *Fundamentals of Renewable Energy Processes*. Amsterdam, Netherlands, Elsevier Academic Press, 2005.

[7] C. Honsberg and S. Bowden. Photovoltaic Education Network. [Online] Available: http://pveducation.org/, [Accessed March 2017].

[8] H. Mousazadeh, A. Keyhani, A. Javadi, H. Mobli, K. Abrinia and A. Sharif, "A review of principle and sun-tracking methods for maximizing solar systems output", *Renewable and Sustainable Energy Reviews*, vol 13, no. 8, 2009, pp. 1800 - 1818.

[9] G. Boyle. *Renewable Energy, Power for a sustainable future*, third edition, Oxford University Press, 2012.

[10] G. Hou et al. "Life cycle assessment of grid-connected photovoltaic power generation from crystalline silicon solar modules in China", *Applied Energy*, vol. 164, 2016, pp. 882 - 890.

[11] E. Rome-Cadaval, G. Spagnuolo, L. G. Franquelo, C.-A. Ramos-Paja, T. Suntio and W.-M. Xiao, "Grid-Connected Photovoltaic Generation Plants: Components and operation", *IEEE Industrial Electronics Magazine*, vol. 7, no. 3, 2013, pp.6-20.

[12] T. Blæsterdalen, "Wind resource assessment using mesoscale modelling-A case study at the potential wind farm site Rieppi", M.S. thesis, UiT The Arctic Univ. of Norway, Tromsø, Norway, 2016.

[13] The Weather Research & Forecasting Model. (n.d.). The Weather Research & Forecasting Model, [Online]. Available: http://www.wrf-model.org/index.php. [Accessed April 2017].

[14] C. S. Solanki. *Solar Photovoltaics*, third edition, Delhi, India, PHI Learning Private Limited, 2015.

[15] J. Nelson, *Physics of solar cells*, London, England, Imperial College press, 2013.

[16] F. Kreith, *Principles of Sustainable Energy Systems*, second ed. Boco Raton, CRC Press, 2014.

[17] J. Andrews and N. Jelley, *Energy Science: Principles, Technologies and Impacts*, Oxford, Oxford University Press, 2007.

[18] S. Sunanda and S.S Chandel. "Review of software tools for hybrid renewable energy systems number", *Renewable and Sustainable Energy reviews*, vol. 32, April, 2014, pp. 192-205.

[19] I. A. Gondal and Dr M. H. Sahir, "Review of Modelling Tools for Integrated Renewable Hydrogen Systems" in *2011 2nd International Conf. on Environmental Science and Technology IPCBEE vol.6*, Singapore, IACSIT Press.

[20] R. D. Prasad, R.C. Bansal and Atul Raturi, "Multi-faceted energy planning: A review", *Renewable and Sustainable Energy Reviews*, vol. 38, 2014, pp. 686–699.

[21] D. Connolly, H. Lund, B.V. Mathiesen and M. Leahy, "The first step towards a 100% renewable energy-system for Ireland". *Applied Energy*, vol. 88, 2011, pp. 502–507.

[22] Z. Huang, H. Yu, Z. Peng and M. Zhao, "Methods and tools for community energy planning: A review". *Renewable and Sustainable Energy Reviews*,

vol. 42, 2015, pp. 1335–1348.

[23] S.D Firincaă and I. Mircea, "Simulation of the systems with renewable energy sources using Homer software", *Journal of Sustainable energy*, vol. 6, no. 4, December, 2015, pp. 60-64.

[24] D. M. Riley and C. W. Hansen, "Sun-Relative Pointing for Dual-Axis Solar Trackers Employing Azimuth and Elevation Rotations". *Sandia Report*, April, 2014.

[25] Apogee Instruments, SP-230 All- Season Pyranometer. [Online]. Available: http://www.apogeeinstruments.com/content/sp-230.pdf, [Accessed Jan 2017].

[26] Y.-M. Chen, C.-S. Cheng, and H-C. Wu. "Grid-Connected Hybrid PV/Wind Power Generation System with Improved DC Bus Voltage Regulation Strategy". *IEEE Applied Power Electronics Conference and Exposition*, March, 2006. pp. 1088- 1094.

[27] M. A. Martínez, J. M. Andújar and J. M. Enrique, "A New and Inexpensive Pyranometer for the Visible Spectral Range", *Sensors*, vol. 9, no. 6,, June, 2009, pp. 4615-4634.

[28] B. Zeqiang, L. Wenhua, S. Yizhuo, H. Xiaolei and C. Wei, "Research on Performance Test Method of Silicon Pyranometer", *2013 The 11th IEEE International Conf. on Electronic Measurement & Instruments*, vol. 1, pp. 43-48.

[29] D. Lingfors. "Solar Variability Assessment and Grid Integration: Methodology Development and Case Studies", Faculty of Science and Technology, Uppsala University, Uppsala, 2015.

[30] P. Nema, R.K Nema, S. Rangnekar, "A Current and fututre state of the art development if hybrid energy systems using wind and PV-solar: A review". *Renewable and Sustainable Energy Reviews*, vol 13, no. 8, 2009, pp. 2096-2103.

[31] Y.-M. Chen, Y.-C. Liu, S.-C. Hung and C.-S. Cheng, "Multi-Input Inverter for Grid-Connected Hybrid PV/Wind Power System". *IEEE Transactions on power electronics*, vol. 22, no. 3, May, 2007, pp. 1070-1077.

[32] G. Yuan, J. Chai and Y. Li, "Vector Control and Synchronization of Doubly Fed Induction Wind Generator system", in *The 4th International Power Electronics and Motion Control Conference 2004, IPEMC 2004.*, vol. 2, pp.886-

890.

[33] Campbell Scientific, Instruction manual for the SP- 230 Heated Pyranometer. [Online]. Available: https://s.campbellsci.com/documents/us/manuals/sp230.pdf, [Accessed January 2017].

[34] S. Li, T. A. Haskew, D. Li and F. Hu, "Integrating photovoltaic and power converter characteristics for energy extraction study of solar PV systems". *Renewable Energy*, vol. 36, no. 12, 2011, pp. 3238 - 3245.

[35] N. Gokmen et al. "Investigation of wind speed cooling effect on PV panels in windy locations", *Renewable Energy*, vol. 90, 2016, pp. 283 - 290.

[36] C.-M. Hong, T.-C. Ou and K.-H. Lu, "Development of intelligent MPPT (maximum power point tracking) control for a grid-connected hybrid power generation system", *Energy*, vol. 50, 2013, pp. 270 - 279.

[37] NVE, Norges Vassdrag og Energidirekorat. [Online]. Available: https://www.nve.no/, [Accessed Nov 2016]

[38] Kipp & Zonen CM 11/14 Pyranometer/Albedometer Instruction Manual, 2000. [Online]. Available: *https : //www.google.no/url?sa = t&rct = j&q = &esrc = s&source = web&cd =* 1*&ved =* 0*ahUKEwjK*5*eL*1 *− enSAhXmO*5*oKHQogDAAQFggfMAA&url = http*%3*A*%2*F*%2*Fwww.kippzonen.com*%2*FDownload*%2*F*48%2*FCM−* 11 *− Pyranometer − CM −* 14 *− Albedometer − Manual&usg = AFQjCNFP*64*khI*2*AnifoPzM*9*pWD*8*sSO*0*tw&bvm = bv.*150120842*, d.bGs&cad = rja* [Accessed January 2017].

[39] F. Monforti, T. Huld, K. Bódis, L. Vitali, M. D'Isidoro, R. Lacal-Arántegui. "Assessing complementarity of wind and solar resources for energy production in Italy. A Monte Carlo approach", *Renewable energy*, vol. 63, 2014, pp. 576 - 586.

[40] K. Solbakken, B. Babar, and T. Boström, "Correlation of wind and solar power in high-latitude arctic areas in Northern Norway and Svalbard", *Renew. Energy Environ. Sustain*, vol. 42, no. 1, EDP Sciences, Sept, 2016.

[41] M. H. Nehrir, C. Wang, K. Strunz, H. Aki, R. Ramakumar, J. Bing, Z. Miao, and Z. Salameh, "A Review of Hybrid Renewable/Alternative Energy Systems for Electric Power Generation: Configurations, Control, and Applications", *IEEE transactions on sustainable energy*, vol. 2, no. 4, Oct, 2011 pp. 392-403.

[42] V. Khare, S. Nema, P. Baredar, "Solar–wind hybrid renewable energy system: A review", *Renewable and Sustainable Energy Reviews*, vol. 58, 2015, pp. 23 - 33.

[43] S. Weitemeyer, D. Kleinhans, T. Vogt and C. Agert, "Integration of Renewable Energy Sources in future power systems: The role of storage", *Renewable Energy*, vol. 75, 2015, pp. 14-20.

[44] T. U. Daim, X. Li ,J. Kim and S. Simms" "Evaluation of energy storage technologies for integration with renewable electricity: Quantifying expert opinions", *Environmental Innovation and Societal Transitions*, vol. 3, 2012, pp. 29 - 49.

[45] G. L. Shevlyakov and H. Oja. *Robust Correlation: Theory and Applications*, Wiley, 2016.

[46] R. Guerrero-Lemus, R. Vega, T. Kim, A. Kimm, L.E. Shephard, "Bifacial solar photovoltaics- A technology review", *Renewable and Sustainable Energy Reviews*, vol. 60, 2016, pp. 1533 - 1549.

[47] F. Fertig, S. Nold, N. Wöhrle, J. Greulich, I. Hädrich, K. Krauß, M. Mittag, D. Biro, S. Rein and R. Preu, "Economic feasibility of bifacial silicon solar cells", *Progress in photovoltaics: research and applications*, vol. 24, no. 6, June, 2016, pp. 800-817.

[48] M.P Brennan, A.L. Abramase, R.W. Andrews and J.M. Pearce, "Effects of spectral albedo on solar photovoltaic devices", *Solar Energy Materials & Solar Cells*, vol. 124, 2014, pp. 111 - 116.

[49] U. A. Yusufoglu, T. M. Pletzer, L. J. Koduvelikulathu, C. Comparotto, R. Kopecek, and H. Kurz, "Analysis of the Annual Performance of Bifacial Modules and Optimization Methods". *IEEE Journal of Photovoltaics*, vol. 5, no. 1, Jan, 2015, pp. 320-328.

[50] G. Quesada, L. Guillon, D. R. Rousse, M. Mehrtash, Y. Dutil and P.-L. Pardis, "Tracking strategy for photovoltaic solar systems in high latitudes", *Energy conversion and Management*, vol. 103, 2015, pp. 147 - 156.

[51] S. C. Bhattacharyya, "Economic Analysis of Energy Investments", *Energy Economics: Concepts, Issues, Markets and Governance*, London, UK, Springer, 2011, ch. 7.

[52] J. J. Roberts, A. A. M. Zevallos and A. M. Cassul, "Assessment of photovoltaic performance models for system simulation ", *Renewable and*

Sustainable Energy Review, 2016.

[53] M. A.M. Ramli et al. "On the investigation of photovoltaic output power reduction due to dust accumulation and weather conditions", *Renewable Energy* , vol. 99, 2016, pp. 836 - 844.

[54] Homer Energy, Homer energy help manual. [Online]. Available: http://www.homerenergy.com/pdf/HOMERHelpManual.pdf, [Accessed March 2017].

[55] IRENA, " Renewable Power Generation Costs in 2014", IRENA, 2015.

[56] S. Kouro et al. "Grid-Connected Photovoltaic Systems: An Overview of Recent Research and Emerging PV Converter Technology", *IEEE Industrial Electronics Magazine*, vol. 9, no. 1, 2015, pp. 47-61.

[57] B. Thorud, S. Merlet, "Solenergi i Norge: Status og framtidsutsikter", *Energi og Klima*, vol 5, June 2015.

[58] NREL, Best research-cell efficiencies. [Online]. Available:https://www.nrel.gov/pv/assets/images/efficiency-chart.png, April 2017. [Accessed May 2017].

[59] IRENA, "The power to change: Solar and wind cost reduction potential to 2025", IRENA, July, 2016.

[60] Solar Edge, [Online]. Available: https://www.solaredge.com/us. [Accessed April 2017]

[61] D. Zaitsev et al., "Mot Lysere Tider Solkraft i Norge – Fremtidige muligheter for verdiskaping", accenture and WWF, April 2016.

[62] Statistikk- bruk av solenergi i Norge. (n.d). Norsk solenergiforening. [Online]. Available: http://solenergi.no/statistikk/. [Accessed April 2017].

[63] Solar technologies Scandinavia AS. [Onlie]. Available:http://solarts.no/. [Accessed April 2017].

[64] Elspot Prices_2016_Hourly_NOK from Historical Market Data. (n.d.). Nord Pool. [Online]. Available: http://www.nordpoolspot.com/historical-market-data/. [Accessed April 2016].

[65] W. C. Skamarock et al. "A Description of the Advanced Research WRF Version 3", *National Center of Atmospheric Research*, Boulder, Colorado,

USA, 2008.

[66] R. Godina et al. "Sustainable energy system of El Hierro Island", *International Conference on Renewable Energies and Power Quality*, La Coruña, Spain, 2015.

[67] L. Plitt, "The greenest island in the world?", *BBC:magazine*, October 5, 2015. [Online] Available: http://www.bbc.com/news/magazine-34424606. [Accessed April 25, 2017].

[68] C. R. A. Hallam et al. "Hybrid Closed-loop Renewable Energy Systems: El Hierro as a Model Case for Discrete Power Systems", *2012 Proceedings of PICMET '12: Technology Management for Emerging Technologies*, pp. 2957-2969.

[69] Homer Energy. (n.d). [Online].Available: http://www.homerenergy.com. [Accessed April 2017].

[70] V. Quaschning, *Understanding Renewable Energy Systems*, London, England, Earthscan, 2005.

[71] seNorge- vær, "Stasjon Fakken". [Online]. Available: http://www.senorge.no/index.html?p=senorgeny&st=weather. [Accessed May 2017].

[72] D. C. Jordan and S. R. Kurtz, "Photovoltaic Degradation Rates — An Analytical Review", *Progress in photovoltaics: Research and applications*, vol. 21, no. 1, 2013, pp. 12-29.

[73] D. Carvalho et al. "A sensitivity study of the WRF model in wind simulation for an area of high wind energy", *Environmental Modelling & Software*, vol. 33, 2012, pp. 23-34.

[74] John Gerrard, "Weathering and mass movement", *Mountain Environments: An Examination of the Physical Geography of mountains*, MIT press, 1990, pp. 98

[75] "Area solar radiation". [Online]. Available: http://desktop.arcgis.com/en/arcmap/10.3/tools/spatial-analyst-toolbox/area-solar-radiation.htm, July 2012. [Accessed May 2017].

[76] K. Branker et al. "A review of solar photovoltaic levelized cost of electricity ", *Renewable and Sustainable Energy Reviews*, vol. 15, no. 9, 2011, pp. 4470 - 4482.

[77] SMA, "Products". [Online] Available: https://www.sma.de/en/products/system-solutions-packages/mv-power-station-2200sc-2500sc-ev.html, [Accessed May 2017]

[78] K. Zipp, "The new age in solar inverter conversion efficiency: 99%", *Solar Power World*, Feb 2015. [Online], Available: http://www.solarpowerworldonline.com/2015/02/new-age-solar-inverter-conversion-efficiency-99/. [Accessed May 2017].

[79] Mark Fedkin and John A. Dutton, "Utility and solar power concentration" Department of Energy and Mineral Engineering, Penn State. [Online] Available: https://www.e-education.psu.edu/eme812/node/738. [Accessed May 2017].

[80] P. M Rodrigo et al. "DC/AC conversion efficiency of grid-connected photovoltaic inverters in central Mexico", vol. 139, 2016, pp. 650-665.

[81] M. A. Green1 et al. "Solar cell efficiency tables (version 49)", *Progress in Photovoltaics: Research and Applications*, Wiley Online Library, vol. 25. no. 1, 2017, pp. 3-13.

[82] NIBIO, Norsk institutt for bioøkonomi, "Landbruksmetrologisk tjeneste". [Online]. Available: http://lmt.bioforsk.no/agrometbase/getweatherdata.php. [Accessed May 2017].

[83] Statistisk sentralbyrå, "Energiforbruk is husholdninger 2012". [Online]. Available: https://www.ssb.no/energi-og-industri/statistikker/husenergi/hvert-3-aar/2014-07-14.

[84] Eurostat statistics explained, "Electricity prices statistics". [Online] Available: http://ec.europa.eu/eurostat/statistics-explained/images/d/do/Disaggregated_price_data_for_household_consumers%2C_2016s2_%28in_EUR_kWh%29.png, May 2017. [Accessed May 2017].

[85] T. Phillips, "China builds world's biggest solar farm in journey to become green superpower", *The Guardian*, January 19, 2017. [Online]. Available: https://www.theguardian.com/environment/2017/jan/19/china-builds-worlds-biggest-solar-farm-in-journey-to-become-green-superpower. [Accessed April 25, 2017].

[86] W. Fang et al. "Optimal sizing of utility-scale photovoltaic power generationcomplementarily operating with hydropower: A case study of

theworld's largest hydro-photovoltaic plant", *Energy Conversion and Management*, vol. 136, 2017, pp. 161 - 172.

[87] IHA central office, "2015 Hydropower Status rapport", iha international hydropower association, London, 2015.

[88] ISET and SMA, "Kythnos IslandNew Generation of Modular Hybrid Power SupplyBased on AC-Coupling20 Years' Experience of System Technology for Renewable Energies", Technical report, Germany.

[89] "RE islands: RE hybrid systems integration", *REfocus*, London, vol. 3. no. 4, July/August 2002. pp. 54-57.

[90] FF. Le and J. Qiu, "Multi-objective optimization for integrated hydro–photovoltaic power system ", *Applied Energy*, vol. 167, 2016, pp. 377–384.

[91] "Treasure island" , Giltemeister Energy solutions, 8 Aug, 2013. [Online]. Available:http://energy.gildemeister.com/en/company/news/pellworm-cellcube-installation/261096. [Accessed April 2017].

[92] S. Koopmann et al. "Multifunctional operation of a virtual power plant in an active distribution grid: Modelling approaches and first field test experiences from the SmartRegion Pellworm project", *IEEE PES Innovative Smart Grid Technologies Europe*, Oct 2014, pp. 1-6.

[93] "Germany's first large-scale photovoltaic plant is being refurbished", Sun & Wind energy, Aug 2015. [Online] Available: http://www.sunwindenergy.com/sectors. [Accessed April 2017].

[94] A. Risso et al. " A PV WIND HYDRO HYBRID SYSTEM WITH PUMPED STORAGE CAPACITY INSTALLED IN LINHA SETE, APARADOS DA SERRA, SOUTHERN BRAZIL" *Modeling and Dynamic Behaviour of Hydropower Plants*, March 2017. [Online]. Available: http://digital-library.theiet.org/content/books/10.1049/pbp0100e_ch10. [Accessed April 2017].

[95] "Best research cell efficiencies", National Renewable energy laboratory (NREL), *Photovoltaic research*. [Online]. Available: https://www.nrel.gov/pv/. [Accessed: May 2017].

[96] Solbes, [Conversations with Øystein Kleven by phone and email], Available: http://solbes.no/, May 2017.

[97] K. Ingebrigtsen, "Case Study of a Large-Scale Solar, Wind and Hydro Power Hybrid system in Skibotndalen, Troms", M. S thesis, UiT, The Arctic Univ. of Norway, Tromsø, 2017.